The *Leishmania* Phagosome: Isolation by Dual-Fluorescence Sorting

Freya Mayhew-Smith

MSc by Research

University of York

Biology

December 2025

Abstract

This project developed a novel, efficient technique for isolating *Leishmania donovani*-containing phagosomes to enable in-depth proteomic analysis, offering critical insight into host-pathogen interactions and the macrophage host response to infection. Building upon methods used for isolating other pathogen-containing vacuoles (like those of *Salmonella* and *Legionella*), and adapting prior work on other *Leishmania* species, our technique uses Fluorescence-Activated Cell Sorting (FACS). Mouse bone marrow-derived macrophages (BMDMs) were infected for 24 hours with a TdTomato fluorescent *L. donovani* line. The macrophages were then lysed via nitrogen cavitation, a gentle method that preserves intracellular amastigotes and the integrity of the phagosomes. The phagosomal membrane was stained using CellVue Burgundy, and *L. donovani*-containing phagosomes were subsequently isolated by FACS based on dual fluorescence (parasite and phagosome membrane stain). The established method successfully yields highly intact, isolated parasite-containing phagosomes, providing a strong foundation for future research. This successful isolation technique creates a reliable basis not only for the initial goal of proteomics but also for broader 'omics' studies, including lipidomics and interactomics, to fully characterize the *Leishmania donovani*-containing phagosome environment. While the results are promising, future optimization steps are outlined to enhance efficiency and validity for high-throughput applications.

Author's declaration

I declare that this thesis is a presentation of original work and I am the sole author. This work has not previously been presented for a degree or other qualification at this University or elsewhere. All sources are acknowledged as references.

Acknowledgements

I'd like to thank both my supervisors Jeremy Mottram and Elmarie Myburgh for sharing all their knowledge and expertise with me throughout my project as well as for their continued support. I'd also like to thank the rest of the Mottram lab and H block for all their help, advice, wonderful cakes and sunny BBQs! I'd like to give a special mention to Megan Pierce in the Mottram lab for being the best lab buddy I could've asked for to help me get through all the highs and lows of my project.

Lastly, thank you to all my friends and family who have cheered me on all the way through, I couldn't have done it without all your encouragement and words of wisdom.

Table of Contents

Chapter 1: Background

1.1 Leishmaniasis

1.1.1 Outline

Leishmania are kinetoplastid protozoan parasites transmitted to humans via bites from female phlebotomine sand flies, causing diseases of varying severity (Debrabant et al., 2004; Mougneau et al., 2011; Ready, 2014). The most severe, Visceral Leishmaniasis (VL), causes serious illness and in 95% of untreated cases, death (Kumar and Nylén, 2012; Torres-Guerrero et al., 2017; Yeshaw et al., 2020). Although found across 88 countries worldwide, VL is most prevalent in India, East Africa, and Brazil, causing significant health complications for up to 400,000 people per year as well as up to 40,000 deaths annually (Kumar et al., 2014; Ready, 2014). The lack of a vaccine or effective chemoprophylaxis highlights the need for greater understanding of the parasite's survival mechanisms within the human host (Van Griensven and Diro, 2012).

1.1.2 Clinical presentations and variants

Leishmaniasis presents with varying symptoms, dependent on the infectant parasite species and clinical sub-type of disease. There are four different clinical categories of disease; Cutaneous Leishmaniasis (CL), Mucocutaneous Leishmaniasis (MCL), Visceral Leishmaniasis (VL) and Post Kala-Azar Dermal Leishmaniasis (PKDL) (Abadías-Granado et al., 2021). CL is the most common clinical presentation and is often caused by the *Leishmania mexicana*, *Leishmania braziliensis, Leishmania tropica, Leishmania amazonensis* and *Leishmania major* species, among others (David and Craft, 2009). Symptoms typically appear as a self-healing papule that will sometimes then ulcerate and become a larger lesion (Abadías-Granado et al., 2021; David and Craft, 2009; Pace, 2014). The lesion is localised to the bite site, meaning they are most often seen on exposed areas of the body such as the ears, face and neck (Abadías-Granado et al., 2021; Pace, 2014). MCL is a more severe and fatal manifestation of CL, most commonly developing in CL cases that have received inadequate treatment of lesions (David and Craft, 2009). The risk of disease progression between these sub-types is relatively small as it requires dissemination of the parasite to mucosal areas such as the oral and upper respiratory tract mucosal linings through the bloodstream or lymphatic system (Abadías-Granado et al., 2021; Pace, 2014).

VL causes the highest number of deaths of all the clinical sub-types of disease and is most commonly caused by the *Leishmania donovani* and *Leishmania infantum* species (Mann et al., 2021). Instead of developing the dermatological symptoms, this form of disease is systemic with parasites spreading

throughout the body to the liver, spleen, bone marrow and lymph nodes (Kumar and Nylén, 2012). Initial symptoms include fevers, fatigue and weight loss and then far more severe symptoms such as hepatosplenomegaly, thrombocytopenia and immunosuppression develop as the disease progresses, eventually resulting in death in many cases (Chappuis et al., 2007; Kumar and Nylén, 2012). PKDL arises as a complication of VL and is seen in less than 10% of cases in Asia but up to 60% of cases in East Africa (Pace, 2014). Patients develop PKDL due to an immunological reaction to the parasites and so is most often seen in those immunocompromised (Chappuis et al., 2007; Pace, 2014). These cases appear as a nodular skin rash, with each lesion containing large numbers of parasites, making this clinical form highly contagious (Chappuis et al., 2007). With a fatality rate of almost 100% without treatment, it is clear how essential effective intervention is for patient survival (Alemu et al., 2023).

1.1.2 Epidemiology

The epidemiology of Leishmaniasis differs by region and parasitic strain. In most regions Leishmaniasis is considered to be zoonotic, with disease transmitting from person to person via the sandfly vector, although in some endemic areas of India, VL is considered anthroponotic (Lysenko, 1971; Singh et al., 2013). There have also been a very small number of reported cases where transmission has occurred via blood transfusion and needle sharing, differing from other vector-transmitted diseases such as American trypanosomiasis, where these transmission routes lead to many more cases (Gradoni, 2018). In South America, the disease is considered as zoonotic due to high incidences of transmission of *L. infantum* from dogs to humans (Ready, 2014; Torres-Guerrero et al., 2017). Studies in Italy, China and parts of South America have all suggested that domestic dogs can act as 'reservoirs of infection' in the transmission of multiple species by the sandfly but particularly *L. brasiliensis* and *L. infantum* (Dantas-Torres, 2007; Ferroglio et al., 2018). This outlines how complex and multifaceted the transmission of Leishmaniasis is and indicates why prevention can be so challenging.

Primarily, Leishmaniasis effects those in poor and rural communities of developing countries, which is often characteristic of neglected tropical diseases (NTDs) (Okwor and Uzonna, 2016; Sunyoto et al., 2019). Poverty plays a key role in the spread of the disease with unsanitary housing conditions offering favourable environments for sandfly breeding and people being forced to migrate to endemic villages due to urban areas becoming too expensive (Sunyoto et al., 2019). The lack of access to affordable treatment also increases the prevalence of disease in these areas with small villages mostly offering only private healthcare that many can't afford and treatment prices sometimes being higher than the average household income as seen in Nepal (Okwor and Uzonna, 2016; Sunyoto et al., 2019). This may also begin to explain the underreporting of Leishmaniasis cases, with tests being unavailable or

overpriced in these communities as well as social stigmas around those infected (Clem, 2010; Elfaki et al., 2024).

1.2 Diagnosis, treatment and prevention

1.2.1 Diagnostic methods and current patient prognosis

There are several methods for the diagnosis of *Leishmania* infection, most of which require clinical diagnosis from a hospital (Ready, 2014). The most common method for diagnosis is microscopically which can be done by the staining of blood samples where the parasite can be seen easily under a light microscope or through liver and spleen biopsies (Ready, 2014). These methods are cheap and easy to perform. There are also molecular and serological diagnostic tools such as PCR, enzyme-linked immunoassay (ELISA) and rK39-ICT (Srivastava et al., 2011). PCR tests are highly sensitive and therefore often give accurate results however the process of performing them is expensive and so is not feasible for diagnosis in poorer areas (Srivastava et al., 2011). ELISA tests allow detection of anti-α-galactosyl antibodies that are present in the serum of CL patients following *L. tropica* and *L. major* infection (Abadías-Granado et al., 2021). The issue with this diagnostic method is the specificity of the test and that it may fail to detect infection of other *Leishmania* strains that don't cause the production of the same antibodies (Abadías-Granado et al., 2021). The rK39-ICT rapid test is often the most practical diagnostic technique as it only consists of a dipstick that is used to detect anti-K39 antibodies in the bloodstream and shows a sensitivity of over 90% in symptomatic patients (Piscopo and Mallia Azzopardi, 2007).

Currently, patients with CL have a good prognosis, with lesions self-healing after a period of 3-18 months in over 90% of cases, particularly if treatment is given (Piscopo and Mallia Azzopardi, 2007). Although the fatality rate is relatively low, patients can be left with scarring from the lesions which may affect their quality of life due to social isolation (Roatt et al., 2020). In patients that have any immunosuppressive coinfections, such as HIV or Malaria, the lesions will be much less likely to self-heal and the disease will often develop into the systematic MCL, making fatalities much higher in these individuals (Alemu et al., 2023; David and Craft, 2009; Ornellas-Garcia et al., 2023; Van Griensven et al., 2014). Lack of treatment is a critical determining factor to CL becoming ulcerative and patient prognosis worsening (Roatt et al., 2020). The prognosis of patients with VL is markedly worse, with 95% of untreated and up to 20% of treated cases being fatal, with death typically occurring two years post-infection (Ready, 2014).

1.2.2 Existing therapeutics

Currently, treatments are generally based on chemotherapy and antimonial drugs that must be administered intravenously and have other issues such as side effects and high costs (Sasidharan and Saudagar, 2021; Torres-Guerrero et al., 2017). Of the antimonial drugs, the pentavalent antimonials are the most common and although it's mechanism of action is not fully clear, the antileishmanial effect is produced when this prodrug is reduced to trivalent antimonial (Sasidharan and Saudagar, 2021; Torres-Guerrero et al., 2017). This group of drugs are most effective against parasites in the amastigote stage, targeting their glycolytic and oxidative pathways in fatty acid synthesis (Goto, 2012; Roatt et al., 2020). This class of treatments causes dangerous side effects such as arthralgia, myalgia and vomiting as well as being toxic to the heart, kidneys, liver and pancreas, meaning some patients (e.g. pregnant and elderly) may not be able to receive them (Goto, 2012; Santos et al., 2008; Sasidharan and Saudagar, 2021). Amphotericin B is another common treatment and is an antibiotic that targets parasites in both the promastigote and amastigote stages (Goto, 2012; Roatt et al., 2020; Santos et al., 2008). It functions by binding to the sterols on the surface membrane of the parasite, increasing permeability and influx of ions and parasite death (Goto, 2012; Roatt et al., 2020; Sasidharan and Saudagar, 2021). This drug is often used for the treatment of VL patients who have developed resistance to other antimonial drugs (e.g. pentamidine) however, the cost of production is very high meaning those who often need this treatment the most cannot access it (Santos et al., 2008). AmBiosome is a liposomal formulation of amphotericin B that, although not currently available on the market, has shown to be effective for the treatment both CL and VL, as well has having a lowered incidence of adverse effects compared to other treatments (Frézard et al., 2022). Its efficacy, however, is highly variable, based on immunological response type (e.g. Th1 vs Th2, further discussed in section 1.6.2) and clinical manifestation (Frézard et al., 2022). Lastly, Miltefosine is currently the only oral anti-leishmanial drug that has been approved for use and is based upon other chemotherapy drugs used in the treatment of cancer (Clem, 2010; Goto, 2012; Roatt et al., 2020). Miltefosine works by inhibiting parasite synthesis of phospholipids and sterols (Goto, 2012). Initially, this drug proved to have high effectiveness in the treatment of VL but after many years of use this decreased due to drug resistance and now this therapeutic is more often used in the treatment of CL (Dirkx et al., 2022; Roatt et al., 2020). Its uses are limited even further due to its high levels of toxicity in the gut, liver and kidneys and its induction of developmental malformations *in utero* (Goto, 2012). To date, there are no licenced vaccines for Leishmaniasis and prevention strategies are centred around vector control (Clem, 2010; Mutiso et al., 2013). Sandfly populations can be easily controlled through the use of insecticides, nets and the wearing of longer clothing (Clem, 2010). This lack of safe, effective treatment as well as biological prevention methods indicates the critical need for more research into *Leishmania* survival mechanisms within the host and its potential vaccine targets.

1.2.3 Drug resistance

As outlined above, antimonial drugs were used successfully for decades, and it is only in the last 30 years that resistance to the drugs has become an obvious problem (Croft et al., 2006). Clinical resistance variation causes an ongoing problem in the use of antimonial drugs with some people being more sensitive to certain compounds such as sodium stibogluconate than others, causing varying effectiveness of these drugs (Croft et al., 2006; Herwaldt and Berman, 1992). Misuse of this class of medications has been a suggested contributor to this problem, with patients able to purchase them over the counter and then not follow the treatment protocol adequately (Croft et al., 2006). This has become a particular issue in endemic regions of India (Croft et al., 2006). In the use of Miltefosine, different parasite species and lifecycle stages naturally have a greater sensitivity to the drug activity, with *L. donovani* being the most sensitive species in both the promastigote and amastigote stages (Croft et al., 2006).

There is also a rise in parasite strains that are themselves resistant to antimonial treatments. Some resistant parasites can reduce intracellular drug levels by overexpression of ABC transporters and efflux of the drug from within the parasite (Croft et al., 2006). This also leads to an influx of thiols that neutralise the reactive oxygen species (ROS) that accumulate under the action of the drug (Magalhães et al., 2018; Mukherjee et al., 2006; Ponte-Sucre et al., 2017). Conversely, the data on *Leishmania* resistance to Miltefosine shows to be somewhat more promising for the ability to continue use of this treatment for years to come. Currently, very few clinical isolates have shown any Miltefosine resistance, meaning naturally resistant strains are less prevalent and slower to emerge compared to strains resistant to other drugs (Croft et al., 2006; Perezvictoria et al., 2006; Ponte-Sucre et al., 2017). This reiterates the need for increased *Leishmania* experimentation with a view to developing new therapeutics before resistant strains render current treatments ineffective.

1.3 Parasite lifecycle

1.3.1 Overview

Leishmania is a digenetic parasite, meaning it has two distinct lifecycle stages in the sandfly and mammalian hosts (Dostálová and Volf, 2012; Gossage et al., 2003). The parasite enters the mammalian host once the female sandfly takes a blood meal (Gossage et al., 2003). The parasites take on several different morphologies within their lifecycle such as long, flagellated promastigotes that can be either procyclic (non-mammalian infective) or metacyclic (mammalian infective) and shorter, rounder

amastigotes that are the intracellular form (Gossage et al., 2003; Mougneau et al., 2011; Torres-Guerrero et al., 2017).

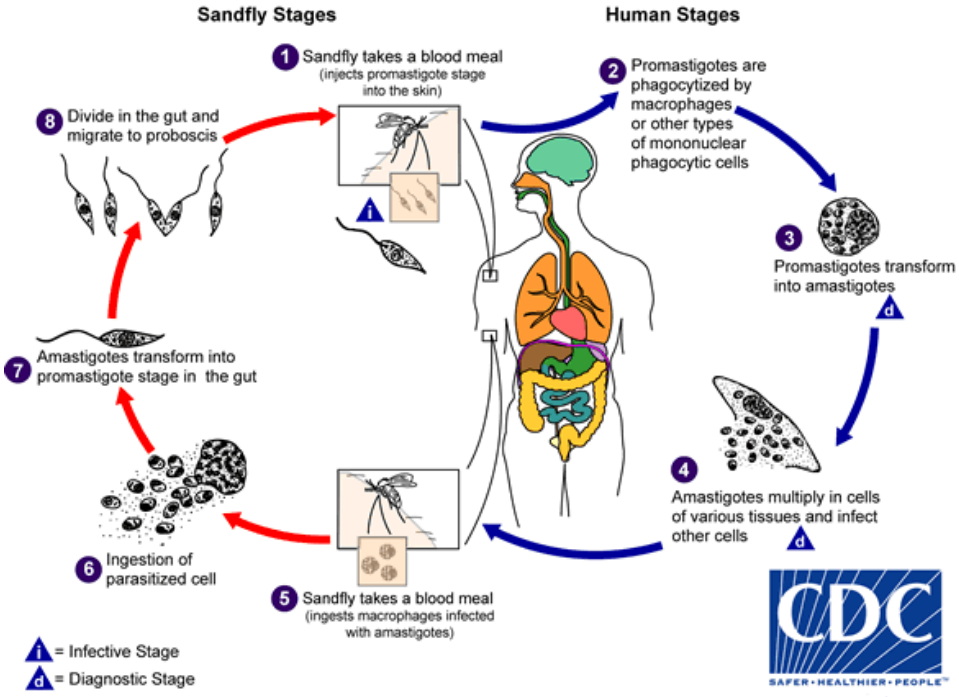

Figure 1: The *Leishmania* lifecycle. This figure shows the complex digenetic life cycle of Leishmania, with its distinct sand fly and human infective stages. Sandfly stages are shown in red and human host stages shown in blue. Amastigotes transform into promastigotes within the sand fly gut. The female sand fly takes a blood meal from a human host, inoculating the promastigotes. Following phagocytosis, promastigotes transform into amastigotes in human phagocytic cells, which then replicate until their release. Taken from Centre of Disease Control and Prevention (www.cdc.gov).

1.3.2 Infection of mammalian hosts

Metacyclic promastigotes enter the mammalian bloodstream via a bite from an infected sandfly (Mougneau et al., 2011). This triggers an immune response is triggered, releasing chemoattractants such as MCP-1 and CXCL1, which recruit monocytes and neutrophils respectively to the site of infection (Mougneau et al., 2011). Neutrophils have been shown to play a key role in the immediate stages of the response against *L. donovani, L.major and L. amazonensis*, responsible for parasite killing through the release of DNA traps called neutrophil extracellular traps (NETs) which cause the parasite to be taken up for degradation alongside the dead neutrophil (Mougneau et al., 2011; Séguin and Descoteaux, 2016). Neutrophils also become transiently infected following phagocytosis of parasites, providing temporary 'shelter' from the host immune system (Podinovskaia and Descoteaux, 2015). The metacyclic promastigotes cannot differentiate into the long-term infective amastigotes within neutrophils, hence only offering temporary survival (Podinovskaia and Descoteaux, 2015). Proteophosphoglycans originating from the sandfly midgut are inoculated alongside the metacyclic promastigotes and act as a strong signal for macrophage recruitment (Podinovskaia and Descoteaux,

2015). The macrophages then either phagocytose the metacyclic promastigotes directly or phagocytose parasites within apoptotic neutrophils and infection is then established (Podinovskaia and Descoteaux, 2015). The uptake of parasites within apoptotic neutrophils causes an immunosuppressive response to further aid persistence of the infection (Séguin and Descoteaux, 2016). Monocytes are recruited to the bite site slightly later, around two weeks post-infection, where they differentiate into monocyte-derived dendritic cells that are able to capture amastigotes (Mougneau et al., 2011).

Once internalised, promastigotes begin to modify the intracellular environment of the phagosome, forming a parasitophorous vacuole (PV) to aid their long term survival (Podinovskaia and Descoteaux, 2015; Real and Mortara, 2012). Some species, like *L. mexicana*, reside in large communal vacuoles, while others, like *L. donovani* and *L. infantum*, form smaller individual vacuoles (Liévin-Le Moal and Loiseau, 2016; Semini and Aebischer, 2018). Within the phagosome, metacyclic promastigotes transform into smaller amastigotes (Dias et al., 2018; Gossage et al., 2003; McConville et al., 2007). In order to survive long term within this PV, the parasites halt the maturation of the vacuole to disrupt the later stages of phagocytosis and trafficking to the lysosome for degradation (Liévin-Le Moal and Loiseau, 2016; Séguin and Descoteaux, 2016). The promastigote uses its virulence factors (discussed in section 1.5.1) such as lipophosphoglycan (LPG) upon entry into the host cell (Séguin and Descoteaux, 2016; Vinet et al., 2009). LPG inserts into the lipid domains of the macrophage membrane and disrupts their structure, which blocks normal NADPH-oxidase activity on the PV membrane and maturation along the endocytic pathway (Séguin and Descoteaux, 2016; Vinet et al., 2009). As a result, proton-ATPases cannot fuse to and enter the vacuole, which stops vacuolar acidification and prevents downstream parasite degradation (Liévin-Le Moal and Loiseau, 2016; McConville et al., 2007; Séguin and Descoteaux, 2016). To further disrupt the later stages of phagocytosis, LPG also induces F-actin accumulation within the periphagosomal space to form a physical barrier that impedes endosome fusion and prevents phagolysosome formation (Séguin and Descoteaux, 2016; Semini and Aebischer, 2018; Vinet et al., 2009). These macrophage lipid domains are also essential for the recruitment of the exocytosis regulatory protein Synaptotagmin (Syt) V, which in the absence of *Leishmania*, associates with the phagosome throughout maturation to mediate the delivery of hydrolytic enzymes that acidify the phagosome to begin degrading its contents (Arango Duque et al., 2013; McConville et al., 2007; Séguin and Descoteaux, 2016; Vinet et al., 2009). In *L. donovani*, the disruption of the lipid microdomains by LPG causes exclusion of Syt V from the phagosome, preventing vesicle fusion and the delivery of further hydrolases (Vinet et al., 2011). The phagosome is therefore not acidified any further, ensuring the safety of the parasites, at which point transformation into amastigotes

(amastigogenesis) takes place. This differentiation can be characterised by a reduction in growth rate and a shift to a unique metabolic state (further detailed in section 1.4.1) as well as morphological changes in size and shape (Podinovskaia and Descoteaux, 2015; Sasidharan and Saudagar, 2021). At this stage, the amastigotes proliferate to allow persistence of infection, causing macrophages to eventually rupture and release the mature amastigotes which are then able to disseminate to infect further host cells (Sasidharan and Saudagar, 2021).

1.4 The Phagosome

1.4.1 The phagosome environment

The phagosome is an acidified vacuole with a pH ranging from approximately 4.5-5.5 depending on the species and amastigotes are highly adapted to thrive within this harsh environment (Glaser et al., 1988; Real and Mortara, 2012). Firstly, the decrease in pH acts as a signal for the beginning of amastigogenesis after the promastigote has halted the later stages of phagocytosis and ensured long-term safety within the PV (Batista et al., 2020; Burchmore and Barrett, 2001; Séguin and Descoteaux, 2016). For effective metabolism once living intracellularly, amastigotes must maintain an intracellular neutral pH, which they are adapted to do at pH levels as acidic as 4-5 (Burchmore and Barrett, 2001). This allows effectual degradation of macromolecules that are delivered to the phagosome, which the parasites are then able to take up (detailed further in section 1.4.2) (McConville et al., 2015; McConville and Naderer, 2011). This switch to the amastigote form also allows the parasite entry into a slowed metabolic rate, that can be described as 'semi-quiescence', meaning that many highly energy-consuming processes are suppressed and this has been demonstrated in several species such as *L. infantum*, *L. major*, *L. donovani* and *L .mexicana* (Dirkx et al., 2024; Jara et al., 2017; McConville et al., 2015). Without the acidity of the phagosome environment this transformation would not take place, and the parasites may not survive. This semi-quiescent state causes lowered replication rates with some studies discovering populations of amastigotes with varying rates (Jara et al., 2017). For example, some amastigotes had a doubling time of approximately 60 hours whereas others were considered non-replicating (Jara et al., 2017).

The nature of this environment also allows close mimicry of a mature phagolysosome, displaying similar surface markers that subvert the host immune system and prevent further attack (Burchmore and Barrett, 2001; Lodge and Descoteaux, 2005; McConville and Naderer, 2011). Although the recruitment of some of these markers, such as Lysosome-associated membrane proteins (LAMPs) , is delayed, by 48 hours following parasite engulfment, the phagosome displays the key characteristics

of a phagolysosomal compartment (Lang et al., 1994). LAMP proteins (1 and 2) are essential for the fusion of the phagosome with the lysosome and therefore the final degradation of the engulfed material (Huynh et al., 2007). The delayed nature of the accumulation of LAMP proteins on the phagosome membrane means that the phagosome does not fuse with a lysosome to form the phagolysosome, however the host immune system does not recognise this due to the eventual display of these proteins (Boggiatto et al., 2014; Rodríguez et al., 2011). Similarly, *L. donovani* upregulates the early endosome protein Rab5a to further delay phagosome maturation and lysosome fusion (Batista et al., 2020). Phagosomes also contain a highly controlled level of the hydrolases that are characteristic of a phagolysosome (Handman and Bullen, 2002). This allows the PV to be acidified to the required pH for amastigogenesis and appear to the host as a phagolysosome, but it will not be acidified enough that the parasites become degraded (Lodge and Descoteaux, 2005; McConville et al., 2015). These key features of the phagosome environment allow the parasites to thrive within the host as well as remain undetected.

1.4.2 Nutrient acquisition

The phagosome also provides a constant supply of nutrients that allow the amastigotes long term survival (Burchmore and Barrett, 2001; Landfear, 2011). While the parasite is auxotrophic for specific host-derived molecules such as purines and specific amino acids, other nutrients such as lipids and vitamins are also trafficked to the phagosome from the host (Burchmore and Barrett, 2001; McConville and Naderer, 2011). These are exploited as carbon and energy sources, despite amastigotes possessing the machinery to synthesise these molecules *de novo* (Burchmore and Barrett, 2001; McConville and Naderer, 2011). These nutrients are delivered to the phagosome via vesicles from multiple pathways (e.g. endocytic, autophagic and phagocytic) as well as from the endoplasmic reticulum (ER) (McConville et al., 2015; Naderer and McConville, 2007). The hydrolases (e.g. cathepsins and glucuronidases) within the phagosome can then break down these host molecules to produce sugars, amino acids and lipids that are free for uptake by the amastigotes to provide essential carbon (Burchmore and Barrett, 2001; McConville et al., 2015). To ensure that this supply is sufficient, amastigotes divert the host endocytic system towards the parasite-containing phagosomes to increase the delivery of host molecules (Burchmore and Barrett, 2001; Liévin-Le Moal and Loiseau, 2016). The mTOR/AMPK pathway that mediates autophagy is modulated by the parasite for increased nutrient uptake, being upregulated in the later stages of infection (Thomas et al., 2018). Approximately 24 hours post-infection, activation of the cellular resource sensor, AMPK, becomes elevated through upstream switches, mediated by the parasite (Moreira et al., 2015). This causes

increased scavenging for nutrients by the host and higher levels of autophagy, delivering greater recycled molecules to the phagosomes for the parasites to utilise (Ferreira et al., 2021).

The diverted vesicles also carry Transferrin (which is usually recycled within the host through clathrin-mediated endocytosis) to the phagosome, to provide a source of iron once degraded by the amastigote, essential for growth and replication (Borges et al., 1998; Burchmore and Barrett, 2001; Mayle et al., 2012). *Leishmania* are also unable to synthesise purines intrinsically, despite them being essential for cell signalling and energy production (Boitz et al., 2012; Landfear, 2011). Nucleoside transporters were first identified in *L. donovani* and have shown to allow recovery of purines (alongside other free nucleosides) from the host via proton-coupled transport across the plasma membrane (Boitz et al., 2012; Burchmore and Barrett, 2001; Landfear, 2011). In summary, although *Leishmania* must scavenge for several of its essential nutrients once within the host, phagosomes typically contain high enough levels of these molecules to facilitate long-term survival and meet the metabolic requirements of the amastigotes (Naderer and McConville, 2007).

1.5 Mammalian host cell types

1.5.1 Phagocytic cell types

Immediately following the sand fly bite, professional phagocytic cells such as neutrophils and tissue-resident macrophages are recruited to the bite site, beginning the host immune response (Mougneau et al., 2011; Séguin and Descoteaux, 2016; Valigurová and Kolářová, 2023). As *Leishmania* parasites lack the machinery used by other parasites (e.g. *Toxoplasma* and *Plasmodium*) to actively invade host cells, phagocytic cells are easy targets for invasion, with binding to the host cell surface opsonins enough to trigger phagocytosis and allow entry into host cells (Valigurová and Kolářová, 2023). The parasites then begin to infect recruited dendritic cells, inflammatory monocytes and eosinophils, which support long term *Leishmania* survival (Mougneau et al., 2011; Valigurová and Kolářová, 2023). The nature of dendritic cells particularly promotes dissemination and visceralisation of the infection due to their migration abilities (Kima, 2007; Valigurová and Kolářová, 2023). Interestingly, although initially neutrophils only offer temporary shelter for *Leishmania* (as discussed in section 1.3.3) as their environment does not support amastigogenesis, neutrophils can support the replication of amastigotes if taken up in this lifecycle stage (Hurrell et al., 2017; Valigurová and Kolářová, 2023). This form of passive entry via phagocytic uptake is the most well studied form of internalisation used by *Leishmania*. This, alongside infection studies in different macrophage types, suggests differences in

permissiveness of different host cell types to parasite growth (Mandell et al., 2022; Valigurová and Kolářová, 2023).

1.5.2 Non-phagocytic cell types

Leishmania can also exist latently in other, non-phagocytic cell types such as fibroblasts, osteoclasts, haematopoietic stem cells and adipocytes, supporting parasite survival for long time periods before the appearance of symptoms (Bogdan et al., 2024, 2000; Dirkx et al., 2022; Valigurová and Kolářová, 2023). This greatly enhances the persistence of *Leishmania* as these cells can provide safety from destruction by host defences whilst the parasites continue to replicate, building up reservoirs that are hidden from the host immune system (further discussed in section 1.5.3) (Bogdan et al., 2000; Valigurová and Kolářová, 2023). Entry into non-phagocytic cells may be possible through several mechanisms, with one currently being proposed as the most feasible. *Trypanosoma cruzi*, a close relative of *Leishmania*, enters non-phagocytic cells during lysosome exocytosis following injury to the host cell membrane (Fernandes et al., 2011; Valigurová and Kolářová, 2023). The membrane damage causes an increase in intracellular calcium ions, which stimulate lysosome exocytosis (Cavalcante-Costa et al., 2019; Valigurová and Kolářová, 2023). Within this process, endocytosis of the damaged membrane allows the parasite to enter the cell, thereby infecting it (Fernandes et al., 2011; Valigurová and Kolářová, 2023). It has been proposed that *Leishmania* may use this same mechanism, particularly for the invasion of fibroblasts (Cavalcante-Costa et al., 2019; Valigurová and Kolářová, 2023).

1.5.3 Latency and infection recurrence

As previously mentioned, *Leishmania* can cause latent infections in non-phagocytic host cells whereby the parasites are replicating at very low rates (doubling times of several days), undetected by the host immune system because of their intracellular nature (Bogdan et al., 2024; Jara et al., 2017; Kloehn et al., 2015; Valigurová and Kolářová, 2023). Additionally, some *Leishmania* species, alongside other intracellular parasites, can form non-replicating cells that are still viable for infection (Dirkx et al., 2022). This allows long-term persistence of infection (Bogdan et al., 2024). These large reservoirs play a critical role in causing the relapse of infection following treatment with antileishmanial drugs (Dirkx et al., 2022). Studies into latent populations within long-term haematopoietic stem cells (LT-HSCs) suggests that this particular bone marrow niche can offer protection from drug action, allowing re-infection even after the administration of treatment (Dirkx et al., 2022). Moreover, this hypoxic environment also protects from oxidative stress and the antimicrobial action of ROS, further supporting the persistence of the latent parasites (Dirkx et al., 2022). Other intracellular pathogens such as *T. cruzi* and *Mycobacterium tuberculosis* have shown to survive latently in adipocytes, and

recent studies in mice have suggested that *L. infantum* may do the same (Schwing et al., 2021). Similarly to in LT-HSCs, adipocytes types have no intrinsic anti-microbial activities, making them ideal cells for long-term survival (Schwing et al., 2021; Valigurová and Kolářová, 2023). The parasites within these reservoirs are released when the host cells undergo apoptosis, making them free to infect macrophages that will be recruited to the area, to begin active infection (Baars et al., 2023; Mandell and Beverley, 2017). This causes issues in the development of vaccines due to the latent populations being immunologically 'silent' and not able to be killed by vaccine-stimulated macrophage action (Panahi et al., 2022; Schwing et al., 2021).

1.6 Host immune evasion

1.6.1 Parasite virulence factors

LPG is one of the key virulence factors that *Leishmania* uses to infect the mammalian host, being highly expressed in the promastigote stage and then downregulated following amastigogenesis (Al-Khalaifah, 2022; Séguin and Descoteaux, 2016). LPG is responsible for many of the processes that ensure survival such as Syt V exclusion, NET release, host protein kinase C (PKC) inhibition and arrested phagosomal maturation (Liévin-Le Moal and Loiseau, 2016; Olivier et al., 2012; Séguin and Descoteaux, 2016; Shadab and Ali, 2011; Vinet et al., 2011). Although the importance of LPG for parasite virulence differs between *Leishmania* species (e.g. less crucial for experimental *L. mexicana*), it is generally considered to be crucial for persistence of infection, with LPG negative mutants having been shown to be more susceptible to particular host immune defences (Ilg, 2000; Späth et al., 2003, 2000). LPG also allows modulation of the host immune responses, to interrupt many of the key strategies used for pathogen destruction (detailed further in section 1.6.3).

Beyond LPG, *Leishmania* uses other pathogenicity factors to establish and maintain persistent intracellular infection. GP63 is a surface metalloprotease, that can also be present in exosomes, that alters host cell signalling upon secretion (Isnard et al., 2012; Olivier et al., 2012; Séguin and Descoteaux, 2016). In the promastigote stage, GP63 has been shown to interrupt host complement action by cleaving C3b, which normally binds to pathogens to mark them for destruction (Dunkelberger and Song, 2010; Olivier et al., 2012). This cleavage causes the generation of the iC3b molecule which aids parasite entry into macrophages by acting as an opsonin to trigger phagocytosis and parasite engulfment (Gurjar et al., 2025; Olivier et al., 2012). Like LPG, GP63 expression is also reduced in amastigotes and although detectable, its function following amastigogenesis requires further elucidation (Olivier et al., 2012). Additionally, GP63 targets key host signalling pathways to

disrupt the release of TNF, IL-12 and nitric oxide (NO) which are all critical for pathogen clearance (detailed further in section 1.6.2) (Séguin and Descoteaux, 2016). Glycosylinositol phospholipids (GIPLs) are a smaller group of virulence factors, present on the surface of both promastigotes and amastigotes (Olivier et al., 2012). *L. donovani* GIPLs have been shown to interact with receptors on the macrophage surface to further inhibit PKC activity alongside LPG (Olivier et al., 2012). Uniquely, GIPLs are almost equally expressed in the promastigote and amastigote stages, however there is some differential expression of particular classes in a stage-specific manner (Schneider et al., 1993). This difference in GIPL class expression is also species-dependent with *L. major* showing greater stage-specific variation compared to *L. donovani* (Schneider et al., 1993).

1.6.2 Activation of the Th2 response

Although living within the phagosome provides protection from attack by host immune cells, *Leishmania* also utilises strategies to actively suppress host responses (Batista et al., 2020; Goto and Lindoso, 2004; Séguin and Descoteaux, 2016; Semini and Aebischer, 2018). One of these strategies is the disruption of pro-inflammatory cytokines and activation of a Th2 response. *Leishmania* infection can cause the suppression of IL-12 production by reducing NF-κB signalling and therefore downstream IL-12 transcription (Alexander and Bryson, 2005; Shweash et al., 2011). IL-12 is a critical pro-inflammatory cytokine that is released during a Th1 response and has been associated with infection resistance and greater wound healing following infection (Alexander and Bryson, 2005; Gupta et al., 2013). This lack of IL-12 signalling, alongside the upregulation of IL-4 production drives the differentiation to a Th2 immune response, associated with the non-healing and visceral infections caused by *L. donovani* (Alexander and Bryson, 2005; Goto, 2025; Rossi and Fasel, 2018). The absence of IL-12 also means that IFN-γ secretion is suppressed, blocking NO accumulation in the macrophage and pathogen killing (Alexander and Bryson, 2005).

Leishmania also drives the release of immunosuppressive cytokines such as TGF-β. The apoptotic neutrophils that the parasites are engulfed within have a surface display of phosphatidylserine (PS) that some *Leishmania* species are then able to themselves present following internalisation (Batista et al., 2020). This PS signal causes apoptotic mimicry, appearing to phagocytes as apoptotic cells (Séguin and Descoteaux, 2016). The PS-displaying promastigotes then stimulate TGF-β secretion by the neutrophils, inhibiting the expression of transcription factor T-bet and to driving the immune response towards the Th2 lineage (Birge et al., 2016; De Freitas Balanco et al., 2001; Goto and Lindoso, 2004; Wanderley et al., 2013). This shift to the Th2 response allows greater parasite persistence and survival (Alexander and Bryson, 2005).

1.6.3 Inhibition of antimicrobial strategies

After engulfment, macrophages typically utilise a technique of ROS accumulation within the phagosome to cause the pathogen oxidative stress which eventually leads to its death known as the 'oxidative burst' (Canton et al., 2021; Martínez-López et al., 2018; Rossi and Fasel, 2018). NADPH oxidases are essential for the production of these ROS and must be translocated to the lipid microdomains of the phagosome membrane to perform this function (Lodge and Descoteaux, 2006; Rossi and Fasel, 2018; Vinet et al., 2011). As discussed previously, *Leishmania* LPG disrupts these microdomains and this causes interference with NADPH oxidase assembly on the surface of the phagosome, stopping its ROS-producing capabilities (Lodge and Descoteaux, 2006, 2005; Vinet et al., 2009). GP63 also aids this by cleaving host phosphatases that are part of the signalling cascade that activates MAP kinase (MAPK), which would usually activate NAPDH oxidase activity (Frey et al., 2009; Gomez et al., 2009). This inability to activate MAPK further impedes the ability of NADPH oxidase to cause antimicrobial build-up of ROS within the phagosome. These are just some of the many pathways through which *Leishmania* can subvert and interfere with the mammalian host signals to ensure its survival.

1.7 Proteomics

1.7.1 Overview of proteomics

Broadly, proteomics is the study of proteins within cells, tissues or organisms from multiple aspects such as protein abundance, protein localisation, protein interactions and protein modifications post-translation (Alsagaby, 2019). There are four major steps involved in the process of proteomics; protein extraction from a sample, fractionation for protein separation, mass spectrometry and protein identification (Alsagaby, 2019). This method allows the collection of large volumes of protein data from a single experiment, recognising up to thousands of proteins that can then be characterised and further investigated (Alsagaby, 2019). Although somewhat dependent on sample complexity and preparation, the sensitivity of this process also allows detection of proteins that are low in abundance and therefore only produce limited sample (Aebersold and Mann, 2016). Additionally, the sensitivity allows detection of very small changes in protein abundance, structure or interaction, yielding highly detailed data (Cox and Mann, 2011). The goal of performing such experimentation is to develop deeper understanding of cell behaviour through its signalling and metabolic pathways, by studying the proteins that make up these pathways (Anderson et al., 2000). This can identify new targets and biomarkers that can be exploited for drug development and clinical testing (Vitzthum et al., 2005).

1.7.2 Proteomics of *Leishmania*

Within *Leishmania* research, proteomics has already helped to further elucidate many aspects of parasite behaviours and the proteins that facilitate them, from protein remodelling between lifecycle stages to secreted proteins that modulate host processes (Sanchiz et al., 2020; Tsigankov et al., 2013). Much research has also focused on creating a well-annotated reference genome to provide a database for protein identification following mass spectrometry (Sanchiz et al., 2020). There are, however, several factors that cause *Leishmania* proteomics to be more problematic. In dual proteomics, parasite proteins can be hard to detect because host proteins appear in much higher abundances (Gioseffi et al., 2020; Moradimotlagh et al., 2023). This limitation arises from the dynamic range of protein abundance, whereby low abundance parasite proteins may not reach the detection threshold of mass spectrometry, rather than issues in the separation process itself (Zubarev, 2013). Therefore, approaches that enrich for parasite-derived proteins have the potential to overcome this constraint, such as using FACS to reduce the abundance of background host proteins, as presented in this study. Species specific variation also limits the ability to find proteins that share structure and function across all species, which adds complexity when trying to target them (De Rezende et al., 2017). These challenges increase in studying phagosome proteomics, since *Leishmania* remains inside the phagosome for most of its time in the mammalian host (Gioseffi et al., 2020; Moradimotlagh et al., 2023). The amount of amastigote protein in a sample depends on the level of infection and the number of phagosomes formed, and host proteins can mask parasite proteins when infection rates are low (Gioseffi et al., 2020; Moradimotlagh et al., 2023). Mass spectrometry will also detect host proteins from the cell surrounding the phagosome, which complicates efforts to identify parasite proteins present.

Profiling the proteomes of amastigote-containing phagosomes could provide crucial insights for identifying vaccine and drug targets, but this is dependent on advancing sample preparation methods specifically for phagosome proteomics. One method for doing so involves the isolation of amastigote-containing phagosomes from the surrounding cell prior to proteomics (Chatterjee et al., 2025; Semini and Aebischer, 2018). Although this has been tested further using bacterial pathogens (detailed further in section 1.7.4) some experimentation has begun to adapt techniques for larger *L. amazonensis* and *L. mexicana*-containing phagosomes (Chatterjee et al., 2025; Real, 2020; Semini and Aebischer, 2018). Several strategies have been trialled with varying levels of success. As vesicles contain a unique display of the transmembrane protein calnexin on their surface, some studies have aimed to exploit this by using anti-calnexin antibodies to select for PVs following fractionation (Kima

and Dunn, 2005; Semini and Aebischer, 2018). This showed limited potential as it was only able to efficiently isolate PVs containing promastigotes, not amastigotes due to issues in binding affinity (Kima and Dunn, 2005; Semini and Aebischer, 2018). More recently, protocols using fluorescence-activated cell sorting (FACS) following gradient centrifugation have been developed, showing success in isolating larger *L. mexicana*-containing phagosomes (Chakraborty et al., 1995; Semini and Aebischer, 2018). However, there has been little work in altering this technique for use in isolating *L. donovani*-containing phagosomes, despite this species being the causing the more lethal clinical manifestation of disease. Differences in phagosome size between these two species means that this technique must be optimised and tested further for use in *L. donovani*, which is what this project has aimed to achieve (Liévin-Le Moal and Loiseau, 2016). In addition to these approaches, previous related work at York has shown that mechanical disruption can release L. donovani-containing phagosomes for downstream analysis (Saunders, 2016). Saunders (2016) applied a mechanical breakage method to infected macrophages and used magnetised LV9 (MHOM/ET/67/HU3) *L. donovani* amastigotes to recover parasite-containing compartments for proteomics. This demonstrates that phagosome isolation through mechanical methods is feasible within the *Leishmania* system allowing this project to build on this foundation by using controlled pressure-based disruption through nitrogen cavitation, preserving phagosomal integrity (Saunders, 2016). This then supports subsequent purification and analysis of *L. donovani* containing phagosomes.

1.7.3 Phagosome proteomics of other pathogens

1.7.3.1 Legionella

Legionella pneumophila is a bacterial pathogen that exists intracellularly for part of its lifecycle, residing transiently in alveolar macrophage-derived phagosomes immediately following infection (Shevchuk et al., 2009). Similarly to *Leishmania*, its ability to subvert phagosome maturation attracts interest and some research has now turned to the isolation of *Legionella*-containing phagosomes for proteomic study (Shevchuk et al., 2009). Using a host model of the amoeba *Dictyostelium discoideum*, which closely mimics the action of a human macrophage, infected with *Legionella spp.*, phagosomes were isolated through cellular fractionation and proteins identified through mass spectrometry (Shevchuk et al., 2009). The use of multiple *Legionella* species, exhibiting variations in virulence, produced interesting findings showing greater abundance of certain proteins in more infective species (Shevchuk et al., 2009). This research offered valuable insight into proteins that aid the pathogenicity of the bacteria and therefore proteins of interest that could be exploited for therapeutic development (Shevchuk et al., 2009). Examples of these proteins are Coronin, which interacts with NADPH oxidase and protein kinase C inhibitors to help the bacteria avoid death by oxidation and the Rho GDP-

dissociation inhibitor which is downregulated in phagosomes where the bacteria shows high replication levels (Shevchuk et al., 2009).

1.7.3.3 *Mycobacterium tuberculosis*

The bacterium *Mycobacterium tuberculosis* resides within membrane-bound phagosomes derived from host macrophages (Russell, 2001). Once again, *M. tuberculosis*, halts the acidification of the phagosome to ensure its survival and because of this, performing proteomics on the bacteria-containing phagosomes is of interest (Chakraborty et al., 1995; Russell, 2001). To date, these studies have used less advanced techniques, using metabolic labelling to identify macrophage proteins, immunoblotting to analyse phagosomal proteins and microscopy to confirm that the isolated phagosomes remained intact (Chakraborty et al., 1995). The cells containing the phagosomes were lysed through a process of nitrogen cavitation, utilising pressure to disturb the cell surrounding the phagosome but not the pathogen-containing phagosome itself (Chakraborty et al., 1995). This proved to be more successful for *M. tuberculosis* phagosomes compared to those containing *L. mexicana* (which was also trialled in this study) due to the larger size of the *L. mexicana* phagosomes (Chakraborty et al., 1995). This suggests that the use of this technique to remove cellular matter surrounding the *Leishmania*-containing phagosomes may be more effective to use in macrophages infected with species that form smaller vacuoles, such as *L. donovani*. Once compared to inert bead-containing phagosomes, the results again provided enhanced understanding of phagosome proteins (Chakraborty et al., 1995).

1.7.3.3 Salmonella

Salmonella enterica serovar Typhimurium (STM) is another intracellular bacterium that, like *Leishmania*, resides within the phagosomes of phagocytic cells following engulfment (Chatterjee et al., 2025). Novel research has now successfully utilised a combination of fluorescent labelling of *Salmonella* and their phagosomes, ultracentrifugation and FACS to isolate *Salmonella*-containing phagosomes from infected macrophages to perform proteomics (Chatterjee et al., 2025). Previous to this, FACS had been used to isolate the bacteria from within its phagosome and analyse phagosomal sub-populations but this was the first time that whole bacteria-containing phagosomes had been successfully collected (Chatterjee et al., 2025). This study revealed new information on how *Salmonella* interacts with its host intracellularly and identification of new *Salmonella* effector proteins such as novel putative proteins that shape the intracellular phagosome niche and secreted lipoproteins that show differences in abundance between the wildtype and mutant species (Chatterjee et al., 2025). The use of inert bead-containing phagosomes allowed as a comparator allowed the differentiation between host and pathogen proteins as well as showing how host proteins

are changed in the presence of *Salmonella* (Chatterjee et al., 2025). Several difficulties arose in the optimisation of this technique, primarily in the centrifugation stage as the bacteria showed to have a similar density to the host mitochondria, making separation of these proteins challenging (Chatterjee et al., 2025). Nonetheless, the successful development of this protocol forms a robust basis from which the isolation of *Leishmania*-containing phagosomes can be based upon.

Chapter 2: Project details

2.1 Project aims

The overarching goal of this project is to use proteomics to analyse the protein contents of *L. donovani* containing phagosomes to better understand how *Leishmania* parasites interact with the host from within the phagosome. To achieve this, work focused on meeting the following aims:

Aim 1 - To create a fluorescent *L. donovani* parasite line to be used to infect bone marrow macrophages for isolation of *Leishmania*-containing phagosomes.

Aim 2 - To optimise a protocol of nitrogen cavitation and fluorescence activated cell sorting to isolate fluorescent parasite-containing phagosomes from infected macrophages.

Aim 3 - To use proteomics to investigate the protein composition of the *L. donovani* phagosome and identify *Leishmania*-specific proteins.

This work has facilitated the optimisation of a protocol that allows greater elucidation of amastigote behaviour within its host, through its proteome, as well as a deeper insight into the proteomic environment of the phagosome. This will enable further discovery of how the phagosome composition is adapted to promote *L. donovani* survival and how *L. donovani* amastigotes modulate their host, offering potential for finding therapeutic targets.

Chapter 3: Methods

3.1 Parasite line selection and infection testing

3.1.1 TdTomato *L. donovani* testing

3.1.1.1 TdTomato *L. donovani* infection studies

Bone marrow macrophages from 10-week-old C57BL/6 (B6) female mice were generated by taking the femurs and tibia from two mice and flushing out the bone marrow with sterile FCS-free DMEM (Gibco). The bone marrow was then centrifuged at 300xg for 6 minutes and resuspended in 5ml DMEM with 10% FCS (Gibco) with a small sample being diluted in Trypan Blue (Gibco) for counting. After counting, cells were resuspended in MΦ Medium (DMEM with 20% FCS (Gibco), 2mM L-glutamine (Gibco), 1% Penicillin-Streptomycin (Sigma-Aldrich), non-essential amino acids (Gibco) and 20ng/ml M-CSF (BioLegend)) at approximately $5x10^5$ cells/ml. Cells were plated out with 10ml on each 9cm petri dish and cultured at 37°c, 5% CO2 for 3 days. On day three, an additional 5ml of MΦ Medium with 40ng/ml M-CSF was added to each plate and incubated for 3 further days. On day six, the medium was replaced with fresh, M-CSF-free MΦ Medium and the cells rested for a further day at 37°c, 5% CO2. The cells were then harvested on day seven by removing the media, replacing it with 3ml cold, calcium- and magnesium-free HBSS (Sigma-Aldrich) and then transferring this to a tube. This was repeated twice more, retaining the HBSS with each wash. The cells were then centrifuged at 300xg for 10 minutes, resuspended in DMEM with 10% FCS and counted with Trypan Blue. Finally, the macrophages were plated out at a concentration of $2.2x10^6$ cells per plate. The following day, the macrophages were harvested from the plates using three washes with cold calcium- and magnesium-free HBSS and counted. They were then added to 3 wells of twelve 16-well chamber slides at a concentration of $5x10^6$ cells/ml in volumes of 100µl per well, ready for infection. This was done in parallel to the experiments detailed in 3.1.3.6.

TdTomato-expressing *Leishmania donovani* LV9 (MHOM/ET/67/HU3) promastigotes (Beattie et al., 2010; Cruz et al., 2024) were grown in HOMEM (Gibco) with 10% FCS, 1% Penicillin-Streptomycin and 25µg/ml G418 (InvivoGen) at 25°c, 5% CO_2 until the third day of the stationary phase of growth. Parasites, suspended in DMEM with 20% FCS, 2mM L-glutamine, 1% Penicillin-Streptomycin and non-essential amino acids, were added in triplicate to the macrophages at an MOI of 20, 30 and 50 and incubated at 37°c, 5% CO_2 for 6 hours. The samples were then washed three times with DMEM containing 20% FCS, 2mM L-glutamine, 1% Penicillin-Streptomycin and non-essential amino acids to remove external parasites. The wells were again washed once in PBS and then fixed in 3% paraformaldehyde (PFA) at room temperature for 10 minutes. Following another PBS wash, the samples were permeabilised with 100% cold MetOH for 10 minutes and then washed in distilled water.

The water was then fully removed and the slides mounted with Fluoroshield™ mounting medium with DAPI (Sigma-Aldrich). The fixation, permeabilization and mounting steps were repeated with further slides that were incubated until reaching 24-, 48- and 72-hours post-infection after the washing steps at 6 hours. The slides were then imaged on a ZEISS AxioObserver, images analysed using FIJI software and data plotted using GraphPad Prism®.

3.1.1.1 Flow cytometry of TdTomato-expressing *L. donovani* parasites

Wildtype and TdTomato-expressing *L. donovani* LV9 promastigotes were grown in HOMEM (Gibco) with 10% FCS and 1% Penicillin-Streptomycin (addition of 25µg/ml G418 to TdTomato line) at 25°c, 5% CO_2 until reaching the log phase of growth. Control samples of unstained wildtype and single-stain TdTomato parasites alongside one LIVE/DEAD™ Fixable Dead Cell Stain (ThermoFisher) stained sample for each parasite line were set up by adding $3x10^5$ cells of the relevant parasites to separate tubes. A further $1.2x10^6$ parasites of each line were then centrifuged at 1200xg for 5 minutes, washed twice in FCS-free HBSS and resuspended in PBS with 0.5% FCS at $3x10^6$ cells/ml. Stained cells from each genotype were divided into 100µl samples; two wildtype and two TdTomato samples were fixed in 1% PFA for 15 minutes at room temperature, leaving two of each unfixed. For the LIVE/DEAD samples, half the cells were heat killed by incubation at 65°c for 15 minutes and added back to the rest of the sample, before washing in PBS, addition of 100µl LIVE/DEAD stain and incubation on ice for 15 minutes. Finally, the parasites were washed twice and resuspended in 200µl of MACS buffer (sterile PBS with 10% 05.mM EDTA and 2% FCS). All samples were then run on the CytoFLEX S flow cytometer and analysed in FCS-express 7 software.

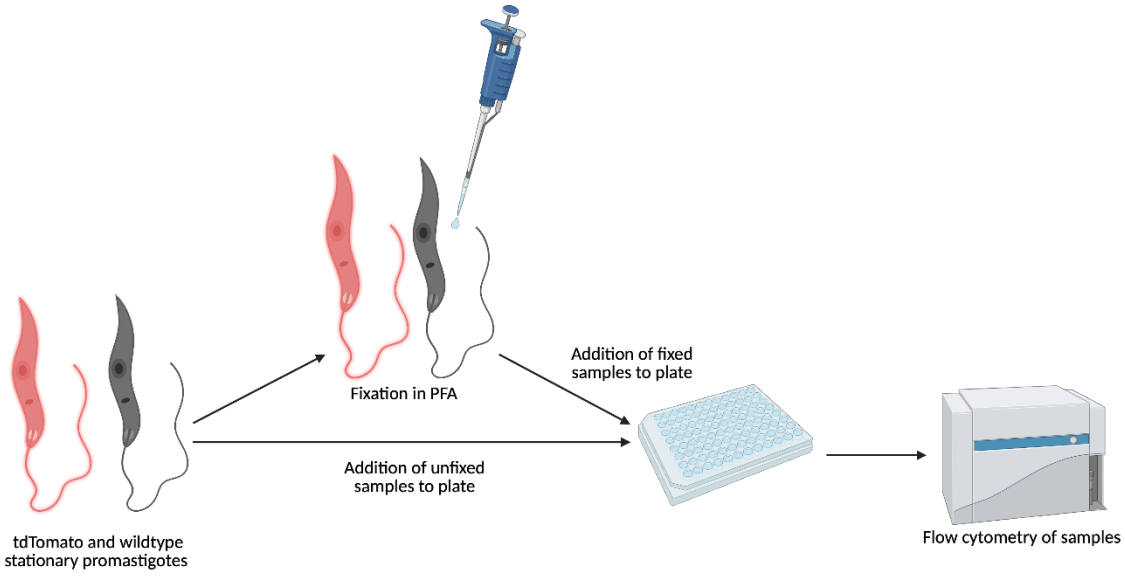

Figure 2: Workflow of methods for flow cytometry testing of fixed and unfixed of *L. donovani* parasites.
Created in BioRender.

3.1.2 CMFDA staining of wildtype *L. donovani*

A 10 mM CellTracker™ Green CMFDA fluorescent dye (Invitrogen) stock solution was prepared by dissolving 50µg of dye in 10µl DMSO (ThermoFisher). Log- and stationary-phase *L. donovani* parasites were harvested and resuspended in FCS-free HOMEM. Parasites were then aliquoted in 100µl volumes each containing 2×10^6 parasites. CMFDA (0.5 µl or 1 µl) was added to test samples, with an unstained tube serving as a control. After 20 minutes at 25°C, 5% CO_2, DAPI was added for 10 minutes, and samples were mounted for live fluorescence microscopy. This was repeated with a 15-minute stain in PBS. To optimize CMFDA staining, parasites were then incubated with CMFDA (1:250 or 1:500 dilutions in HOMEM or PBS) at 25°C or 37°C for 15 or 30 minutes. After staining, parasites were washed three times with DMEM, incubated for 15 minutes at 25°C, and mounted for live fluorescence imaging. Images were then taken using a ZEISS AxioObserver and images analysed using ZEISS Zen image analysis software.

3.1.3 mNeonGreen-expressing *L. donovani* line creation and testing

3.1.3.1 Plasmid construction

Existing backbone and vector plasmids (De Oca et al., 2023; Soysa et al., 2015) were transformed into *E. coli* through overnight incubation at 37°c and DNA extracted using the QIAprep Spin Miniprep Kit (Qiagen). Required sections of this DNA were amplified through PCR using Q5 Hi-Fi polymerase (New England Biolabs). Amplification of the backbone using specially designed primers (pGL2553_fwd - OL15250 and pGL2553_rev- OL15251) (Table 1) used cycling conditions of 5.5 minutes at 98°c, 30 seconds at 72°c, 4 minutes and 5 seconds at 72°c, 10 minutes at 72°c and resting at 4°c until DNA is required. Amplification of the vector using specially designed primers (pGL2666_fwd - OL15252 and pGL2666_rev - OL15253) (Table 1) used cycling conditions of 5.5 minutes at 98°c, 30 seconds at 61°c, 22 seconds at 72°c, 10 minutes at 72°c and resting at 4°c until DNA is required. Gel electrophoresis confirmed the presence of the desired products based on the expected size of the resultant fragments. The resulting DNA fragments were then purified using the QIAquick PCR Purification Kit (Qiagen) and concentrations quantified at 52.1ng/µl of vector and 129ng/µl of insert DNA. Gibson assembly of these fragments was then performed using the NEBuilder® HiFi DNA Assembly Cloning Kit (New England Biolabs) at a 2:1 vector to insert DNA mass ratio (325ng of vector DNA and 57.9ng of insert DNA) based on fragment length. The new complete plasmid was then transformed into *E. coli* through overnight incubation at 37°c. Under aseptic conditions, 100µl of this bacterial broth was spread onto an ampicillin (InvivoGen) agar plate to allow colonies to grow at 37°c overnight. Ten individual colonies were then selected from the plate using a pipette tip to undergo a colony PCR using the PCRBIO HS Taq Mix Red protocol (PCR Biosystems) (primers pGL3093_fwd – OL15256 and pGL3093_rev – OL15257 shown in

table 1). Gel electrophoresis confirmed the presence of the expected plasmid section in three of the ten colonies, which were then grown overnight at 37°c and the DNA extracted.

Name of primer	**Primer sequnce (5' to 3')**
pGL2553_fwd - OL15250	ATTGTATAAGTGAGGCCGGGCTGGCCAG
pGL2553_rev- OL15251	CTTTCGAGACCATGGCCCAGGTGGCCTC
pGL2666_fwd - OL15252	CTGGGCCATGGTCTCGAAAGGTGAGGAAG
pGL2666_rev - OL15253	CCCGGCCTCACTTATACAATTCGTCCATCCC
pGL3093_fwd – OL15256	TAAAGGCACAGGCTTCCCAG
pGL3093_rev – OL15257	TTCCGTGTTTTCACGTCGGA

Table 1: Primers for PCR reactions for amplification of insert and backbone DNA sections and colony PCR.

3.1.3.2 Transfection of plasmid

Early passage wildtype *Leishmania donovani* LV9 promastigotes in complete HOMEM (with 10% FCS and 1% Penicillin-Streptomycin) and complete Schneider's insect media (Sigma-Aldrich) (with 10% FCS, 0.1% 2.5mg/ml Hemin (Sigma-Aldrich) in NaOH (Fisher Scientific), 0.1% 10mM 6-Biopterin (Sigma-Aldrich) and 1% Penicillin-streptomycin) were passaged to $1x10^5$ cells/ml and allowed to grow at 25°c, 5% CO_2until in the log phase of growth (3-$6x10^6$ cells/ml).

For plasmid linearisation, 10µg of newly constructed pGL3093 per transfection was digested using the NotI-HF enzyme (New England Biolabs). A double digest using both the NotI-HF and XhoI (New England Biolabs) enzymes was also set up with a 1µg sample of the plasmid DNA as a positive control. Both digests were incubated overnight at 37°c. Gel electrophoresis of all samples confirmed the successful linearisation of the plasmid and the single digested DNA was then purified using ethanol precipitation. Clonal mNeonGreen-expressing *L. donovani* LV9 were obtained by transfection of pGL3093 plasmid into log-phase wildtype promastigotes via electroporation in the 4D-Nucleofector® X Unit (Lonza) using the Cell Line Nucleofector Kit V (Lonza). Parasites were then recovered in their respective media for the appropriate time (Schneider's 8 hours; HOMEM 20 hours) with an additional 10% FCS before addition of with 25µg/ml G418 and plating out at several dilutions; 1:6, 1:66, 1:726, 1:7986. The transfection, electroporation and plating steps were repeated, using an equal volume of water in place of DNA, for control samples. Clonal populations were allowed to grow at 25°c, 5% CO_2 for 14 days in 96-well plates, before the transfer of selected clones into 3ml cultures of respective media with 10% FCS and 25µg/ml G418 in 12-well plates, and further passage into 5ml cultures 5 days later. Green

fluorescence of the line was confirmed by visualisation of parasites under the EVOS M5000 Cell Imaging system (Invitrogen).

3.1.3.3 EC50 determination of G418 drug in Schneider's media

Complete Schneider's insect media was treated with varying concentrations of G418 ranging from 200µg/ml-25µg/ml. The treated media was plated out with 50µl being added to each well of a 96-well plate, with each concentration in octuplicate. Wildtype *L. donovani* parasites grown in complete Schneider's at 25°c were counted and passaged to a density of $5x10^3$ cells/ml in complete HOMEM before 50µl of parasites was added to each well, creating final drug concentrations of 100µg/ml-12.5µg/ml. Control wells with equal volumes of parasite culture and untreated media as well as with only untreated culture were included on each plate. This was repeated a further two times to create three final plates to be assessed at 5-, 7- and 10-day time points. At each time point, 20µl of 0.49mM Alamar blue solution (Sigma-Aldrich) was added to each well and then the plate incubated at 25°c, 5% CO_2 for 6 hours. The levels of Alamar blue remaining in each well was then detected using a BMG LABTECH CLARIOstar® microplate reader at a wavelength of 590nm and the average for each concentration calculated.

3.1.3.4 Clone selection via microscopy

mNeonGreen-expressing *L. donovani* LV9 parasites were grown in complete HOMEM with 25µg/ml G418 or complete Schneider's insect media (at 25°c, 5% CO_2, post-transfection until reaching the log phase of growth. Per culture, $3x10^6$ parasites were centrifuged at 1200xg for 5 minutes, washed in FCS-free HBSS twice, and finally resuspended in PBS. The cells were then fixed by incubation in an equal volume of 2% PFA at room temperature for 15 minutes, washed in PBS and incubated with DAPI at 1µg/ml at room temperature for 5 minutes. After a further wash and resuspension in PBS, the sample was added to a slide for imaging. The slides were then imaged on a ZEISS AxioObserver, images analysed using ZEISS Zen software and relative fluorescence unit (RFU) data plotted using GraphPad Prism®.

3.1.3.5 mNeonGreen-expressing *L. donovani* growth curve

Log-phase mNeonGreen-expressing *L. donovani* LV9 parasites, originating from three different clonal populations, were inoculated in 10ml complete HOMEM or 10ml complete Schneider's insect media with 25µg/ml G418 at a density of $1x10^5$ parasites per ml. Cultures were grown at 25°c, 5% CO_2 for 10 days. Each day, a sample of each flask was immobilised using 2% PFA in PBS and counted. Parasite density was calculated for each day plotted onto a log growth curve using Microsoft Excel.

3.1.3.6 mNeonGreen-expressing *L. donovani* infection testing

Bone marrow macrophages were generated from a 10-week-old female C57BL/6 (B6) mouse as detailed above in section 3.1.1.1 and added to 6 wells of twelve 16-well chamber slide at a density of $5x10^6$ cells/ml. This was done in parallel to the experiments detailed in 3.1.1.1. Wildtype and mNeonGreen-expressing *L. donovani* LV9 promastigotes were grown in complete HOMEM (addition of 25µg/ml G418 to mNeonGreen line) at 25°c, 5% CO_2, until the third day of stationary phase. Parasites, suspended in DMEM with 10% FCS, 2mM L-glutamine, 1% Penicillin-Streptomycin and non-essential amino acids, were added in triplicate to the macrophages at an MOI of 10, 20 and 50, leaving two wells of uninfected macrophages on each slide, and incubated at 37°c for 6 hours. The samples were then washed with three washes of DMEM with 10% FCS, 2mM L-glutamine, 1% Penicillin-Streptomycin, non-essential amino acids to remove external parasites. The wells were again washed in one wash of PBS and then fixed in 3% PFA at room temperature for 10 minutes. Following another PBS wash, the samples were permeabilised with 100% cold MetOH for 10 minutes and then washed in distilled water. The water was then fully removed and the slides mounted with Fluoroshield™ mounting medium with DAPI. After the washing steps at 6 hours, the fixation, permeabilization and mounting steps were repeated with further slides that were incubated until reaching 24-, 48- and 72-hours post-infection. The slides were then imaged on a ZEISS AxioObserver, images analysed using FIJI software and RFU data plotted using GraphPad Prism®.

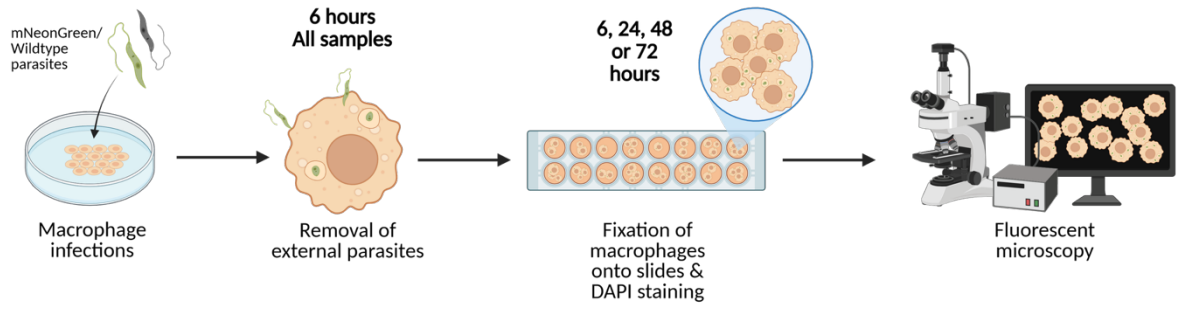

Figure 3: Workflow of methods for bone marrow macrophage infections with mNeonGreen *L. donovani* parasites.
Created in BioRender.

3.2 CellVue Burgundy membrane dye testing

3.2.1 CellVue Burgundy staining of macrophages for flow cytometry

Bone marrow macrophages were generated from a female C57BL/6 (B6) mouse as detailed above in section 3.1.1.1. Instead of addition to chamber slides, the macrophages were plated out into 9cm petri dishes at a concentration of $1.5x10^6$ cells per plate.

Macrophages were harvested from the plates using three washes with cold calcium- and magnesium-free HBSS and counted. The cells were washed with more HBSS and $6x10^5$ cells removed for single stain and unstained samples, before a final resuspension containing $1.5x10^6$ macrophages in Diluent C from the CellVue™ Burgundy Cell Labelling Kit (ThermoFisher) at a density of $2x10^7$ cells/ml. To create a final labelling concentration of 2µM, an equal volume of 4µM CellVue Burgundy dye in Diluent C was then added to the macrophage suspension and incubated at room temperature for 5 minutes, mixing with a pipette periodically. An equal volume of serum was then added to the sample and allowed to sit for a minute to stop the labelling. The samples were then centrifuged at 200xg for 5 minutes and washed in three washes of MACS buffer (sterile PBS with 10% 05.mM EDTA and 2% FCS), with one sample being added to a 96-well plate at this stage to serve as a CellVue™ Burgundy single stain sample. A live/dead stain was then added to all four CellVue™ Burgundy stained samples and incubated at room temperature for 15 minutes. For one unstained sample, half the cells were heat killed by incubation at 65°ᶜ for 15 minutes and added back to the rest of the sample, before washing in PBS, addition of 100µl live-dead stain and incubation on ice for 15 minutes. All samples were then centrifuged at 400xg for 5 minutes and washed in 3 washes of MACS buffer and made up to a final volume of 100µl per 96-well plate well. Finally, the samples were then added to the plate and another 100µl of MACS buffer added to each well. The samples were then run through the CytoFLEX LX375 flow cytometer and the results analysed using FCS express 7 software.

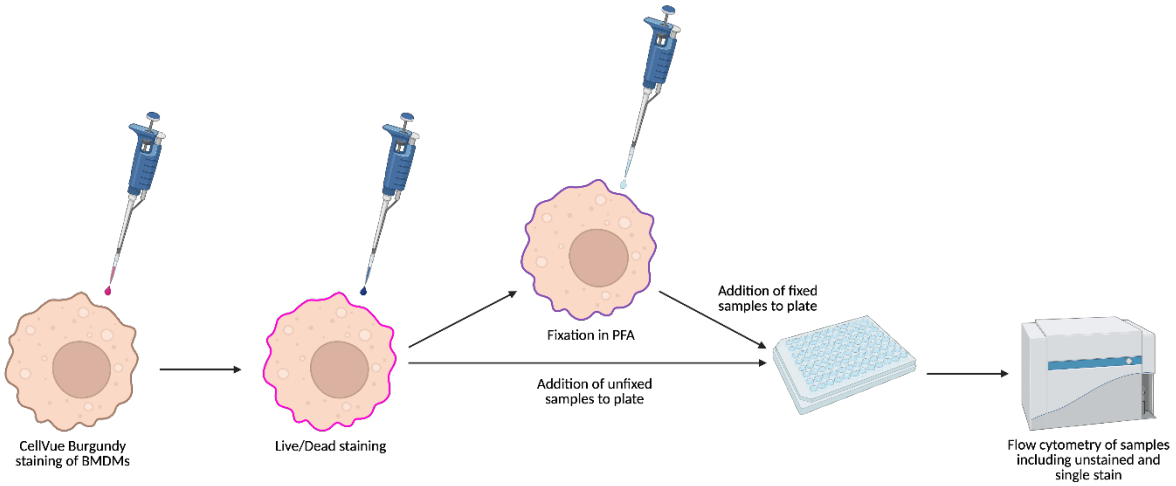

Figure 4: Workflow of methods for CellVue Burgundy staining of bone marrow macrophages. Created in BioRender.

3.2.2 CellVue Burgundy staining of *L. donovani* promastigotes

Wildtype *L. donovani* LV9 were grown in complete HOMEM or complete Schneider's insect media at 25°ᶜ, 5% CO_2, until either log phase or third-day stationary phase. Per sample, $3x10^6$ parasites were centrifuged at 1200xg for 5 minutes, washed in FCS-free HBSS twice, and finally resuspended in Diluent

C from the CellVue™ Burgundy Cell Labelling Kit at $4x10^7$ cells/ml. The parasites were then dyed using the CellVue™ Burgundy Cell Labelling Kit as detailed in section 3.2.1, centrifuged at 1200xg for 5 minutes, resuspended in PBS and incubated with DAPI at 1µg/ml at room temperature for 5 minutes. After two washes in PBS, the cells were then fixed by incubation in PFA at room temperature for 15 minutes, washed in PBS and resuspended in PBS and finally added to a microscope slide for imaging. The slides were then imaged on a ZEISS AxioObserver, images analysed using ZEISS Zen software and RFU data plotted using GraphPad Prism®.

3.3 Parasite-containing phagosome isolation

3.3.1 Isolation of *L. mexicana*-containing phagosomes

Bone marrow macrophages from 10-week-old C57BL/6 (B6) female mice were thawed following preparation as detailed in section 3.1.1.1. Macrophages were plated out at a density of $1x10^5$ cells per 9cm petri dish. Wildtype *Leishmania mexicana* parasites were thawed and cultured in complete HOMEM at 25°c, 5% CO_2, until reaching the third day of the stationary growth phase. A subset of parasites was stained with CMFDA dye. For staining, parasites were centrifuged at 1200xg for 5 minutes, washed twice with PBS, and resuspended in 50µl HOMEM. This suspension was mixed with an equal volume of CMFDA dye diluted to 1:125 in HOMEM, and parasites were incubated at 25°c for 15 minutes. The stained parasites were then centrifuged at 1200xg for 5 minutes with an additional 50 µl of DMEM containing 10% FCS. The supernatant was then discarded, and the pellet resuspended in 100µl DMEM supplemented with 10% FCS.

Macrophages were infected with either CMFDA-stained or unstained wild-type *L. mexicana* at an MOI of 10 and incubated at 37°c, 5% CO_2, for 24 hours. After this initial incubation, extracellular parasites were removed by three washes with DMEM containing 10% FCS, and cultures were incubated for a further 24 hours. At 48 hours post-infection, macrophages were washed twice with sucrose buffer (250 mM sucrose, 10 mM HEPES (Gibco), pH 7.4, 2 mM EDTA, pH 8 and complete EDTA Free Protease Inhibitor Cocktail), then incubated on ice for 15 minutes in the same buffer to release adherent cells. Cells were subsequently lysed by nitrogen cavitation at 200psi for 20 minutes. The lysates were supplemented with Halt™ EDTA-free protease inhibitor cocktail (100X) (ThermoFisher) and an additional 3 ml fresh sucrose buffer. Samples were then centrifuged at 200xg for 5 minutes, followed by membrane and DNA staining with CellVue™ Burgundy Cell Labeling Kit as detailed in section 3.2.1 and 1 µg/ml DAPI, respectively. Stained samples were mounted onto glass slides and imaged using a ZEISS AxioObserver microscope. Image analysis was performed with FIJI and ZEISS Zen software.

3.3.2 Isolation of *L. donovani*-containing phagosomes

Bone marrow macrophages were generated from 11 week old female C57BL/6 (B6) mice as detailed above in section 3.1.1.1. The macrophages were plated out at a density of $5x10^6$ cells per 9cm petri dish, with a total of 12 plates. Wildtype and TdTomato-expressing *Leishmania donovani* LV9 parasites were defrosted and cultured in complete HOMEM (addition of 25µg/ml G418 to TdTomato line) at 25°c, 5% CO_2, until reaching the third day of the stationary growth phase. Macrophages were infected with either wildtype *L. donovani* at an MOI of 10 (1 plate) or TdTomato-expressing *L. donovani* at an MOI of 20 (11 plates) in DMEM supplemented with FCS and incubated at 37°c for 6 hours. Following this incubation, extracellular parasites were removed by three washes with DMEM containing 10% FCS, after which the cultures were incubated for a further 18 hours. At 24 hours post-infection, macrophages were washed twice with sucrose buffer (250 mM sucrose, 10 mM HEPES, pH 7.4, 2 mM EDTA, pH 8 and complete EDTA Free Protease Inhibitor Cocktail), then incubated on ice for 15 minutes in the same buffer to release adherent cells. Cells were subsequently lysed by nitrogen cavitation at 200 psi for 20 minutes. The lysates were supplemented with Halt™ EDTA-free protease inhibitor cocktail (100X) and an additional 3 ml of fresh sucrose buffer. Samples were then centrifuged at 200xg for 5 minutes and resuspended in 100µl fresh sucrose buffer. This was performed in parallel across five biological replicates of TdTomato-infected macrophages, one TdTomato-infected control, and one wildtype–infected control. Control samples were used as single-stain and unstained controls for calibration of the flow cytometer. The wildtype control was divided into two 50 µl aliquots: one left unstained, while the other was stained using the CellVue™ Burgundy Cell Labelling Kit, together with all five TdTomato test replicates. All samples were then centrifuged at 200xg for 8 minutes, resuspended in PBS containing 1 mM EDTA, and fixed by incubation at room temperature with an equal volume of 2% PFA, giving final concentration of 1% PFA. PBS containing 1mM EDTA was then added to each sample for a final volume of 500µl.

The samples were then sorted by flow cytometry using the BD FACSDiscover™ S8 Cell Sorter, collecting double positives (TdTomato+ and CellVue Burgundy+, referred to as $TdT^{+}CVB^{+hi}$). In the CellVue Burgundy channel the excitation was set to 683nm and emission to 707nm. In the TdTomato channel, the excitation was set to 554nm and the emission to 581nm. The gating strategy involved identification of phagosomes based on high intensity signals in both channels, measured against the signals from the single stain and unstained controls. Analysis of the flow plots was performed using FCS express 7 software. A sample of the $TdT^{+}CVB^{+hi}$ sorted group was then mounted onto glass slides and imaged using a ZEISS AxioObserver microscope. Image analysis was performed with FIJI and ZEISS Zen software.

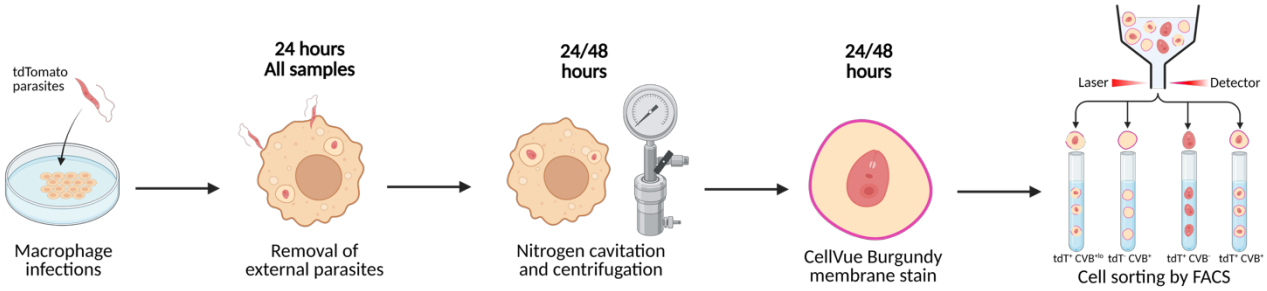

Figure 5: Workflow of methods for isolation of *L. donovani*-containing phagosomes
Created in BioRender.

3.4 Latex bead infection studies

Bone marrow macrophages were prepared as outlined in section 3.1.1.1 from 10 week old female C57BL/6 (B6) mice were thawed. The cells were added to chamber slides at a density of $5x10^4$ cells per well and onto 12mm round coverslips at a density of $1x10^5$ cells per coverslip.

Fluoresbrite® YO carboxylate microspheres (4.50 µm diameter; Polysciences) were sonicated for 1 minute and resuspended in DMEM supplemented with 10% FCS at concentrations of $5x10^6$ beads/ml (for bead to cell ratio of 10) or $2.5x10^6$ beads/ml (for bead to cell ratio of 5). The bead suspension was vortexed before addition to macrophages, with 100µl added to each chamber well and 200µl added to each coverslip. Cells were incubated with beads at 37°c for 6 hours, after which extracellular beads were removed by washing with DMEM containing 10% FCS. Cells were then maintained at 37°c until 24 hours post-bead addition, depending on the experimental time point. Following incubation, samples were washed twice with sterile PBS, fixed with 2% PFA, and permeabilised with 0.1% Triton X-100 (ThermoFisher). Macrophage nuclei were stained using 1 µg/ml DAPI incubated for 15 minutes at room temperature. Finally, samples were mounted with ProLong™ Diamond Antifade Mountant (Invitrogen) and cured overnight. Imaging was conducted using a ZEISS AxioObserver microscope, and image analysis was performed with FIJI and ZEISS Zen software.

Chapter 4: Results

4.1 Parasite line selection and infection testing

4.1.1 TdTomato *L. donovani* testing

4.1.1.1 Initial infection testing

For parasites to be visible by microscopy and detectable in fluorescence activated cell sorting (FACS), they must either be stained with fluorescent dyes or fluorescence genes introduced. This is particularly important for the isolation of infected phagosomes in this project as the fluorescence the parasites produce will allow these phagosomes to be distinguishable within the sample. TdTomato is a tandem dimer red fluorescence protein that allows detection of *L. donovani* parasites (Morris et al., 2010). To assess differences in infectivity between TdTomato-expressing and wildtype promastigote-stage *L. donovani*, bone marrow derived macrophages (BMDM) were infected with both parasite lines at multiplicities of infection (MOIs) of 5 or 10, at day 3 stationary phase, and infections analysed at 3, 24 and 72 hours by the counting of parasites from microscopy images (Figure 6). TdTomato-expressing parasites showed a significantly lower number of parasites per 100 macrophages after 24 and 72 hours compared to the wildtype at both MOIs, suggesting that the genetic modification and expression of the TdTomato gene reduces the virulence of this line. This lowered infection rate would also lead to a decrease yield of phagosomes, which may hinder later stages of the experiment and was an important consideration on whether to use this line within this project. Based on these results, an MOI of 20 could offer TdTomato infection rates more similar to macrophages infected with wildtype parasites at an MOI of 10, due to the number of parasites per 100 macrophages being approximately half that of the wildtype at the 24 hour time point.

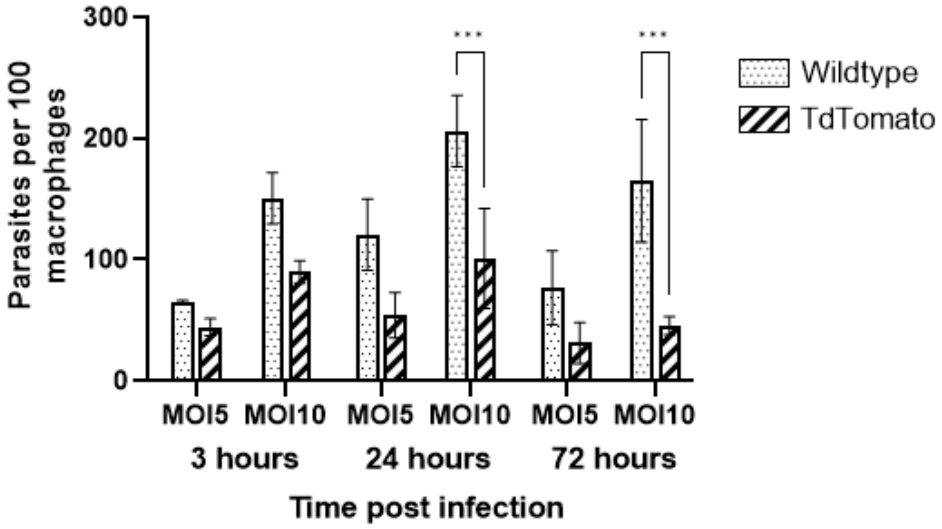

Figure 6: TdTomato expressing *L. donovani* parasites display decreased infectivity.
Wildtype and TdTomato expressing *L. donovani* promastigotes at day 3 stationary phase were used to infect mouse bone marrow derived macrophages at either an MOI of 5 or 10 (n=3). Macrophages were incubated with parasites for the relevant time with external parasites being removed at 24 hours for the two later time points. Fluorescence microscopy images were used to assess infectivity of both parasite lines. Macrophage and parasite numbers were counted using FIJI and number of parasites per 100 macrophages was calculated. All significance values calculated in GraphPad Prism using a two-way ANOVA, * = $p<0.05$, ** = $p<0.005$, *** = $p<0.005$, **** - $p<0.0001$, N=2.

4.1.1.2 Optimisation of infection

Due to the reduced virulence of the parasite line, yielding a sufficient number of phagosomes required infecting macrophages at a higher MOI than is typically used for wildtype parasites. As a consequence, after leaving parasites to be internalised for 24-hours (as in section 4.1.1.1), many parasites were only partially internalised. This allowed the development of parasites with partial, immature phagosome membranes around them, which could've led to issues during later phagosome isolation experiments. As well as this, the increased parasite load requires more washing steps to remove extracellular parasites, which increases the risk of removing macrophages from the plate.

To establish how these issues could be eliminated, bone marrow macrophages were infected with third day stationary TdTomato parasites at an MOI of 20, 30 or 50 and external parasites washed off after 6 hours rather than 24. After washing, further samples were incubated until 24, 48 and 72 hours post-infection, allowing full internalisation of any parasites that are in early stages of being phagocytosed. From these results we observed no significant difference between the percentage of macrophages infected at MOIs of 20 versus 30 at any time point (Figure 7A). This indicated that an MOI of 30 would not be used for further infections as it offers no significant benefit to the infection rates compared to an MOI of 20, which requires less washing steps following infection and therefore lowers the risk of

losing macrophages. At all time points MOIs of 20 and 50 showed a significant difference in the number of parasites per infected macrophage (Figure 7B). At the critical 24-hour timepoint, an MOI of 20 showed an average of 5 parasites (and therefore individual *L. donovani* phagosomes) per infected macrophage, compared to an average 6.8 phagosome per macrophage with an MOI of 50 (Figure 7B), although the level of significance in the difference was decreased at this timepoint compared to others. These results indicated a potential greater phagosome yield with infections performed using an MOI of 50. Interestingly, when looking more broadly at the number of parasites per 100 macrophages, there was no significant difference between MOIs at any time point, suggesting that when using an MOI of 50, the infection rates are less consistent compared to an MOI of 20, further supported by the greater standard deviation those infections showed (Figure 7C).

Based on these results and those shown in section 4.1.1.1, we decided that in all future experiments, macrophages would be infected with TdTomato *L. donovani* at an MOI of 20 as it struck the best balance between infection rates, phagosome yields and limiting washing steps to remove external parasites. We would also continue to wash at the earlier 6-hour timepoint to reduce the number of parasites that are only partially internalised and therefore likelihood of these parasites being sorted into the phagosome sample.

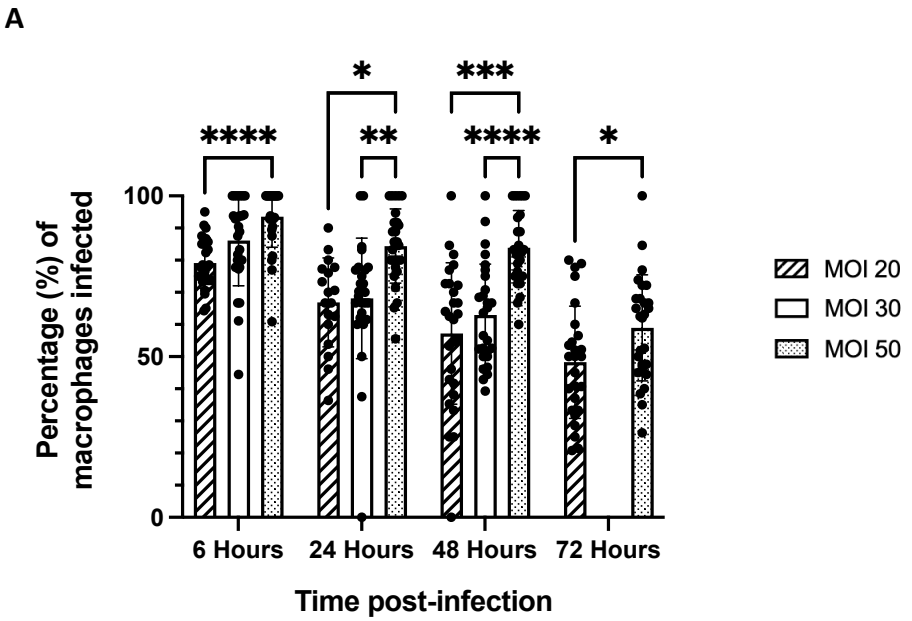

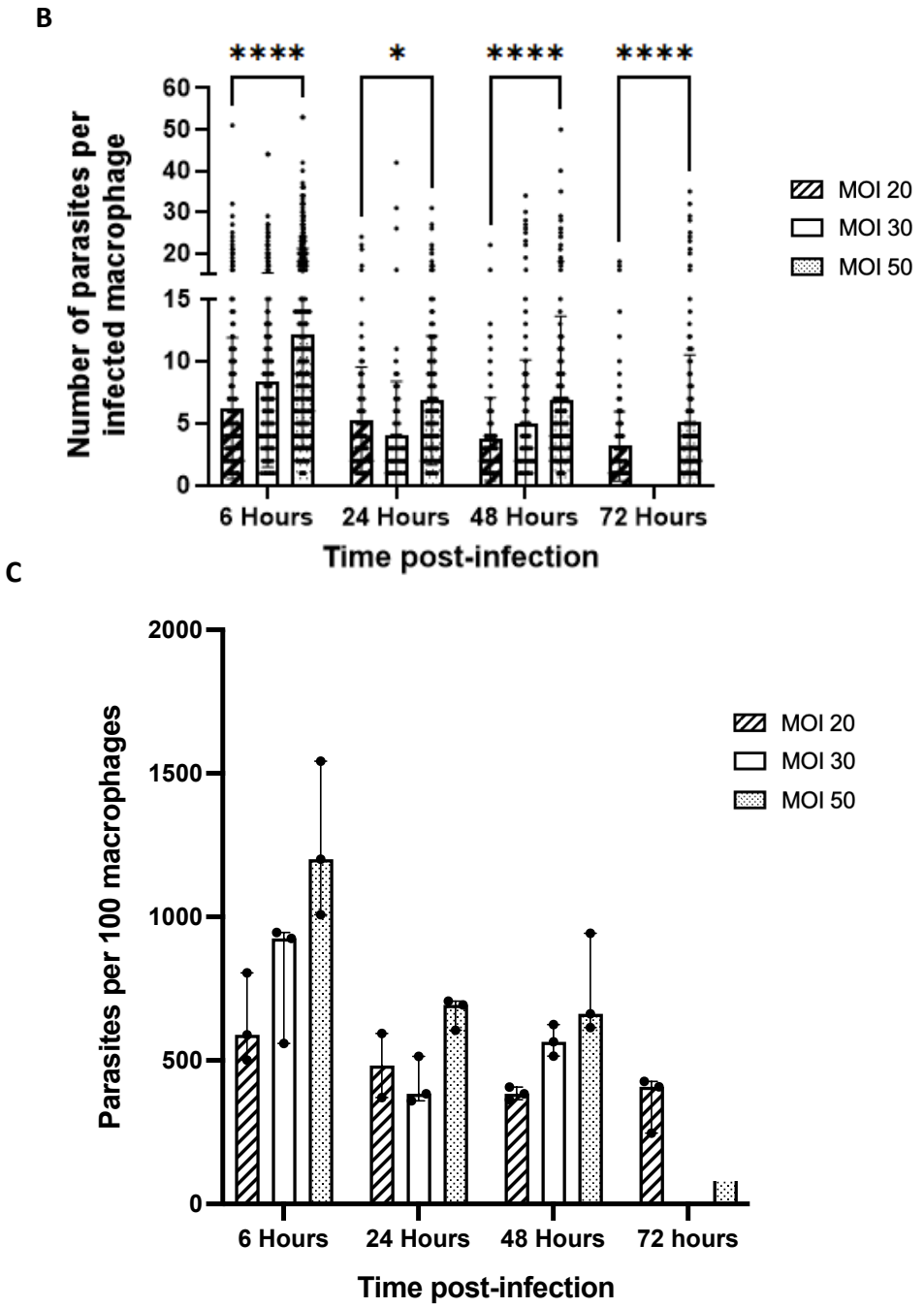

Figure 7: TdTomato parasite infection of macrophages are significantly increased using a higher MOI. TdTomato expressing *L. donovani* promastigotes were used at day 3 stationary phase to infect mouse bone marrow derived macrophages at either an MOI of 20, 30 or 50. Macrophages were incubated with parasites for the relevant time with external parasites being removed at 6 hours for all time points. Fluorescence microscopy images captured at a x63 magnification using a ZEISS AxioObserver were used to assess infectivity of both parasite lines. Macrophage and parasite numbers were counted using FIJI. **A** Both infected and non-infected macrophages were counted in each image to give the percentage of macrophages that were infected. **B** For each infected macrophage, the number of parasites within it were counted as an indication of the number of phagosomes present. **C** An average of parasites per 100 macrophages was calculated for each chamber slide well using the total number of parasites engulfed per image. All significance values calculated in GraphPad Prism using a two-way ANOVA, * = $p<0.05$, ** = $p<0.005$, *** = $p<0.005$, **** - $p<0.0001$, N=1.

4.1.1.3 Flow cytometry testing of TdTomato-expressing *L. donovani*

It was important to check that the TdTomato-expressing parasites were detectable by flow cytometry, again to ensure effective sorting of phagosomes in later experiments. To do this, TdTomato and wildtype parasites were run on the flow cytometer, both live and fixed. Samples were stained with live-dead stain to allow exclusion of signals from heat-shocked cells (Figure 8). A distinct fluorescence intensity was detected in the TdTomato (Y675) channel, which distinct from the intensity of the wildtype (Figure 8). The results demonstrated that TdTomato parasites produce a sufficiently strong signal for detection by flow cytometry and the rightward shift in fluorescence intensity relative to the wildtype confirms successful TdTomato expression. In addition, there were no observable differences in the signal intensities between the fixed and unfixed sample, confirming that the fixation process does not interfere with the reading of the TdTomato protein expression and that the phagosomes can be fixed without impeding the sorting of the sample.

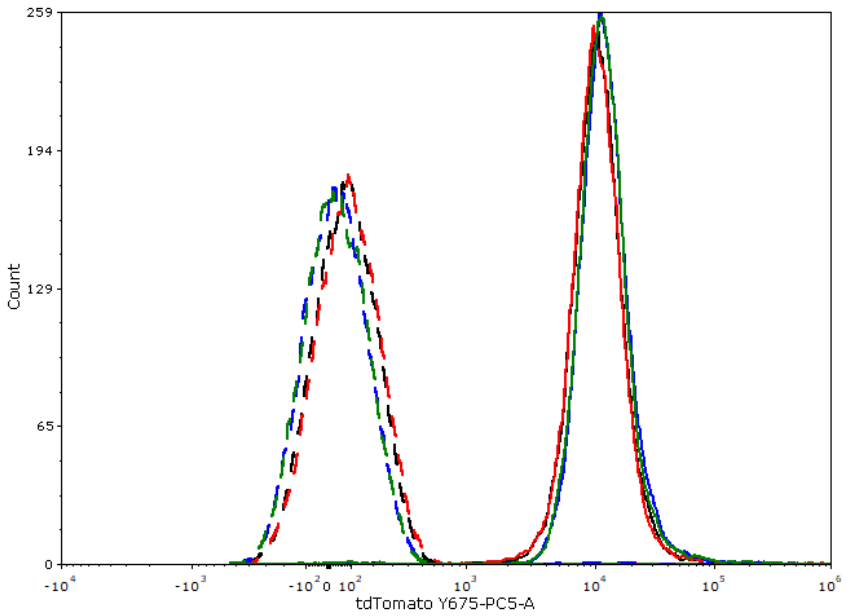

Figure 8: Fixation of parasites does not disrupt detection of TdTomato by flow cytometry.
Wildtype (dotted lines) and TdTomato (solid lines) promastigotes were added to a 96-well plate, with half the parasites fixed (shown in black and red) and half left unfixed (shown in blue and green). Data analysed in FCS-express 7 software. N=1.

4.1.2 5-Chloromethylfluorescein diacetate (CMFDA) stained wildtype *L. donovani*

CMFDA staining was then evaluated as an alternative to fluorescent protein, as it should not interfere with parasite infectivity. CMFDA is a membrane-permeable, non-fluorescent marker that becomes fluorescent upon cleavage by esterases in the cytosol, making it suitable for visualising live parasites in cells (Dagley et al., 2015). Previous studies have demonstrated its use in microscopy of *Trypanosoma*

cruzi and macrophage infection studies of *Leishmania mexicana* suggesting its suitability for this project (Dagley et al., 2015; Sarkar et al., 2009).

After a 30-minute stain at 1:250 or 1:500 dilution, both stationary and log phase promastigotes exhibited green fluorescence, confirming successful staining at both concentrations, with control unstained promastigote showing no autofluorescence (data not shown). This suggested that CMFDA staining could be a viable method for generating fluorescent *L. donovani*. A further experiment trialling a 15-minute stain in PBS, however, did not result in fluorescence (data not shown), indicating that the longer stain in HOMEM yielded better results. Further optimisation of the protocol was then carried out to achieve the best staining for future experiments. A series of stains were conducted with varying CMFDA concentrations, incubation times, temperatures, staining media, and an additional 15-minute incubation after CMFDA removal based on previous studies into optimal conditions for CMFDA staining (Figure 9) (Körner et al., 2006; Sarkar et al., 2009). All samples showed fluorescence in the CMFDA channel and unstained control samples produced no fluorescence. Overall, the differences between test groups were minimal; however, staining in HOMEM at 25°C for 30 minutes with a 1:250 CMFDA dilution produced the most consistently clear staining and therefore this method was selected for future staining.

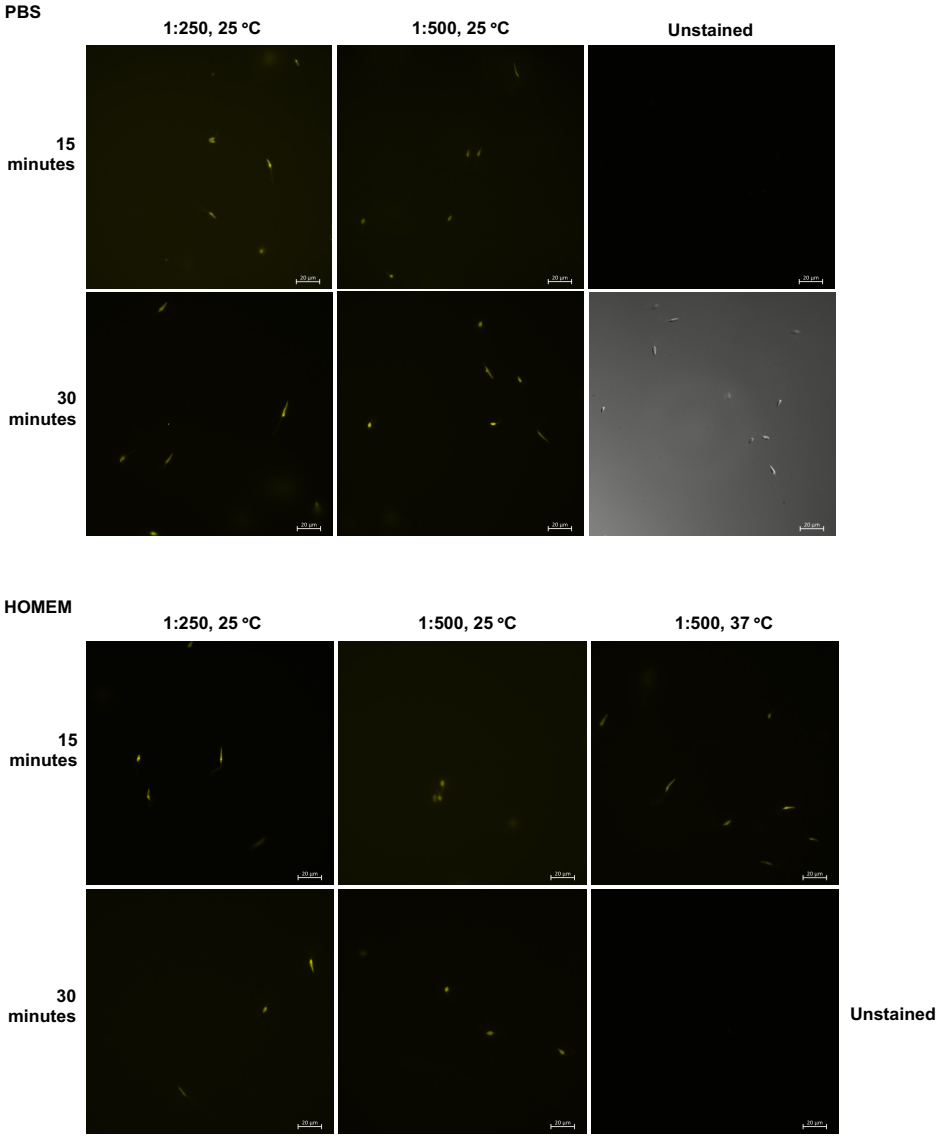

Figure 9: Optimisation of CMFDA staining produces brighter fluorescence
Third day stationary phase *L. donovani* parasites were stained in PBS or HOMEM media for 15 or 30 minutes with a CMFDA solution at 1:250 or 1:500 dilution, incubating at 25 or 37°C. Live fluorescence microscopy images were taken at a x63 magnification using a ZEISS AxioObserver and then analysed in FIJI. Scale bar representative of 20µm. N=2. Figure shows representative images from N=2 experiments.

4.1.3 Creation of mNeonGreen-expressing *L. donovani*

4.1.3.1 Plasmid design

As an alternative to the TdTomato-expressing parasite line, we also investigated whether mNeonGreen-expressing parasites could be a viable alternative and so created a new mNeonGreen (mNG)-expressing *L. donovani* line. mNeonGreen is a green fluorescent monomeric protein that can appear up to three times brighter than conventional GFP, making it a popular choice for *in vivo* tagging, including within *Leishmania* research (Hostettler et al., 2017; Paterou et al., 2025; Steiert et al., 2018). As we found that TdTomato-expressing parasites have a reduced virulence when infecting bone

marrow macrophages, this new line offered an alternative that is still compatible with the CellVue Burgundy membrane stain but with infectivity closer to the wildtype (discussed in section 4.1.3.5) to allow a greater yield of phagosomes for proteomic analysis.

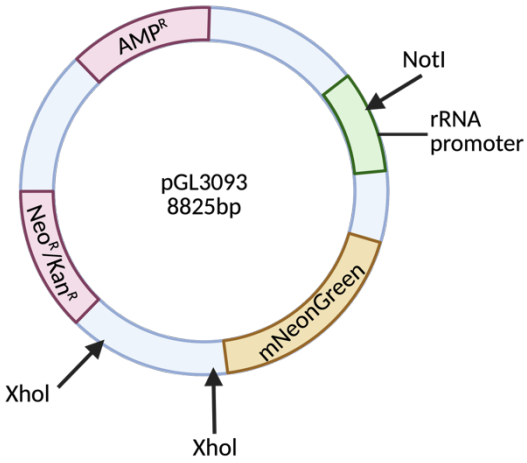

Figure 10: Map of new mNeonGreen plasmid
Map of new plasmid construct after Gibson Assembly of required DNA segments from backbone and insert plasmids. The construct contains the mNeonGreen gene to allow expression of the green fluorescent protein to create parasites that can be detected within phagosomes. The rRNA promoter region allows integration into the parasite genome and the NEO cassette confers Neomycin resistance. The Ampicillin resistance cassette allows selection of bacteria containing the desired DNA when propagating more plasmid. The plasmid is linearised at the NotI restriction site before transfection. Created in BioRender.

The plasmid design allowed for targeted integration of the DNA into the ribosomal locus of the parasite to offer a stable and uniform expression of the fluorescent protein (Figure 10) (Soysa et al., 2015). The plasmid contains homology regions that allow for integration into the parasite genome through homologous recombination; a sequence that encodes the *L. donovani* rRNA promoter to provide a target sequence for integration and allow for RNA polymerase binding, and a region encoding the 28S rRNA gene to act as a terminator (Soysa et al., 2015). The plasmid can then be linearised at the NotI restriction site, situated between the two rRNA components. The plasmid also contains a Neomycin resistance cassette which confers resistance to the parasites once they have taken up this DNA, allowing for selection of clones after transfection. The regulatory elements present within untranslated regions (UTRs) are key for efficient splicing of pre-mRNAs and therefore in controlling overall protein expression levels, so the presence of the *L. major* α-tubulin gene (LmTub) 3'-UTR in the construct ensures the production of stable RNAs during this process (Soysa et al., 2015). Lastly, the *Leishmania* genome shows disparity in the use of synonymous codons and shows certain 'preferred' codons for some amino acids as well as a higher content of G and C nucleotides (Subramanian and Sarkar, 2015).

This plasmid is codon optimised for *Leishmania*, meaning that the DNA sequence encodes for amino acids using the 'preferred' codons (Soysa et al., 2015; Subramanian and Sarkar, 2015). The new plasmid (pGL3093) was constructed by replacing the luciferase gene in an existing 'backbone' plasmid (pGL2553) with the mNG gene from another 'insert' plasmid (pGL2666) through Gibson Assembly (Figure 11). The 'backbone' plasmid has been previously used to produce red shifted luciferase-expressing *L. donovani*, suggesting its suitability to form part of our new plasmid (De Oca et al., 2023). The full plasmid sequence is detailed in section 7.1 of the appendix. Primers (Table 1) were designed using existing plasmid maps so that only the required sections of DNA from the backbone and vector plasmids were amplified during PCR (Figure 11).

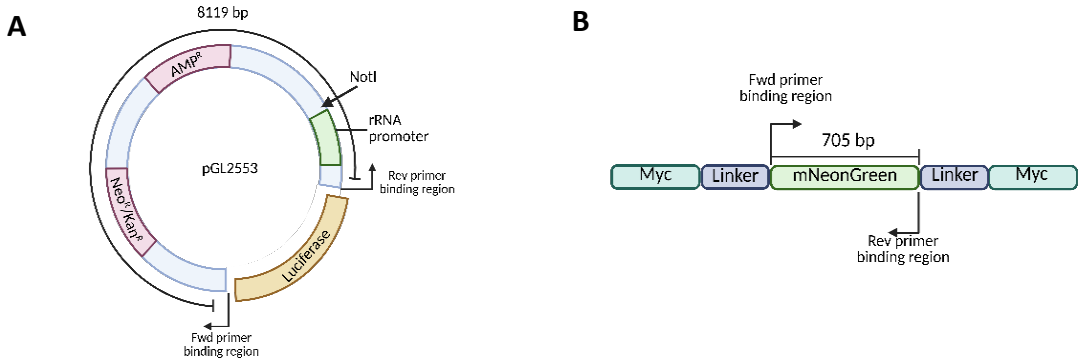

Figure 11: Primer design for mNeonGreen plasmid construction
PCR designs for amplifying required DNA segments to replace the luciferase gene in the backbone plasmid with an mNeonGreen insert. **A:** Plasmid map of existing backbone plasmid, containing rRNA promoter region, Neomycin resistance cassette and Luciferase gene. Primers were designed to bind at either end of the Luciferase gene, so this segment was not amplified. The mNeonGreen gene was then inserted in this position. **B:** Map of insert mNeonGreen gene within original plasmid. Primers were designed to bind at either end of mNeonGreen coding region to amplify only this portion of DNA. Created in BioRender.

Following the Gibson assembly of the plasmid fragments, transformation into *E. coli* and colony PCR (as detailed in section 3.1.3.1) the presence of the new plasmid was confirmed by gel electrophoresis of the colony PCR products prior to restriction digest, which displayed a band at around the 1000bp marker. This confirmed the presence of the 1197bp mNeonGreen - Lm-tub 3' UTR junction DNA segment, only present in the new mNeonGreen plasmid (pGL3093).

4.1.3.2 Transfection troubleshooting

Initial transfection attempts were unsuccessful as no green fluorescence could be visualised when observing the selected parasites, suggesting the plasmid had not been integrated into the parasite DNA. Additionally, the water control samples showed no parasite death, which was indicative of the

drug concentration being too low for selection. The dosage of 25µg/ml that we initially treated the parasites with, was based on dosages given following transfections in HOMEM media, which may differ to Schneider's due to differences in media composition. After conducting an EC_{50} assay (Figure 12) to determine the concentration of drug that produces half the maximal response, (which would kill 50% of the parasites present in the sample), we found an EC_{50} of 8.8µg/ml. The appropriate dosage is then usually three times this concentration, making a dose of 26 µg/ml sufficient to kill all parasites without G418 resistance. As this value was only marginally higher than the original dosage used for transfection, this indicated that the concentration of drug given was likely sufficient and that the failure of the drug selection was caused by another issue.

Previous studies on growth rates have shown that the parasites replicate significantly faster in Schneider's medium than in HOMEM, suggesting that the post-transfection recovery time required for the parasites to begin dividing again may be shorter in Schneider's. Shortening the recovery time before adding G418 could therefore help prevent parasites without the plasmid from growing and reduce the numbers of parasites without the desired DNA in the culture. This would then reduce the number of parasites present in each well at the time of drugging, meaning the drug is used up less quickly, allowing proper selection. Therefore, upon repetition of the transfections, the parasites in Schneider's media were treated with G418 8 hours post-transfection, as opposed to the previous 20 hours.

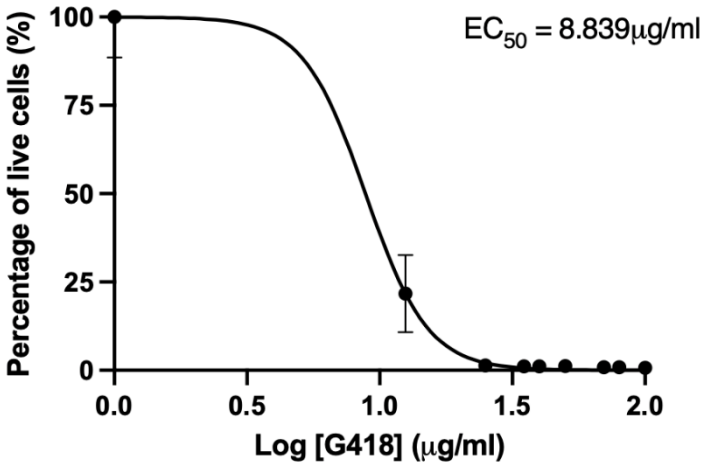

Figure 12: EC_{50} Drug Response Curve for G418 in Schneider's media
Log phase L. *donovani* promastigotes were added to 96-well plates at a concentration of $5x10^3$ cells/ml. The wells were then treated with G418 at concentrations ranging from 12.5µg/ml-100µg/ml and Alamar blue added on days 5, 7 and 10 post-drugging. After 6 hours, the metabolic activity in each well was determined using a BMG LABTECH CLARIOstar® microplate reader at a wavelength of 590nm. N=1.

4.1.3.3 Parasite clone selection via microscopy

To assess which of the clonal populations selected following plasmid transfection may be best to use in further experiments, I conducted microscopy of fixed log-phase parasites. As expected, all the clonal populations that had been transfected in HOMEM showed bright and consistent fluorescence (Figure 13). None of the populations transfected and recovered in Schneider's media showed any fluorescence in the mNeonGreen channel so would not be used any further.

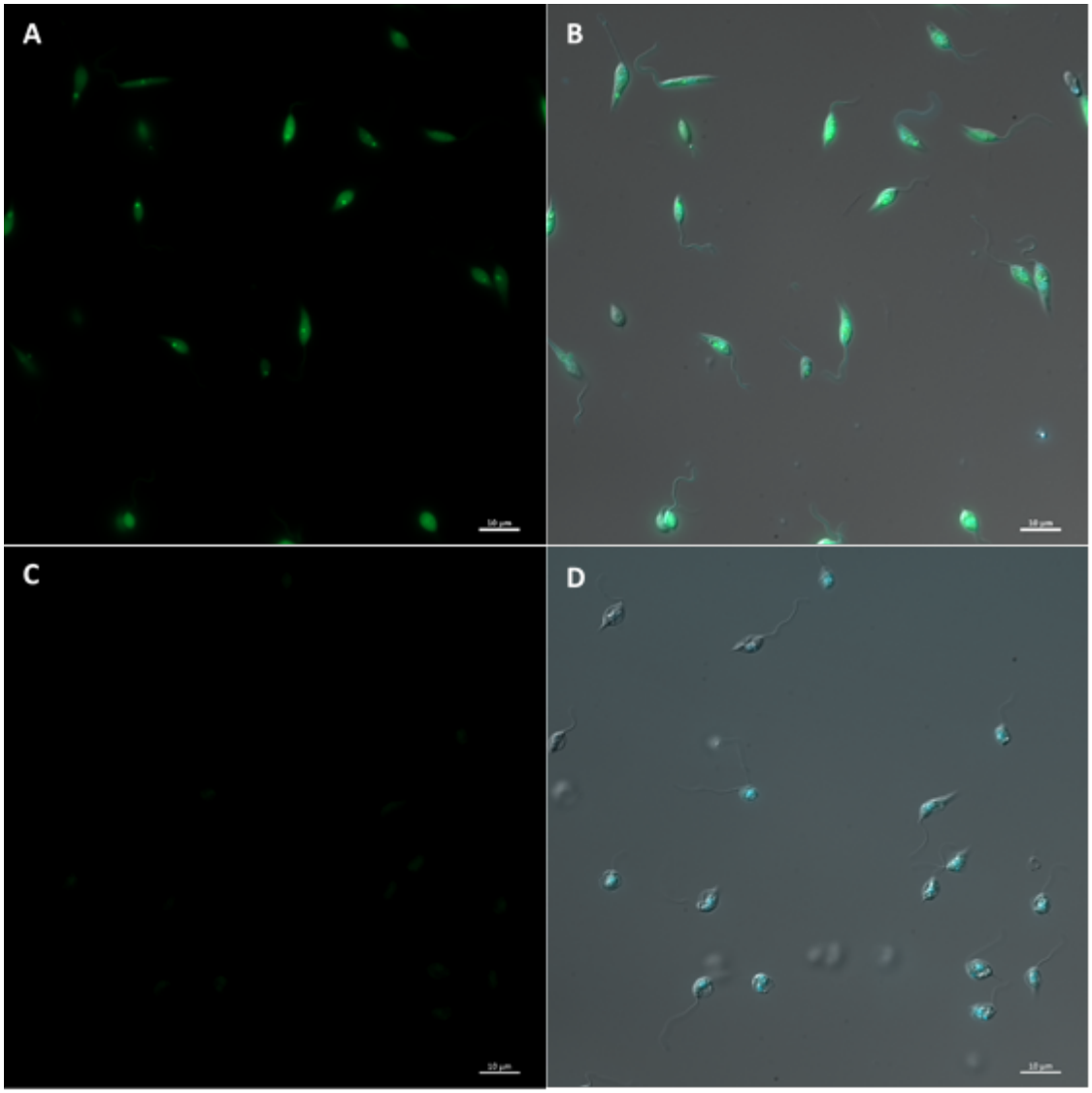

Figure 13: Microscopy of mNeonGreen clones shows successful transfection of plasmid into parasites in HOMEM.

Parasites were transfected with a newly constructed plasmid containing the mNeonGreen gene and selected with G418 . Cultures were grown until log phase and then DAPI stained, fixed and mounted onto slides for microscopy. **A:** Parasites transfected with the plasmid in HOMEM showed bright mNeonGreen expression (shown in green) and therefore successful transfection with the plasmid. **B:** The mNeonGreen fluorescence (shown in green) aligns with the DAPI signals (shown in cyan) and the DIC channel (shown in grey). **C:** Parasites transfected in Schneider's show no mNeonGreen signal at the same exposure levels. **D:** DAPI (shown in cyan) and DIC (shown in grey) channels show the presence of the parasites on the slide, with no mNeonGreen expression. Scale bars representative of 10µm. N=1.

Although visual inspection of the images provided a useful initial indication of clone brightness, analysis using the ZEN image analysis software offered more quantitative data. Fluorescence intensity measurements were collected by defining a region of interest (ROI) around the parasites in each image (Figure 14). To ensure consistency across samples, the same ROI was used for all images. Based on the fluorescence reading of the two HOMEM clones imaged, Clone C appeared to have significantly higher expression levels of the mNeonGreen protein. This technique was used to visualise the localisation of the fluorescence within the parasites to ensure that there were no issues in its expression of the protein which flow cytometry would not reveal.

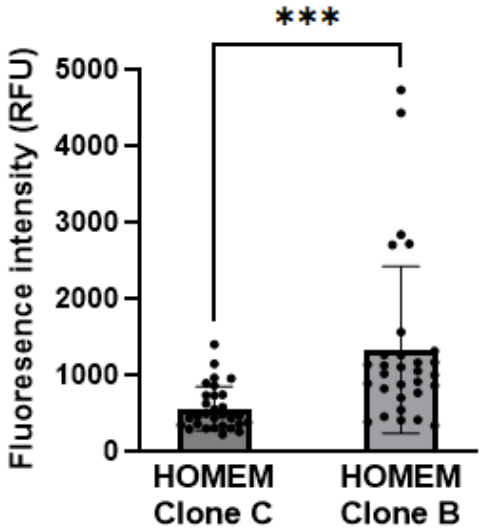

Figure 14: Quantification of fluorescence intensity in two mNeonGreen expression plasmid transfected cell clones.
Following transfection with a DNA plasmid encoding the mNeonGreen protein, fluorescence intensity was measured in two different clonal populations to assess expression levels and brightness. Image analysis was performed using ZEN software, with identical regions of interest (ROIs) applied to each image. The relative fluorescence intensity (RFU) values were plotted to compare clone brightness, providing an indication of which clone may be more suitable for future experiments. All significance values calculated in GraphPad Prism using an unpaired t-test, * = $p<0.05$, ** = $p<0.005$, *** = $p<0.005$, **** - $p<0.0001$, N=2.

4.1.3.4 Growth kinetics

To further assess which clonal population of mNeonGreen expressing parasites would be the most suitable to use for future experiments, a log growth curve on three separate clonal populations were conducted, in both HOMEM and Schneider's media. As expected, all clones grew faster in the Schneider's media compared to in HOMEM. Clones B and C grew at more similar rates in both media, increasing in the number of parasites steadily each day before reaching the stationary phase between days 4 and 5 and parasite numbers dropping on day 10. However, clone A grew very differently in both media, starting off with slower growth, not reaching a true stationary phase by day 10, shown by the continued increase in the number of cells per millilitre of culture. This

suggested that clone A grows much less predictably and would therefore be difficult to use for infection studies as cells must be grown to a precise density prior to infection. Both clones B and C follow what would be considered a normal growth pattern and rate (compared to wildtype parasites), suggesting they are both healthy populations with predicable growth kinetics.

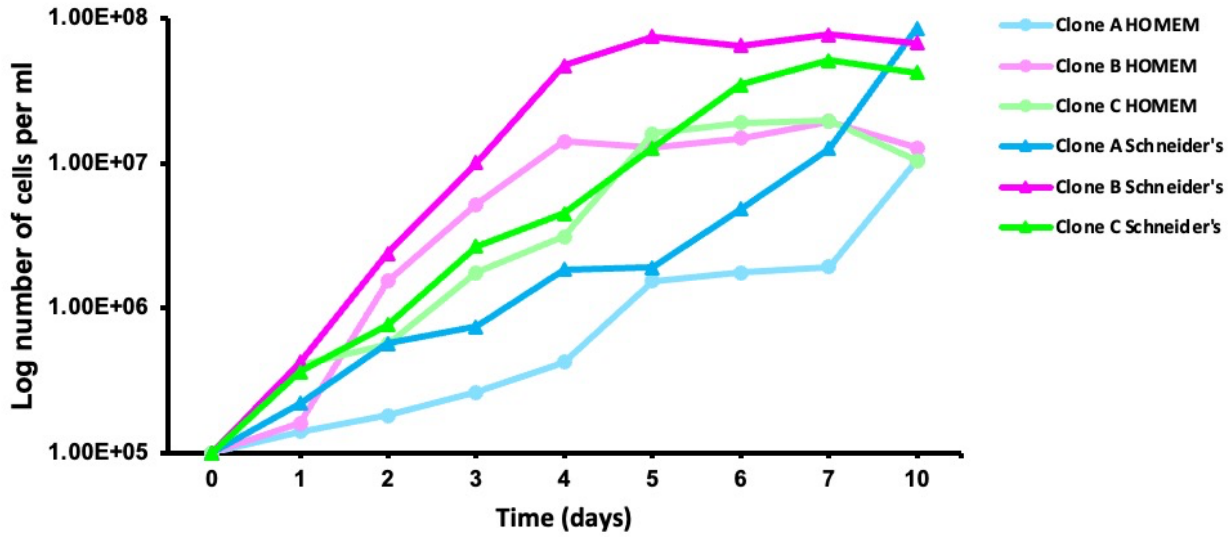

Figure 15: Two clonal populations of mNeonGreen-expressing *L. donovani* parasites show normal growth kinetics.
Promastigotes expressing the mNeonGreen gene from three different clonal populations selected following transfection were grown in either Schneider's or HOMEM media for 10 days from a starting density of $1x10^5$ parasites per ml of culture. Culture densities were counted each day for 10 days and a log growth curve of the data plotted in Excel. N=1.

4.1.3.5 Infection studies of mNeonGreen line

For future phagosome isolation experiments, it was essential that the new mNeonGreen-expressing *L. donovani* parasite line showed sufficient virulence to infect macrophages and yield a substantial number of phagosomes. Therefore, I performed macrophage infection experiments using clonal populations B and C transfected in HOMEM. Bone marrow macrophages were infected with stationary phase mNeonGreen promastigotes. After 6 hours external parasites were washed off and slides mounted for imaging at 6-, 24-, 48- and 72-hours post-infection. Following analysis, there were only significant differences in the percentage of macrophages that were infected between the two parasite lines at the 72 hour timepoint with an MOI of 20. The wildtype parasites here showed to infected 61.9% of macrophages compared to only 33.3% with the mNeonGreen line. This could indicate differences in survival within the macrophages once internalised, with many of the mNeonGreen parasites dying by the 72 hour timepoint (Figure 16A). The other time points suggested that the mNeonGreen-expressing parasites infect macrophages at comparable rates to the wildtype. However, was no significant difference in the number of parasites per 100 macrophages between the two lines

at any time point or MOI. This indicated that not only do both lines initially infect at similar rates, they also both show similar changes in parasite survival once within the macrophage, increasing in number of parasites by 24 hours due to continued phagocytosis and decreasing at 48 and 72 hours as the parasites begin to die (Figure 16B). There was also a significant difference found in the number of parasites found within each infected macrophage at 24 hours with an MOI of 10. Here, the mNeonGreen line showed to have a higher number of parasites (and therefore likely phagosomes) within each macrophage that had been infected, with an average of 3 parasites per macrophage, compared to the wildtype which showed an average of 2.3 (Figure 16C). In combination these results indicate that initially, both lines infect the macrophages at comparable rates, but that each macrophage may take up more mNeonGreen parasites compared to wildtype, with mNeonGreen parasites being less amenable to longer term survival within the macrophage, causing their death by 72 hours.

A

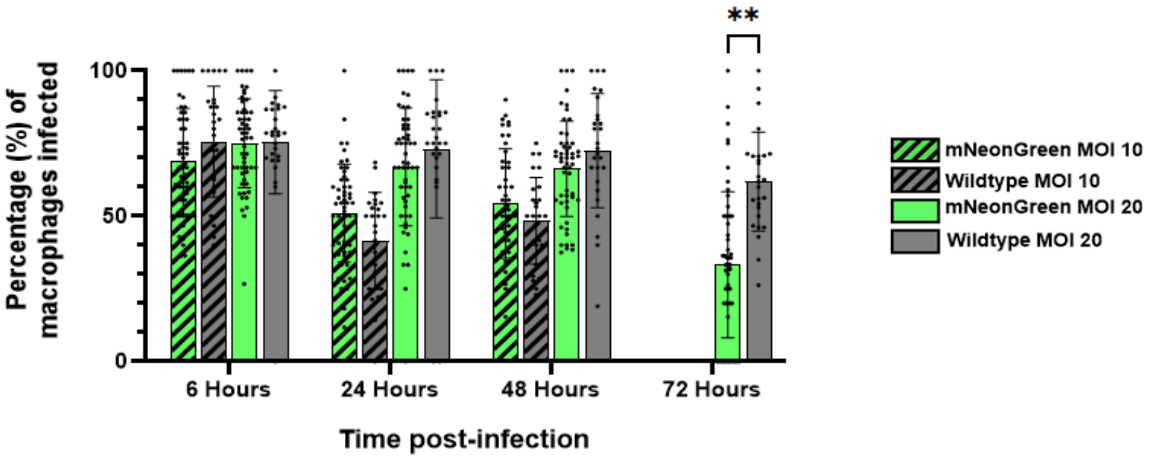
**
Percentage (%) of macrophages infected
100
50
0
6 Hours
24 Hours
48 Hours
72 Hours
Time post-infection
mNeonGreen MOI 10
Wildtype MOI 10
mNeonGreen MOI 20
Wildtype MOI 20

B

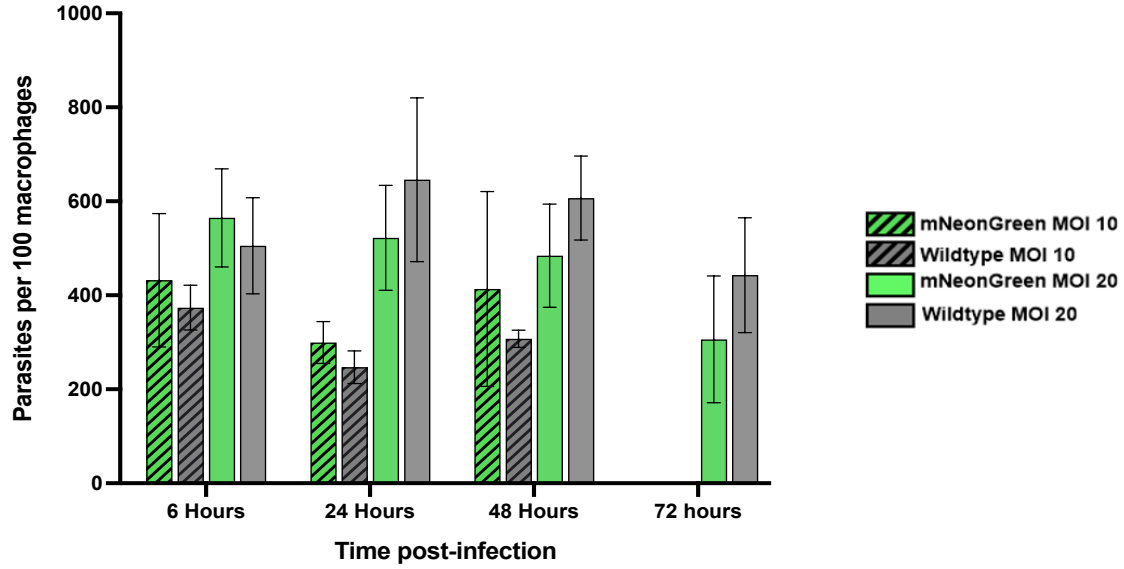
Parasites per 100 macrophages
1000
800
600
400
200
0
6 Hours
24 Hours
48 Hours
72 hours
Time post-infection
mNeonGreen MOI 10
Wildtype MOI 10
mNeonGreen MOI 20
Wildtype MOI 20

C

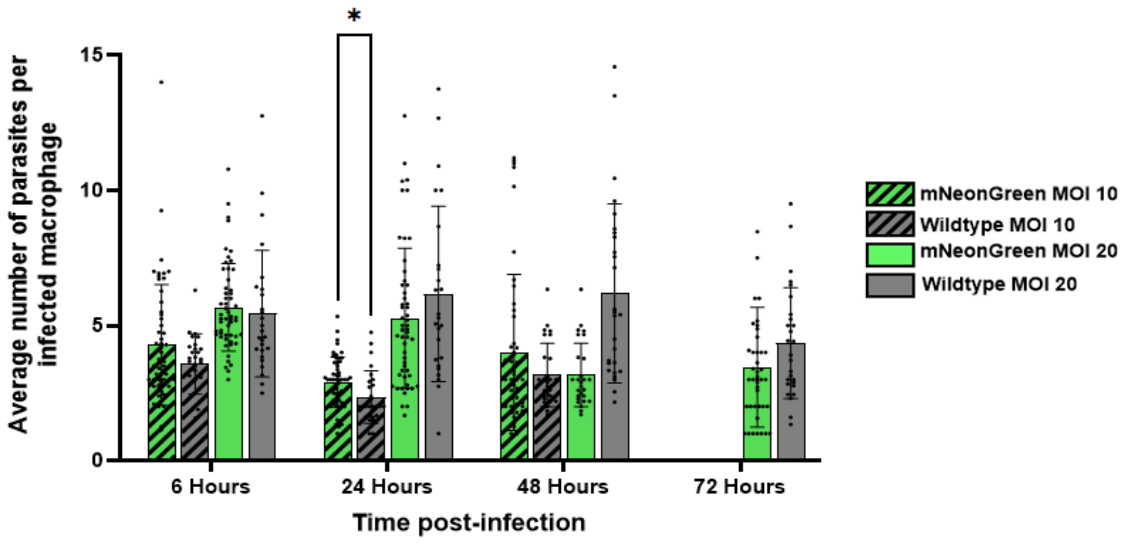
*
Average number of parasites per infected macrophage
15
10
5
0
6 Hours
24 Hours
48 Hours
72 Hours
Time post-infection
mNeonGreen MOI 10
Wildtype MOI 10
mNeonGreen MOI 20
Wildtype MOI 20

Figure 16: mNeonGreen expressing *L. donovani* parasites show similar infection rates compared to wildtype parasites.
MNeonGreen-expressing or wildtype *L. donovani* promastigotes were used at day 3 stationary phase to infect mouse bone marrow derived macrophages at either an MOI of 10 or 20. Macrophages were incubated with parasites for the relevant time with external parasites being removed at 6 hours for all time points. Fluorescence microscopy images captured at a x63 magnification using a ZEISS AxioObserver were used to assess infectivity of both parasite lines. Macrophage and parasite numbers were counted using FIJI. **A** Both infected and non-infected macrophages were counted in each image to give the percentage of macrophages that were infected. Percentage infections were compared to that of the wildtype infected at the same MOI for the same incubation time. **B**. An average of parasites per 100 macrophages was calculated for each chamber slide well using the total number of parasites engulfed per image and compared between wildtype and mNeonGreen-expressing parasites for each MOI and timepoint. **C**. For each infected macrophage, the number of parasites within it were counted as an indication of the number of phagosomes present. This was then compared between the wildtype and mNeonGreen lines. All significance values calculated in GraphPad Prism using a two-way ANOVA, * = $p<0.05$, ** = $p<0.005$, N=1.

4.1.4 Final parasite line selection

Following the testing of these three lines, we selected the TdTomato line for further use in the phagosome isolation experiments. The CMFDA staining showed too much variability to be a viable option, with multiple experiments showing different levels of staining. Furthermore, the staining of the parasites with CMFDA would add an additional step before the macrophages could be infected, making the protocol longer and more complex, leaving more room for error. Although the mNeonGreen line showed higher virulence compared to the TdTomato line, the additional testing performed on the TdTomato line gave more assurance of its viability for use in the phagosome isolation experiments. For example, we performed multiple infection tests on different occasions using this line and gathered consistent results, however infection testing using the mNeonGreen line was only performed once. The TdTomato line also showed successful detection using flow cytometry both fixed and unfixed, which was not performed using mNeonGreen parasites due to time constraints. Some studies have reported that fixation can disrupt the detection of the mNeonGreen protein, making it less bright, suggesting that if using this line, phagosomes could not be fixed before FACS, making the sample more fragile and susceptible to loss of phagosomes (Paterou et al., 2025; Stockmar et al., 2018). Therefore, we selected the TdTomato line with an increased MOI for the future phagosome experiments.

4.2 Phagosome membrane stain testing

4.2.1 Flow cytometry testing

CellVue Burgundy is a lipophilic cell membrane dye that can be used for identification and tracking of cells. Previous literature has shown CellVue stains of various fluorescent wavelengths to be viable for

the detection of the membrane of the phagosome (Chatterjee et al., 2025). The sorting of phagosomes from each sample, following macrophage lysis, requires detection of a positive membrane stain on its surface and therefore it was vital that the CellVue Burgundy dye used in this project could also be detected through flow cytometry. As the phagosomes are very small and easily broken, it is also desirable to fix the sample of collected phagosomes before FACS, meaning it was important to ensure that the fixation process did not disrupt the detection of the membrane stain.

To verify this, bone marrow macrophages were stained with CellVue Burgundy, half the sample fixed in PFA, and the other half left unfixed to gauge whether fixation causes any detection issues (Figure 17). From this experiment, we could conclude firstly, that the signal produced by the CellVue Burgundy stain is distinguishable from that of unstained cells when using flow cytometry. This is shown by a shift of the area reading in the CellVue Burgundy detection channel (R712), representing a greater overall fluorescence intensity across all measured events, compared to the unstained sample (Figure 17). The signals detected from the fixed versus unfixed sample showed minimal differences in fluorescence intensity (Figure 17), suggesting that fixation does not disrupt the staining on the cell membrane or cause any issues in its detection by flow cytometry. Using this same fixation protocol should therefore not cause any issues in the cell sorting of the phagosomes from the sample following macrophage lysis, decreasing the likelihood of destroying any phagosomes throughout the process.

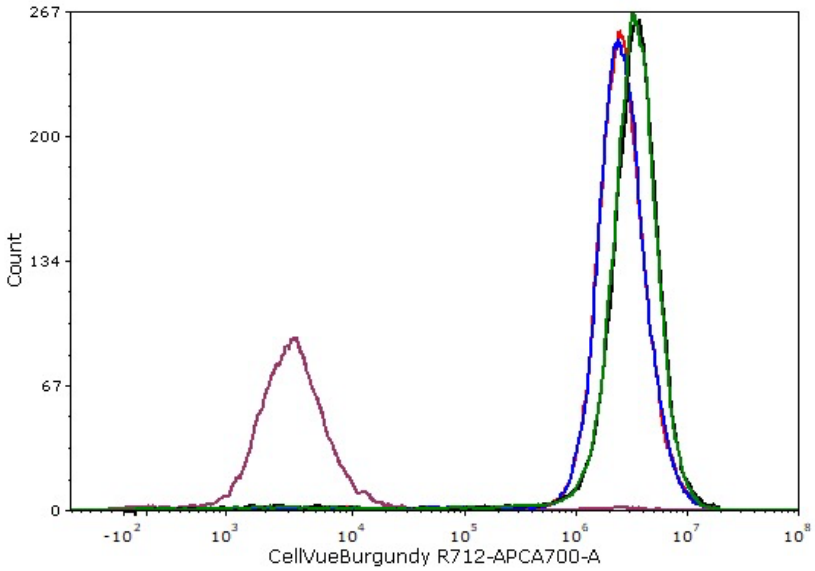

Figure 17: Fixation of CellVue Burgundy stained BMDMs does not disrupt detection by flow cytometry. Bone marrow macrophages were stained with 2µM CellVue Burgundy membrane stain by incubation at room temperature for 5 minutes. The macrophages were washed, and half were fixed with 2% PFA before fixed (shown in blue and red), unfixed (shown in black and green) and unstained (shown in purple) samples were detected by flow cytometry. R712 channel area readings show CellVue Burgundy stained samples to have greater fluorescence intensity in this channel, compared to unstained samples. Fixed and unfixed samples show minimal shift in fluorescence readings compared to one another. N=1.

4.2.2 CellVue Burgundy staining of promastigotes

Through the sorting process, we hoped to obtain a 'double positive' sorted group, with positive signals for both CellVue Burgundy phagosome membrane stain and fluorescent protein, expressed by the parasites. To achieve this, it was important to be certain that the CellVue Burgundy positive events correspond only to phagosomes that have been stained, rather than any other stained particles. To ensure that any free parasites within the sample do not become stained by the CellVue Burgundy, I undertook staining and microscopy of promastigotes, grown in both HOMEM and Schneider's media (Figure 18 A-D). Both log and stationary phase parasites were stained with CellVue Burgundy to assess whether phase of growth affects the staining of the parasites. Although when within the phagosome parasites are in the amastigote stage, we decided to stain promastigotes to ensure that there was no stage-specific staining caused by unique surface content (e.g. lipids and proteins). This removed any doubt that CellVue Burgundy signals could arise from the parasites themselves, such as contaminant promastigotes in the sample that did not successfully infect the macrophages and were not removed during washing.

ZEISS Zen software was used to gather quantitative data on the fluorescence intensity readings of each group. The results of this showed that only 5.36% of parasites become stained. In the stationary phase parasites grown in HOMEM, 22.32% of these parasites were stained with CellVue Burgundy and gave fluorescence readings of above 1000 RFU, which was not observed in any other group (Figure 18E). This could suggest an issue with this group of parasites (stationary phase and grown in HOMEM) taking up the membrane stain, which could cause issues in cell sorting experiments. Additional analysis of these parasites may offer insight into why they exhibit higher fluorescence, such as being dead, at a certain stage of division or a different form of promastigote. There was also a significant difference between the readings of log versus stationary phase parasites in both growth media, suggesting that parasite stage does affect CellVue Burgundy staining.

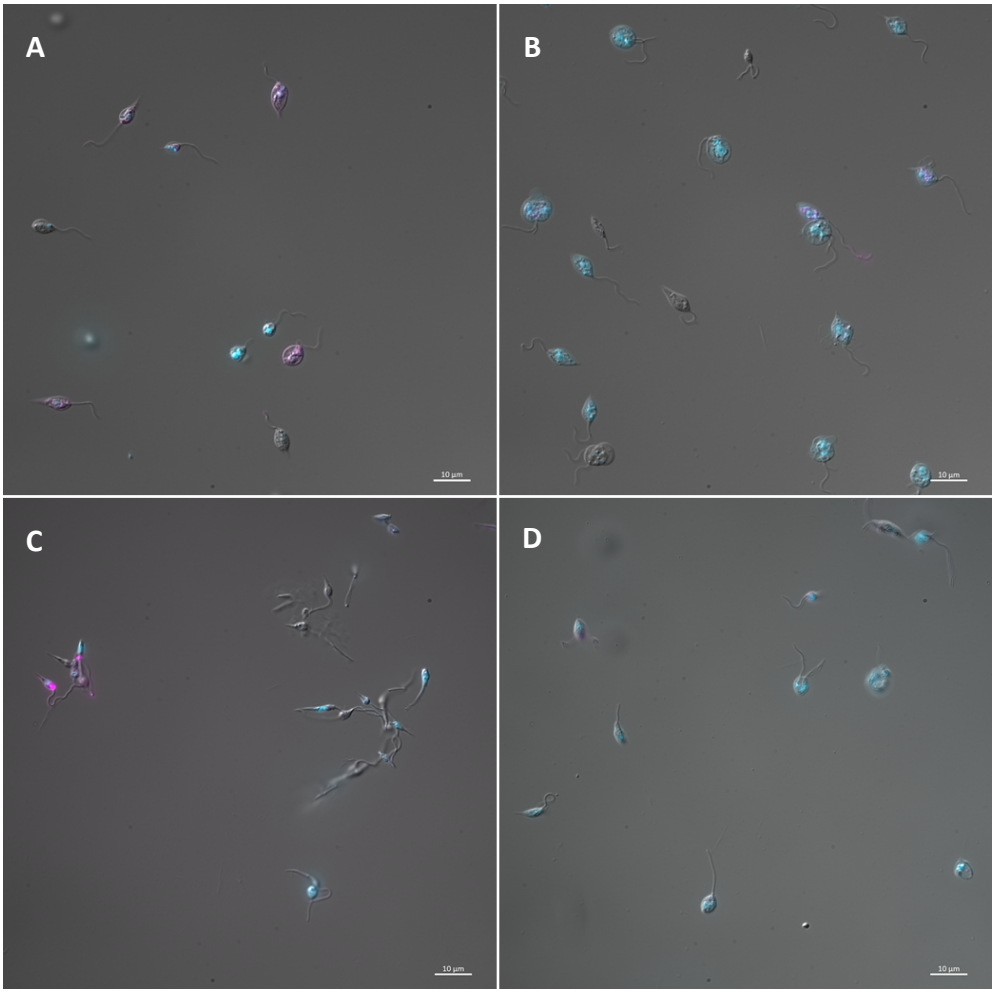

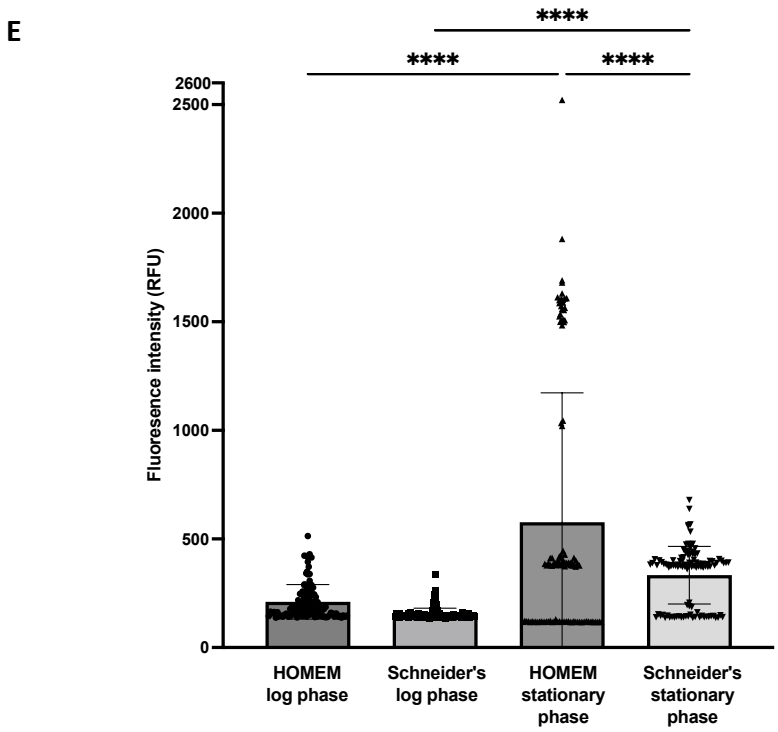

Figure 18: *L. donovani* promastigotes are generally not stained with CellVue Burgundy membrane stain.

A-D: Stationary and log phase promastigotes grown in either supplemented HOMEM or Schneider's were stained with 2µM CellVue Burgundy (shown in magenta) for 5 minutes at room temperature. Parasites were then DAPI (shown in cyan) stained and mounted onto slides for microscopy. N=2, figure shows representative images from N=2 experiments. **A:** Promastigotes grown in HOMEM were stained at log phase. **B:** Promastigotes grown in supplemented Schneider's were stained at log phase. **C:** Promastigotes grown in HOMEM were stained at stationary phase. **D:** Promastigotes grown in Schneider's were stained at stationary phase. **E:** Images were analysed by collecting fluorescence intensity readings of 112 parasites per group in Zen. Data was then plotted and analysed using a one-way ANOVA in GrpahPad Prism, **** = $p<0.001$. Scale bars representative of 10µm.

4.3 Isolation of parasite-containing phagosomes

4.3.1 Isolation of *L. mexicana*-containing phagosomes

As an initial test of the infected macrophage lysis and phagosome staining protocols, macrophages infected with wildtype *L. mexicana* promastigotes were lysed by nitrogen cavitation to release parasite-containing phagosomes. CellVue Burgundy membrane dye was added, alongside DAPI, post-nitrogen cavitation to visualise phagosome membranes and internalised parasites. As this method was untested for *L. donovani*, *L. mexicana* promastigotes were used due to some studies showing successful *L. mexicana* phagosome isolation previously (Chatterjee et al., 2025; Semini and Aebischer, 2018). This would allow for a first trial of the technique using larger phagosomes that are easier to isolate. At 48 hours post infection, the samples produced clear phagosome visualisation (Figure 19). Phagosomes showed fluorescence on their cell membrane, as well as positive DAPI staining of parasite DNA showing an *L. mexicana* parasite contained within the phagosome. Free amastigotes did not exhibit any CellVue Burgundy fluorescence.

These results showed that a protocol of nitrogen cavitation and CellVue Burgundy membrane staining can remove other cell material to leave intact and visible *L. mexicana*-containing phagosomes. This provided a strong base for developing this method to include FACS isolation and the use of *L. donovani* parasites for infection, to yield *L. donovani*-containing phagosomes. Repeating this protocol with *L. donovani* would also allow the use of TdTomato parasites (which were still under virulence testing at the time) to support the sorting stage. We therefore chose to use the TdTomato *L. donovani* line in the next phagosome isolation experiments and to adapt this method that first showed success with *L. mexicana* containing phagosomes.

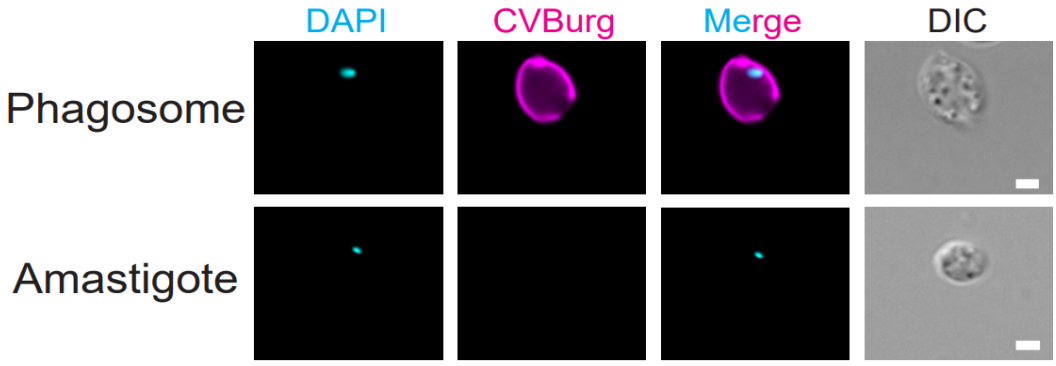

Figure 19: Nitrogen cavitation and membrane staining allows visualisation of parasite-containing phagosomes.
Third day stationary phase wildtype *L. mexicana* were used to infect bone marrow macrophages at an MOI of 10. After 48 hours, macrophages were lysed using nitrogen cavitation and DAPI and CellVue Burgundy stains added. Fluorescent microscopy images were taken at a x63 magnification and then processed in Zen. Scale bars representative of 2µm. N=3, figure shows representative images from N=1 experiments.

4.3.2 Isolation of *L. donovani*-containing phagosomes

Building on the success of the protocol of nitrogen cavitation and CellVue Burgundy staining to isolate fluorescent *L.mexicana*-containing phagosomes, we then utilised the same protocol with TdTomato *L. donovani* promastigotes to assess whether this methodology is also effective for isolating the smaller phagosomes characteristic of this species. Wildtype controls were also included. Macrophages infected with wildtype parasites would produce parasite-containing phagosomes that only emit signals within the CellVue Burgundy channel, to help decide how to gate the sample. This was assessed at two time points, 24 and 48 hours, with external parasites being washed off at 6 hours for all samples to minimise the numbers of partially internalised parasites.

In the next stage of this experiment, we trialled the use of FACS to isolate the phagosomes from the sample, with parasite-containing phagosomes being sorted into a 'double positive' fluorescence group (positive for both CellVue Burgundy membrane stain and TdTomato signal). Following nitrogen cavitation, the sample was sorted into four groups by gating on the cell sorter: $CVB^{+}tdT^{-}$, $CVB^{-}TdT^{+}$, $CVB^{+lo}TdT^{+}$, $CVB^{+hi}TdT^{+}$ (Figure 20). Gates were placed based upon the fluorescence readings of single stain and unstained control samples. The grouping of signals into the two CellVue Burgundy positive groups allowed phagosomes that may have broken membranes or parasites with bits of fluorescent membrane debris stuck to them (CVB^{+lo}) to be sorted out from those with stronger membrane-associated signals (CVB^{+hi}), which are more likely to be intact parasite-containing compartments, although membrane integrity can't be definitively confirmed following mechanical lysis. A small sample of the $CVB^{+}TdT^{+}$ group was then mounted onto slides for microscopy, to confirm that the phagosomes had been appropriately sorted into this group (Figure 20). The $CVB^{-}TdT^{+}$ group was also visualised to ensure that this contained free amastigotes as expected (Figure 21).

The results of this experiment showed that the protocol of nitrogen cavitation, CellVue Burgundy staining and FACS can successfully isolate fluorescent parasite-containing phagosomes. This forms a strong basis for being able to investigate the protein content of the phagosome as the next step of this research (discussed in section 5.2.2). Further to this, the data showed a total of $4x10^4$ phagosomes yielded, suggesting that for proteomic analysis, this experiment would need to be scaled up to yield enough phagosomes to then produce proteomic data of sufficient depth as a minimum of $1x10^5$ phagosomes are typically required.

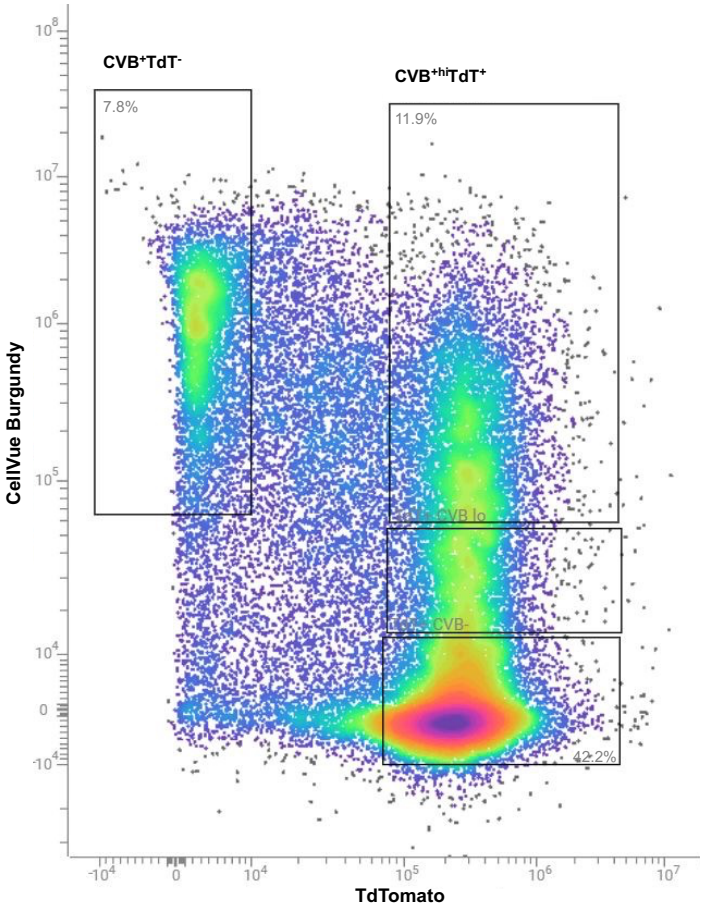

Figure 20: Parasite-containing phagosomes can be isolated by FACS.
Flow cytometry plot showing gating strategy for sorting nitrogen-cavitated particles into four populations based on TdTomato and CellVue Burgundy fluorescence: $CVB^{+}tdT^{-}$, $CVB^{-}TdT^{+}$, $CVB^{+lo}TdT^{+}$, $CVB^{+hi}TdT^{+}$. Events were gated based upon fluorescence readings produced by single stain and unstained controls. N=2, figure shows representative plot from N=1 experiments.

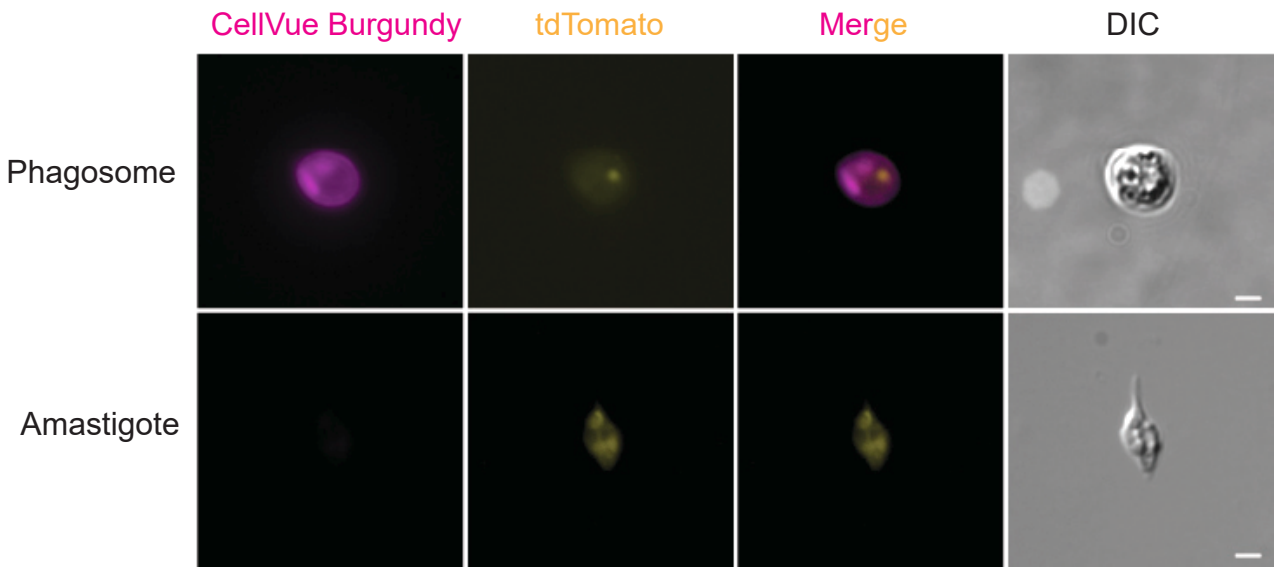

Figure 21: TdTomato parasites within intact phagosomes following isolation by FACS
Third day stationary phase TdTomato-expressing *L. donovani* were used to infect bone marrow macrophages at an MOI of 20. After 48 hours, macrophages were lysed using nitrogen cavitation and CellVue Burgundy stain added. Parasite-containing phagosomes were subsequently isolated using FACS using the gating strategy shown in figure 20. Phagosomes can be differentiated from free amastigotes by absence of CellVue Burgundy staining and size, with phagosomes appearing larger. Fluorescent microscopy images were taken at a x100 magnification and then processed in Zen. Scale bars representative of 2µm. N=2, figure shows representative images from N=2 experiments.

4.4 Latex bead internalisation testing

As a comparator for parasite-containing phagosomes in subsequent proteomic analysis experiments, we assessed the efficiency of internalisation of fluorescent latex beads by bone marrow–derived macrophages (Figure 22). These beads would provide a parasite-free control that enables the differentiation of host- and parasite-derived proteins within isolated phagosomes and allows investigation into how parasite presence alters the phagosomal proteome. Bead to cell ratios of 5 and 10 were tested to determine which would yield phagosome numbers comparable to those observed in TdTomato-expressing parasite infections used previously for phagosome isolation (approximately five phagosomes/parasites per macrophage).

No significant difference was detected in the percentage of macrophages containing latex beads between the two bead to cell ratios, indicating that increasing bead numbers did not increase the proportion of phagocytosing cells (Figure 22A). Likewise, the total number of beads per 100 macrophages did not differ significantly between bead to cell ratios (Figure 22B). Crucially, the number of beads internalised per infected macrophage (reflecting the number of bead-containing phagosomes formed) was also comparable between conditions (Figure 22C), with means of 2.75 and

2.5 beads per infected macrophage for bead to cell ratios of 5 and 10, respectively. These results demonstrated that a higher ratio did not enhance bead uptake per macrophage and that the overall yield of bead-containing phagosomes is markedly lower than that following parasite infection. Overall, these findings indicate that although latex beads are phagocytosed by macrophages, uptake occurs at considerably lower rates than for parasites, and further optimisation will be required before using this approach to generate parasite-free phagosomes for proteomic comparison.

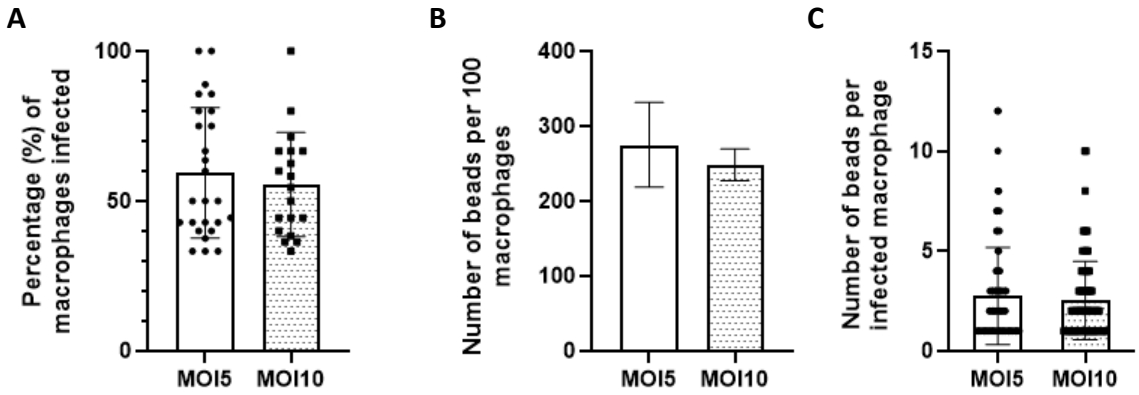

Figure 22: Latex beads are successfully phagocytosed by macrophages at lower rates compared to parasites.

Fluorescent latex beads were added to bone marrow macrophages within chamber slides at bead to cell ratios of 10 and 20, incubated for 6 hours before the removal of external beads and incubation until reaching 24 hours post infection. Macrophage nuclei were stained with DAPI and the slides then mounted ready for imaging using a ZEISS AxioObserver microscope. Images were analysed in FIJI and data analysed in GraphPad Prism. Statistical analysis was performed using an unpaired Welch's t-test $p<0.05$, N=1. **A** Macrophages with and without internalised latex beads were counted to calculate the percentage of macrophages infected with beads. **B** The total number of beads in each image were counted to calculate the number of beads per 100 macrophages in each chamber slide well. **C** The number of beads in each infected macrophage was counted to determine the number of latex bead-containing phagosomes present.

Chapter 5: Discussion

5.1 General discussion

5.1.1 Applications of research

Currently, work to analyse the protein composition of the *Leishmania* phagosome has focused on *L. mexicana* and *L. amazonensis*, with neither showing robust methods of doing so due to low and inconsistent yields (Chatterjee et al., 2025a; Real, 2020; Semini and Aebischer, 2018). These studies show limitations in their extrapolation potential and ability to be further developed for future experiments.

Due to the *Leishmania* species that have been worked with in these studies, these techniques had only proved successful for the isolation of larger, communal phagosomes and so their success in doing so with smaller vacuoles like those formed by *L. donovani* is untested. Additionally, as phagosome composition is dependent on the host cell activation pathway (e.g. Th1 or Th2) induced by the pathogen, the protocols that have been previously tested in some species with particular cell models may not translate to other infection models e.g. with *L. donovani* (Trost et al., 2009). Many of these studies have shown further issues such as low phagosome yield, lack of comparability due to variable methods and protein identification using older, less reliable techniques (Henriques et al., 2003; Kima, 2007; Real, 2020; Semini and Aebischer, 2018). Studies have shown challenges in preventing contamination from other organelles such as endosomal, lysosomal or mitochondrial fragments, highlighting the need for rigorous controls within the development of new techniques (Campbell-Valois et al., 2012). Furthermore, research into the isolation of *Francisella novicidia*-containing phagosomes has presented issues with phagosome integrity after isolation, with only approximately 70% of those isolated remaining intact (Marecic et al., 2017). This causes decreased yield as well as confounded results following proteomic analysis due to debris and artefacts from damaged phagosomes being present within the sample (Marecic et al., 2017).

The applications of these techniques are also limited as they only offer insight into proteins that could be further investigated as potential drug or vaccine targets against CL, which is less of a threat to global health than VL. Study into phagosome proteomics of other parasites such as *Salmonella* typhimurium, *Legionella* and *Mycobacterium tuberculosis*, have shown promising results, with more robust methods such as fractionation and FACS being used, suggesting new combinations of methods that could be adapted for use in *L. donovani* phagosome research (Chakraborty et al., 1995; Chatterjee et al., 2025a; Russell, 2001; Shevchuk et al., 2009).

5.1.2 Overview of findings

5.1.2.1 TdTomato vs mNeonGreen line

Our results offer a good indication of how the TdTomato and mNeonGreen-expressing *L. donovani* lines differ in their virulence at multiple time points, compared to one another and wildtype parasites. Generally, the TdTomato line exhibits a lowered virulence compared to the wildtype line, in contrast to the mNeonGreen line (Figures 7 and 16). When comparing the number of parasites per 100 macrophages for each fluorescent line with the wildtype, TdTomato showed approximately 50% fewer parasites by 24 hours at each MOI. In contrast, the mNeonGreen line showed fewer differences by 24 hours at an MOI of 20, with only a 20-32% decrease, and showed higher parasite counts than the wildtype at every timepoint at an MOI of 10. However, when looking at the percentage of macrophages infected, the differences are less clear. At 24 hours with an MOI of 20, which is the key timepoint and MOI used before phagosome isolation, both fluorescent lines show that 67% of macrophages are infected. This pattern suggests that the TdTomato line shows some variability in infectivity while remaining less virulent overall. This lowered virulence means that TdTomato infections require a higher MOI to produce the same number of infected macrophages per sample. As described in section 4.1.1.2, this creates difficulties in removing external parasites before phagosome isolation, which use of the mNeonGreen line may avoid (further discussed in section 5.1.3.1). Lastly, the infection data also showed that although the TdTomato line infects fewer macrophages, each infected macrophage holds a similar number of parasites to those infected by the mNeonGreen line, with an average of 5 parasites per infected macrophage at 24 hours using an MOI of 20, suggesting that each infected macrophage will yield a similar number of phagosomes for both lines. Together, these findings show that the two lines differ in infectivity, while the yield of phagosomes per macrophage is likely to remain similar, providing useful data for selecting which fluorescent parasite line may best suit future iterations of this technique.

5.1.2.2 Phagosome membrane staining with CellVue Burgundy

Our results have also shown the successful use of CellVue Burgundy staining for visualising the phagosome membrane and allows sorting via FACS. Initial tests showed that CellVue Burgundy staining of BMDMs remains detectable after paraformaldehyde fixation, meaning the fixation step doesn't cause any disruption to the stain (Figure 17). Crucially, this indicated that following nitrogen cavitation, the phagosomes within the sample could be fixed prior to FACS, decreasing the risk of losing any delicate phagosomes throughout processing and keeping the yield as high as possible. Additionally, the use of this stain performed well throughout the subsequent phagosome isolation experiments, showing clearly the membrane of both *L. mexicana* and *L. donovani* phagosomes when imaged via

microscopy (Figure 19 and 21). The sorting via FACS was also very efficient (Figures 20 and 21) and the gating strategy based partially upon the CellVue Burgundy fluorescence allowed efficient sorting of phagosomes from other particles and debris, altogether making the stain a key step in the use of this method for phagosome isolation. However, as nitrogen cavitation may have disrupted membrane integrity, it could not be assumed that all isolated signals in the $CVB^{+hi}TdT^{+}$ group represented fully intact phagosomes without further confirmation as some may instead have consisted of partially disrupted membranes or membrane fragments stuck to parasites. Using CellVue Burgundy allowed the beneficial opportunity to take the $CVB^{+hi}TdT^{+}$ phagosome-containing sample for microscopy imaging so that it could be further analysed, and phagosome presence could be confirmed as the microscope offered a suitable filter set for this stain. Use of another CellVue stain with an emission within the infra-red range (e.g. CellVue™ NIR780 or NIR815) would not allow visualisation via microscopy as there is no microscope filter set within the appropriate range. Other groups, such as the $CVB^{-}TdT^{+}$ group were also imaged. Comparing images of the other sorted groups ($CVB^{+lo}TdT^{+}$, $CVB^{-}TdT^{+}$ and $CVB^{+}TdT^{-}$) to the phagosome-containing group gave assurance that each event had been sorted as intended, which wouldn't be possible with all membrane stains.

From the staining of both stationary and log phase *L. donovani* promastigotes in different media (Figure 18), it was evident that most cells are not stained with CellVue Burgundy, offering some assurance that any particle sorted into the double positive group during FACS would truly be a phagosome, rather than any stained extracellular parasite. However, one subgroup that made up 25% of the HOMEM stationary phase parasites showed detectable staining, with RFUs above 1000. This was more than double the highest RFU seen in the other HOMEM stationary parasites with no staining (Figure 18E). This indicates that there may be some composition differences in the surface membrane of the parasites within this stained sub-group that cause them to take up some of the CellVue Burgundy stain (discussed further in section 5.1.3.2). This is particularly important to investigate following the data in Figure 18E, as it is stationary phase parasites grown in HOMEM that are used for macrophage infections and so could still be present extracellularly within the sample, and would be sorted into the phagosome group. Altogether, the use of CellVue Burgundy has shown to be effective and reliable within this project, however there is some more experimentation required to give complete certainty that it is only able to stain the phagosome membranes.

5.1.2.3 Nitrogen cavitation and FACS for phagosome isolation

The key finding of this project was that using nitrogen cavitation for macrophage lysis together with FACS sorting allows isolation of intact parasite-containing phagosomes, which had not been reported in macrophages infected with *L. donovani*. Our data shows that this process does not disrupt the

parasites or the phagosome membranes. Microscopy of the isolated phagosomes showed a fluorescent parasite enclosed within an undamaged membrane both before FACS (Figure 19) and after FACS (Figure 21). A clear issue that emerged was the reduced TdTomato signal in parasites inside phagosomes compared with free amastigotes. The TdTomato protein expression was visually much less bright when comparing a parasite within a phagosome with a free amastigote. This could be attributed to the metabolic shift that takes place as promastigotes transform into amastigotes, with the expression of the TdTomato gene being downregulated due to the slowed replication rate of amastigotes within the phagosome (Dirkx et al., 2024; Jara et al., 2017; McConville et al., 2015). As overall metabolic activity is lowered, so is translational activity, meaning that less fluorescent protein is produced and it therefore appears less bright (Kloehn et al., 2015). Additionally, the higher levels of reactive oxygen and nitrogen species within the phagosome, which *Leishmania* cannot entirely counteract, can cause alterations in the folding of side chains of the TdTomato protein due to oxidation, causing photobleaching and therefore a reduced brightness within the phagosome (Costantini and Snapp, 2013). Comparison of free amastigotes with parasites inside phagosomes also suggested altered TdTomato localisation, with a smaller area of expression in the intracellular parasites. The cause remains unclear without further experimental work, but several explanations are possible. *Leishmania* sense the acidic and oxidative conditions of the phagosome and change gene expression, surface molecules and intracellular organisation to adapt to this niche, which could shift the distribution of the TdTomato protein within the parasite (Zilberstein, 2021). The promastigote to amastigote transformation also involves remodelling of organelles linked to metabolic changes, which may alter TdTomato localisation (McConville et al., 2007). Studies in other phagosomal parasites support this idea. In *Toxoplasma gondii*, TgPL1 moves from intracellular punctate vesicles into the parasitophorous vacuole in response to host-driven stress, showing that parasites can redirect internal trafficking under these conditions (Tobin Magle et al., 2014). A similar stress-driven shift could change TdTomato localisation in *Leishmania*. Whilst offering some indication, these explanations remain untested in this system and would need direct experimental work before their contribution to the changes in TdTomato brightness or localisation within the phagosome could be confirmed. Although microscopy images show changes in TdTomato expression in the parasite within the phagosome, it is important to note that the data does not indicate this causing any problems for phagosome isolation by FACS and that, although dimmed, the TdTomato expression is still bright enough to be detected.

5.1.3 Experimental troubleshooting

5.1.3.1 Phagosome isolation of mNeonGreen-expressing *L. donovani*

As previously discussed, the TdTomato-expressing parasite line caused difficulties in removing external parasites from infected macrophage plates before nitrogen cavitation as it required a high MOI of 20. The creation and initial testing of the mNeonGreen line (section 4.1.3) offers an alternative that shows virulence more similar to wildtype parasites and achieves comparable infection rates at an MOI of 10. Although this line was not used for phagosome isolation in this project, it could improve outcomes in future experiments using this technique of nitrogen cavitation and FACS. A lower MOI makes it easier to wash away external parasites without losing macrophages that contain valuable phagosomes. Its higher virulence also makes it easier to recover a larger number of phagosomes from infected macrophages, which would provide more material for downstream work such as proteomic analysis (further discussed in section 5.2.2). Furthermore, using this line in place of the TdTomato line could resolve the brightness and localisation differences seen in fluorophore expression in intra-phagosomal parasites, which would reduce the risk of these issues causing complications in later phagosome isolation experiments (Shaner et al., 2005; Steiert et al., 2018; Werner et al., 2020).

On the other hand, the mNeonGreen parasite line has mainly been tested to assess its infectivity and growth kinetics, and we cannot yet be sure how the phagosome isolation procedure may affect fluorescent protein expression. For example, the TdTomato line underwent flow cytometry testing before use to confirm that it was detectable. mNeonGreen is widely used in flow cytometric studies of *Leishmania* and other parasites, and it has served as the basis of gating strategies in FACS experiments, which shows that it is bright enough for this purpose (De Oliveira et al., 2025; Howell et al., 2024). Despite this, fixation may still reduce the brightness of the mNeonGreen protein and affect its detectability. Work in trypanosomes, which are related to *Leishmania*, has shown that fixation with formaldehyde or methanol can reduce fluorescence by up to 50 percent and make detection by flow cytometry more difficult (Paterou et al., 2025). Because of this, the flow cytometry tests carried out with fixed and unfixed TdTomato-expressing promastigotes should be repeated with mNeonGreen-expressing promastigotes. This will clarify whether fixation affects the line generated in this project and whether phagosomes can still be fixed when using it to ensure none are lost during processing. During microscopy used to assess clone brightness during line generation (section 4.1.3.3), the parasites were fixed in PFA and remained clearly visible. This doesn't confirm that fixation wouldn't disrupt detection by FACS, but it suggests that it might not pose a major problem. Overall, despite requiring more testing before use, the newly generated mNeonGreen line offers a promising alternative to the TdTomato line, eliminating issues with virulence and therefore phagosome yield.

5.1.3.2 CellVue Burgundy staining of promastigote sub-group

An important step in troubleshooting potential issues with the CellVue Burgundy stain is to thoroughly investigate the sub-population of parasites that become stained. While most stationary-phase parasites in HOMEM are expected to have differentiated into the typical infective metacyclic form, a small proportion could have differentiated differently, which could alter their surface membrane architecture. During stationary phase, the structure of LPG in the membrane, as well as its GPI anchor, undergoes changes that affect membrane organisation(McConville et al., 1992; Sacks et al., 2000). These shifts could create membrane regions that allow CellVue Burgundy to insert, which would explain staining in only part of the culture (McConville et al., 1992; Sacks et al., 2000). Additionally, as parasites differentiate into metacyclic promastigotes during stationary phase, they may undergo subtle remodelling of their membrane structure, which can vary between individual cells (Silva et al., 2011). In some parasites, this remodelling could involve lipid reorganisation and the formation of membrane invaginations, which might trap CellVue Burgundy and cause these cells to appear stained. Without detailed analysis of the membrane and surface differences between the high-RFU stained and unstained sub-populations, it's difficult to determine precisely why only a subset of the parasites become labelled.

Although this sub-group does show a higher RFU than the other CellVue Burgundy stained parasites, its RFU in the AF647 channel remains lower than that of phagosomes measured with the same region of interest. For example, the phagosome in Figure 21 shows an RFU of 3076, while most parasites in this sub-group show an RFU closer to 1500. This pattern suggests that, although this group takes up more CellVue Burgundy, its signal stays distinguishable from the stronger signal omitted by the stained phagosome membrane. Gating to produce CVB^{+hi} and CVB^{+lo} groups during FACS can reduce the risk of collecting stained parasites in the phagosome sample.

5.1.3.3 CellVue Burgundy staining of axenic amastigotes

Once in the phagosome, promastigotes differentiate into amastigotes, meaning that the phagosomes isolated through FACS contain the parasites in this lifecycle stage (Gossage et al., 2003; McConville et al., 2007). We gained some assurance that the parasites don't become stained with CellVue Burgundy through the staining of promastigotes but, this does not show that free amastigotes within the sample (that are released from damaged phagosomes) will not be stained. Therefore, to ensure this as part of future experiments using this technique, axenic amastigotes should be stained with CellVue Burgundy, as was performed for the promastigotes (detailed in section 4.4.2). The use of axenic amastigotes, as opposed to amastigotes isolated from *in vivo*, would ensure that the parasite does not have any

phagosomal membrane attached to its surface that may take up the stain and appear as staining of the amastigote itself.

Axenic amastigotes can be cultivated through incubation of promastigotes at specific conditions that replicate the environment of the macrophage, such as increased temperatures at 37°^{c}, decreased pH and 5% CO_2 levels (Bates et al., 1992; Debrabant et al., 2004; Doyle et al., 1991; Gupta et al., 2001, 1999). Different species and strains require different conditions such as growth medium and initial density, with some being more amenable to differentiation than others (Gupta et al., 2001). Typically, *L. donovani* is more difficult to culture as axenic amastigotes, with some strains only surviving short periods of time, often making these amastigotes harder to maintain longer term (Gupta et al., 2001, 1999). However, some studies have shown that specific strains such as 1S-C12 and 1S-2D can be maintained for upwards of a year (Doyle et al., 1991; Gupta et al., 2001). Furthermore, *L. donovani* is less resistant to temperature changes than other species, such as *L. mexicana*, meaning that temperature increase must be done in increments to avoid parasite death (Debrabant et al., 2004). It is also essential that the axenic amastigotes replicate the morphology of the amastigotes that differentiate within the phagosome as closely as possible, to give greater assurance that the membrane stain is behaving in the same manner. Some studies have suggested that the amastigotes formed by *L. donovani* strains LV9, the strain used throughout this project, and DD8 only exhibit 'axenic amastigote-like' phenotypes with some parasites still showing external flagellum despite being a more rounded shape (Debrabant et al., 2004). This indicates that the axenic amastigotes formed by *L. donovani* may not be true amastigotes and may be somewhat morphologically different to amastigotes cultivated *in vivo*, limiting the extrapolation potential of staining these parasites.

Leishmania mexicana is more commonly cultured into axenic amastigotes due to its greater resistance to temperature increase and quicker adaptation to altered conditions (Debrabant et al., 2004). Beyond this, it has also been shown that the strict control of CO_2 levels required for differentiation of other species isn't essential to induce differentiation of *L. mexicana* promastigotes, making them easier to cultivate (Debrabant et al., 2004; Gupta et al., 2001). Studies on *L. mexicana* axenic amastigotes have shown that they display the same critical features found in lesion-isolated amastigotes such as the presence of megasomes (which are not found in promastigotes) and the absence of a paraxial rod (Bates et al., 1992; Gupta et al., 2001). This demonstrates that these axenic amastigotes should behave very similarly to amastigotes differentiated *in vivo* and will offer the most reliable insight as to whether free amastigotes or those released from phagosomes become stained by CellVue Burgundy. This would

confirm with certainty that the TdT^+CVB^+ group after FACS is not contaminated with any free amastigotes that have been stained for future experimentation.

5.1.3.4 CellVue Burgundy staining of inert beads

The use of inert beads to infect macrophages and form phagosomes that contain only host proteins, without any parasites, will be highly valuable for future applications of this work such as identifying host proteins that are specifically induced by *L. donovani* infection (discussed further in section 5.2.1). As with free parasites, it is essential that the inert beads don't become stained with CellVue Burgundy, as this would interfere with the sorting process. Therefore, any selected beads should be stained and imaged prior to use. The fluorescent beads used in the initial macrophage infection experiments were polystyrene with carboxylate surface groups. They lack a lipid bilayer, which should make them incompatible with CellVue Burgundy, as this dye requires insertion into lipid membranes. Nonetheless, studies have shown that CellVue dyes can have complications. For example, the dye can form non-specific aggregates that adhere to inert beads or label other debris in the sample, which could result in free latex beads or debris being sorted into the TdT^+CVB^+ gate during sorting (Dehghani et al., 2020). Additionally, inert beads with surface carboxylate groups or other surface modifications can adsorb the dye, forming a stable association that may retain CellVue Burgundy aggregates (Wang et al., 2018). While the only way to determine definitively how the beads will behave during phagosome isolation is to perform the experiment in full, staining the beads with CellVue Burgundy while they are free from macrophages could provide useful insight into potential complications.

5.2 Future directions

5.2.1 Isolation of inert bead-containing phagosomes

The next steps of utilising this technique will involve proteomic analysis to characterise the protein composition of the *L. donovani* phagosome. Currently, isolation and proteomics of phagosomes containing inert beads e.g. latex or polystyrene has been successful, however this alone does not allow for understanding the interactions between the host and the pathogen during infection (Chatterjee et al., 2025a). Proteomics offers a wide range of data such as protein-protein interactions, protein localisation, protein expression levels and more, all from a single sample (Al-Amrani et al., 2021; Herweg et al., 2015). The key aim of studying the phagosome protein composition is to gain a deeper understanding into the general protein landscape within the phagosome and to recognise host proteins that may be modulated specifically because of *L. donovani* infection. Identifying the key

proteins in pathogen-containing phagosomes may provide critical insight into the recruitment of host proteins during infection, potentially revealing mechanisms that facilitate parasite survival.

To do this, phagosomes that contain inert beads can be used as a comparator for protein data from isolated parasite-containing phagosomes. These phagosomes will not contain parasite proteins and will not recruit host proteins that respond only to infection (Chatterjee et al., 2025a). This allows the identification of host proteins that show parasite-driven changes in expression or localisation, which separates proteins involved in normal phagosome maturation from those altered during infection. This approach can extend to time-point studies that compare bead and parasite phagosomes throughout infection. During infection, *Leishmania* promastigotes modulate phagosome maturation by blocking acidification and delaying the recruitment of key host factors through surface molecules such as LPG (Moradin and Descoteaux, 2012; Vinet et al., 2009; Vinet and Descoteaux, 2010). As the phagosome matures, it acquires endosomal and lysosomal markers and incorporates membrane components from several host pathways, which the parasite continues to modulate (Lang et al., 1994; Lodge and Descoteaux, 2005; McConville and Naderer, 2011). The parasite also differentiates into the amastigote form during this process, which changes its interactions with the host (Dias et al., 2018; Gossage et al., 2003; McConville et al., 2007). A time-course study would allow tracking and investigate of these changes within the phagosome, identifying stage-specific host and parasite proteins that single timepoint measurements would not show. This technique can also be combined with imaging and knockout lines to test whether specific proteins are essential for parasite survival. This technique can further be used to study how host cell origin shapes the phagosome proteome by infecting different macrophage types with both beads and parasites. Research has shown that *L. major* replicates more efficiently in peritoneal macrophages than in bone marrow macrophages and retains LPG for longer in less permissive cells, such as BMDMs (Mandell et al., 2022). These differences are likely driven by changes in host protein expression and localisation during phagosome maturation, with the parasite adapting to the specific host cell type. Inert bead-containing phagosomes provide a clear baseline of protein composition for each macrophage type, showing the proteins recruited for normal maturation. Comparing these baselines with parasite-containing phagosomes can reveal proteins that support faster or slower parasite growth. Overall, bead-containing phagosomes offer a strong reference for interpreting protein changes during infection.

5.2.2 Next steps in proteomic analysis of L. donovani-containing phagosomes

Studies on phagosome proteomics in *Salmonella* Typhimurium have shown the enrichment of particular host proteins e.g. mitochondrial, endosomal and lysosomal during infection as well as the

presence of pathogen-secreted effector proteins that cause this modulation (Chatterjee et al., 2025a). *Salmonella* Typhimurium and *L. donovani* both inhibit ROS build-up to aid survival and it has been shown that the recruitment of mitochondrial-derived vesicles to the phagosome in *Salmonella* Typhimurium infection may support this mechanism (Chatterjee et al., 2025a; Rossi and Fasel, 2018). Therefore, this may be an important set of proteins to pay close attention to in the analysis of proteomic data when using our technique. Moreover, this study also showed that *Salmonella* Typhimurium modulates the recruitment of cathepsins to the phagosome throughout its maturation and it is also known that cathepsin modification takes place within other intracellular infections such as *Coxiella burnetii* (Bird et al., 2025; Chatterjee et al., 2025a). *L. mexicana* has also shown changes in host cathepsin abundance within the phagosome throughout infection, again suggesting that these proteins could be of interest in our proteomics (Bird et al., 2025). These are just two examples of proteins that may elucidate the modulation of host protein recruitment and abundance following *L. donovani* infection; however, proteomic data is likely to reveal many candidate proteins for further investigation.

5.2.3 Opening of phagosome compartments

A final stage in expanding the applications of this technique would be to open the isolated phagosomes to allow removal of the parasite, leaving only host phagosome proteins that have been influenced by the previous presence of infection. This could offer several benefits for proteomic analysis of the phagosomes. Removal of the abundant parasite material in intact amastigotes would allow increased sensitivity for lower abundance proteins within the sample, allowing for the potential discovery of host proteins that would usually be masked by the parasite proteins as well as parasite virulence factors secreted into the phagosome (Real, 2020). By lysing the vacuole and fractionating the contents, it would be possible to separate lumenal proteins from membrane-associated ones, then apply short protease or detergent treatments to infer which host proteins face the cytosol, which are internal, and which span the membrane (Benjamin L. Allsup et al., 2024; Garin et al., 2001). This would allow the proteomic analysis of each of these samples separately to give more detailed information about the compartment localisation of each host protein within the phagosome. This type of data could then offer indication as to the function of each protein based on their localisation and association within the phagosome.

Altogether, opening the isolated phagosome and removing the parasite would provide a more refined host-phagosomal proteome than analysing intact, parasite-containing phagosomes. This deeper resolution could reveal low-abundance host factors, and reveal what proteins are present, as well as

where. This is information that parasite-containing proteomics cannot show. Without opening the vacuole, future experimentation would be limited to a mixed overview of phagosomal protein content that amalgamates lumenal, membrane, and parasite-derived proteins, obscuring key structural and functional insights.

5.3 Benefits of a new approach

Using a combined method of nitrogen cavitation, phagosome membrane staining and FACS provides a practical new way to isolate *L. donovani* phagosomes with higher yield and consistency than earlier methods. Nitrogen cavitation lyses cells through controlled pressure release, which preserves membrane-bound compartments far better than mechanical homogenisation to lyse the phagosome-containing host cell (Gotthardt et al., 2002). Studies using this method have shown improved recovery of intact vesicles and small vacuoles because cavitation avoids the more extreme levels of force that damage the fragile phagosome membranes (Lönnbro et al., 2008; Zhou and Philips, 2017). These advantages directly resolve the issues with the low and inconsistent yields reported in previous work on *L. mexicana* and *L. amazonensis* phagosome isolation, where manual homogenisation often disrupted smaller vacuoles and intact phagosomes (Real, 2020; Semini and Aebischer, 2018). Labelling the phagosome membrane using CellVue Burgundy adds a second selection step to reduce contamination. Fluorescent lipid probes and membrane dyes have been previously used to mark pathogen-containing vacuoles in macrophages, increasing the accuracy of phagosome isolation and help overcome the contamination problems described in earlier Leishmania studies, where gradient-based methods pulled down ER, Golgi and endosomal membranes alongside true parasite-containing phagosomes (Henriques et al., 2003; Steinhäuser et al., 2013). As *L. donovani* forms small, tight vacuoles rather than large communal ones, membrane staining is an important additional step that improves detection and recovery of these small vacuoles. FACS provides a final refining step by sorting phagosomes based on fluorescence intensity and scatter, which increases reproducibility across replicates due to the reproducibility of the gating strategy. Flow-sorting of pathogen-containing vacuoles has been successful in bacterial systems, where it produces high-purity, intact phagosomes suitable for proteomic analysis (Chatterjee et al., 2025a). This differs from earlier Leishmania methods that varied between laboratories and produced datasets with limited comparability (Kima, 2007). The improved reproducibility strengthens the validity of the new workflow and supports reliable downstream analysis.

This new technique also aids easier proteomic analysis compared to older methods utilising gradient fractionation. Gradient systems often mix phagosomes with endosomes or mitochondria because

these compartments have similar densities, which leads to contamination and poor reproducibility (Gotthardt et al., 2002). Our technique increases purity and consistency, which strengthens downstream proteomic analysis. Cleaner isolates reduce background proteins within the sample, supporting accurate identification of host factors recruited to PVs (Hoffmann et al., 2018). Together, nitrogen cavitation, membrane staining and FACS offers a cohesive and repeatable method that can fix the yield problems seen in older studies, reduce contamination and support high-quality phagosome proteomics for *L. donovani*.

5.4 Final remarks

The data in this project has shown that combining nitrogen cavitation, CellVue Burgundy staining and FACS is an effective technique for isolating both the larger *L. mexicana* phagosomes and smaller *L. donovani* phagosomes. Although requiring optimisation to upscale for proteomics and strengthen validation of the phagosome sample, it provides a coherent foundation for a phagosome isolation approach that should work across many *Leishmania* species regardless of vacuole size. This offers researchers a straightforward protocol that can be applied in a consistent way and should support more comparable results across studies. There are many benefits to this for future drug and vaccine development for visceral leishmaniasis.

By isolating intact phagosomes containing *L. donovani* parasites and comparing their proteomes to those of inert-bead phagosomes, this method can unmask the precise host pathways and proteins that the parasite manipulates to offer new targets for host-directed therapies (Semini and Aebischer, 2018). It will also reveal parasite-specific protein recruitments that don't occur in uninfected phagosomes, making it possible to distinguish normal trafficking machinery from infection-driven factors (Ndjamen et al., 2010; Vinet et al., 2009). Furthermore, as proteome composition depends on macrophage type, this approach allows the identification of host-cell specific biomarkers (Mandell et al., 2022). Crucially, detecting parasite proteins through proteomic analysis supports the discovery of potential antigens for vaccine development (Singh et al., 2015; Zaidan et al., 2025). Finally, the use of inert-bead phagosomes as a control reduces false positives and strengthens confidence in candidate proteins, guiding more focussed *in vitro* and *in vivo* validation.

Chapter 6: References

Abadías-Granado, I., Diago, A., Cerro, P.A., Palma-Ruiz, A.M., Gilaberte, Y., 2021. Cutaneous and Mucocutaneous Leishmaniasis. Actas Dermo-Sifiliográficas (English Edition) 112, 601–618.

Aebersold, R., Mann, M., 2016. Mass-spectrometric exploration of proteome structure and function. Nature 537, 347–355.

Al-Amrani, S., Al-Jabri, Z., Al-Zaabi, A., Alshekaili, J., Al-Khabori, M., 2021. Proteomics: Concepts and applications in human medicine. World J Biol Chem 12, 57–69.

Alemu, C., Wudu, H., Dessie, G., Gashu, C., 2023. Time to death and its determinant factors of visceral leishmaniasis with HIV co-infected patients during treatment period admitted at Metema hospital, Metema, Ethiopia: a hospital-based cross-sectional study design. Trop Dis Travel Med Vaccines 9, 18.

Alexander, J., Bryson, K., 2005. T helper (h)1/Th2 and: paradox rather than paradigm. Immunology Letters 99, 17–23.

Al-Khalaifah, H.S., 2022. Major Molecular Factors Related to Leishmania Pathogenicity. Front. Immunol. 13.

Alsagaby, S.A., 2019. Understanding the fundamentals of proteomics. Current Topics in Peptide & Protein Research 20, 25.

Anderson, N.L., Matheson, A.D., Steiner, S., 2000. Proteomics: applications in basic and applied biology. Current Opinion in Biotechnology 11, 408–412.

Arango Duque, G., Fukuda, M., Descoteaux, A., 2013. Synaptotagmin XI Regulates Phagocytosis and Cytokine Secretion in Macrophages. The Journal of Immunology 190, 1737–1745.

Baars, I., Jaedtka, M., Dewitz, L.-A., Fu, Y., Franz, T., Mohr, J., Gintschel, P., Berlin, H., Degen, A., Freier, S., Rygol, S., Schraven, B., Kahlfuß, S., Van Zandbergen, G., Müller, A.J., 2023. Leishmania major drives host phagocyte death and cell-to-cell transfer depending on intracellular pathogen proliferation rate. JCI Insight 8, e169020.

Bates, P.A., Robertson, C.D., Tetley, L., Coombs, G.H., 1992. Axenic cultivation and characterization of Leishmania mexicana amastigote-like forms. Parasitology 105 (Pt 2), 193–202.

Batista, M.F., Nájera, C.A., Meneghelli, I., Bahia, D., 2020. The Parasitic Intracellular Lifestyle of Trypanosomatids: Parasitophorous Vacuole Development and Survival. Front. Cell Dev. Biol. 8, 396.

Beattie, L., Peltan, A., Maroof, A., Kirby, A., Brown, N., Coles, M., Smith, D.F., Kaye, P.M., 2010. Dynamic Imaging of Experimental Leishmania donovani-Induced Hepatic Granulomas Detects Kupffer Cell-Restricted Antigen Presentation to Antigen-Specific CD8+ T Cells. PLoS Pathog 6, e1000805.

Allsup, B., Gharpure, S., Bryan D. Bryson, 2024. Proximity labeling defines the phagosome lumen proteome of murine and primary human macrophages.

Bird, L.E., Xu, B., McGowan, E.N.S., Newton, P., Scott, N.E., McConville, M.J., Edgington-Mitchell, L.E., Newton, H.J., 2025. Intralysosomal pathogens differentially influence the proteolytic potential of their niche.

Birge, R.B., Boeltz, S., Kumar, S., Carlson, J., Wanderley, J., Calianese, D., Barcinski, M., Brekken, R.A., Huang, X., Hutchins, J.T., Freimark, B., Empig, C., Mercer, J., Schroit, A.J., Schett, G., Herrmann, M., 2016. Phosphatidylserine is a global immunosuppressive signal in efferocytosis, infectious disease, and cancer. Cell Death Differ 23, 962–978.

Bogdan, C., Donhauser, N., Döring, R., Röllinghoff, M., Diefenbach, A., Rittig, M.G., 2000. Fibroblasts as Host Cells in Latent Leishmaniosis. The Journal of Experimental Medicine 191, 2121–2130.

Bogdan, C., Islam, N.-A.-K., Barinberg, D., Soulat, D., Schleicher, U., Rai, B., 2024. The immunomicrotope of Leishmania control and persistence. Trends in Parasitology 40, 788–804.

Boggiatto, P.M., Martinez, P.A., Pullikuth, A., Jones, D.E., Bellaire, B., Catling, A., Petersen, C., 2014. Targeted extracellular signal-regulated kinase activation mediated by Leishmania amazonensis requires MP1 scaffold. Microbes and Infection 16, 328–336.

Boitz, J.M., Ullman, B., Jardim, A., Carter, N.S., 2012. Purine salvage in Leishmania: complex or simple by design? Trends in Parasitology 28, 345–352.

Borges, V.M., Vannier-Santos, M.A., De Souza, W., 1998. Subverted transferrin trafficking in Leishmania- infected macrophages. Parasitology Research 84, 811–822.

Burchmore, R.J.S., Barrett, M.P., 2001. Life in vacuoles – nutrient acquisition by Leishmania amastigotes. International Journal for Parasitology 31, 1311–1320.

Campbell-Valois, F.-X., Trost, M., Chemali, M., Dill, B.D., Laplante, A., Duclos, S., Sadeghi, S., Rondeau, C., Morrow, I.C., Bell, C., Gagnon, E., Hatsuzawa, K., Thibault, P., Desjardins, M., 2012. Quantitative Proteomics Reveals That Only a Subset of the Endoplasmic Reticulum Contributes to the Phagosome. Molecular & Cellular Proteomics 11, M111.016378.

Canton, M., Sánchez-Rodríguez, R., Spera, I., Venegas, F.C., Favia, M., Viola, A., Castegna, A., 2021. Reactive Oxygen Species in Macrophages: Sources and Targets. Front Immunol 12, 734229.

Cavalcante-Costa, V.S., Costa-Reginaldo, M., Queiroz-Oliveira, T., Oliveira, A.C.S., Couto, N.F., Dos Anjos, D.O., Lima-Santos, J., Andrade, L.O., Horta, M.F., Castro-Gomes, T., 2019. Leishmania amazonensis hijacks host cell lysosomes involved in plasma membrane repair to induce invasion in fibroblasts. Journal of Cell Science 132, jcs226183.

Chakraborty, P., Sturgill-Koszycki, S., Russell, D.G., 1995. Chapter 14: Isolation and Characterization of Pathogen-Containing Phagosomes, in: Methods in Cell Biology. Elsevier, pp. 261–276.

Chappuis, F., Sundar, S., Hailu, A., Ghalib, H., Rijal, S., Peeling, R.W., Alvar, J., Boelaert, M., 2007. Visceral leishmaniasis: what are the needs for diagnosis, treatment and control? Nat Rev Microbiol 5, 873–882

Chatterjee, R., Marin Rubio, J.L., Cianfanelli, F.R., Frey, A., Raymond, B.B.A., Dannoura, A., Valenzuela, C., Meng, M., Heunis, T., Li, M., Sidgwick, F., Enninga, J., Filby, A., Trost, M., 2025a. Flow cytometry-

based isolation of Salmonella-containing phagosomes combined with ultra-sensitive proteomics reveals novel insights into host-pathogen interactions. bioRxiv 2025.04.25.650444.

Chatterjee, R., Marin Rubio, J.L., Cianfanelli, F.R., Frey, A., Raymond, B.B.A., Meng, M., Dannoura, A., Heunis, T., Li, M., Filby, A., Trost, M., 2025b. Flow cytometry-based isolation combined with ultra-sensitive proteomics of *Salmonella* -containing phagosomes reveals novel insights into host-pathogen interactions.

Clem, A., 2010. A current perspective on leishmaniasis. J Glob Infect Dis 2, 124–126.

Costantini, L.M., Snapp, E.L., 2013. Fluorescent proteins in cellular organelles: serious pitfalls and some solutions. DNA Cell Biol 32, 622–627.

Cox, J., Mann, M., 2011. Quantitative, High-Resolution Proteomics for Data-Driven Systems Biology. Annu. Rev. Biochem. 80, 273–299.

Croft, S.L., Sundar, S., Fairlamb, A.H., 2006. Drug Resistance in Leishmaniasis. Clin Microbiol Rev 19, 111–126.

Cruz, M.G.F. de M.L., Santi, A.M.M., Morais-Teixeira, E. de, Caldeira, A.S.P., Siqueira, E.P. de, Oliveira, E., Alves, T.M. de A., Murta, S.M.F., 2024. Anti-Leishmania compounds can be screened using Leishmania spp. expressing red fluorescence (tdTomato). Antimicrob Agents Chemother 68, e0050923.

Dagley, M.J., Saunders, E.C., Simpson, K.J., McConville, M.J., 2015. High-Content Assay for Measuring Intracellular Growth of *Leishmania* in Human Macrophages. ASSAY and Drug Development Technologies 13, 389–401.

Dantas-Torres, F., 2007. The role of dogs as reservoirs of Leishmania parasites, with emphasis on Leishmania (Leishmania) infantum and Leishmania (Viannia) braziliensis. Veterinary Parasitology 149, 139–146.

David, C.V., Craft, N., 2009. Cutaneous and mucocutaneous leishmaniasis. Dermatologic Therapy 22, 491–502.

De Freitas Balanco, J.M., Costa Moreira, M.E., Bonomo, A., Bozza, P.T., Amarante-Mendes, G., Pirmez, C., Barcinski, M.A., 2001. Apoptotic mimicry by an obligate intracellular parasite downregulates macrophage microbicidal activity. Current Biology 11, 1870–1873.

De Oca, M.M., Dey, S., Van Bocxlaer, K., Ashwin, H., Brown, N., Myburgh, E., Dey, N.S., Rani, G.F., Muscutt, E., Osman, M., Perez-Mazliah, D., James, S., Gilbert, L., Chatterjee, M., Kaye, P.M., 2023. UVB modifies skin immune-stroma cross-talk and promotes effector T cell recruitment during cryptic Leishmania donovani infection.

De Oliveira, B., Goes, W.M., Nascimento, F.C., Carnielli, J.B.T., Ferreira, E.R., De Carvalho, A.F., Dos Reis, P.V.M., Pereira, M., Ricotta, T.Q.N., Dos Santos, L.M., De Souza, R.P., Cargnelutti, D.E., Mottram, J.C., Teixeira, S.R., Fernandes, A.P., Gazzinelli, R.T., 2025. Characterization of a novel Leishmania antigen containing a repetitive domain and its potential use as a prophylactic and therapeutic vaccine. mSphere 10, e00097-25.

De Rezende, E., Kawahara, R., Peña, M.S., Palmisano, G., Stolf, B.S., 2017. Quantitative proteomic analysis of amastigotes from Leishmania (L.) amazonensis LV79 and PH8 strains reveals molecular traits associated with the virulence phenotype. PLoS Negl Trop Dis 11, e0006090.

Debrabant, A., Joshi, M.B., Pimenta, P.F.P., Dwyer, D.M., 2004. Generation of Leishmania donovani axenic amastigotes: their growth and biological characteristics. International Journal for Parasitology 34, 205–217.

Dehghani, M., Gulvin, S.M., Flax, J., Gaborski, T.R., 2020. Systematic Evaluation of PKH Labelling on Extracellular Vesicle Size by Nanoparticle Tracking Analysis. Sci Rep 10, 9533.

Dias, B.R.S., De Souza, C.S., Almeida, N.D.J., Lima, J.G.B., Fukutani, K.F., Dos Santos, T.B.S., França-Cost, J., Brodskyn, C.I., De Menezes, J.P.B., Colombo, M.I., Veras, P.S.T., 2018. Autophagic Induction Greatly Enhances Leishmania major Intracellular Survival Compared to Leishmania amazonensis in CBA/j-Infected Macrophages. Front. Microbiol. 9, 1890.

Dirkx, L., Hendrickx, S., Merlot, M., Bulté, D., Starick, M., Elst, J., Bafica, A., Ebo, D.G., Maes, L., Van Weyenbergh, J., Caljon, G., 2022. Long-term hematopoietic stem cells as a parasite niche during treatment failure in visceral leishmaniasis. Commun Biol 5, 626.

Dirkx, L., Van Acker, S.I., Nicolaes, Y., Cunha, J.L.R., Ahmad, R., Hendrickx, R., Caljon, B., Imamura, H., Ebo, D.G., Jeffares, D.C., Sterckx, Y.G.-J., Maes, L., Hendrickx, S., Caljon, G., 2024. Long-term hematopoietic stem cells trigger quiescence in Leishmania parasites. PLoS Pathog 20, e1012181.

Dostálová, A., Volf, P., 2012. Leishmania development in sand flies: parasite-vector interactions overview. Parasites Vectors 5, 276.

Doyle, P.S., Engel, J.C., Pimenta, P.F., P. P. da Silva, Dwyer, D.M., 1991. Leishmania donovani: long-term culture of axenic amastigotes at 37 degrees C. Exp Parasitol 73, 326–334.

Dunkelberger, J.R., Song, W.-C., 2010. Complement and its role in innate and adaptive immune responses. Cell Res 20, 34–50.

Elfaki, N., Alzahrani, M.J., Abdalla, Y., Adeh, A.I., Osman Abdalla, A., Alkhadher, M., Elrefaey, S.R., Abdelmagid, W.H.H., Alshameri, F., Jarelnape, A., Hakami, M., Alghamdi, F.A.A., Elhaj, Y., Dinar, N., Mohamed, A., Abdulrahman, E., Mohamed, D.H.M., Sagiron, E., Ali, M.H., Ahmed, W.A., 2024. Perceived Social Stigma of Cutaneous Leishmaniasis in Hubuna, Saudi Arabia. JMDH Volume 17, 867–876.

Fernandes, M.C., Cortez, M., Flannery, A.R., Tam, C., Mortara, R.A., Andrews, N.W., 2011. Trypanosoma cruzi subverts the sphingomyelinase-mediated plasma membrane repair pathway for cell invasion. Journal of Experimental Medicine 208, 909–921.

Ferreira, C., Estaquier, J., Silvestre, R., 2021. Immune-metabolic interactions between Leishmania and macrophage host. Current Opinion in Microbiology 63, 231–237.

Ferroglio, E., Battisti, E., Zanet, S., Bolla, C., Concialdi, E., Trisciuoglio, A., Khalili, S., Biglino, A., 2018. Epidemiological evaluation of *Leishmania infantum* zoonotic transmission risk in the recently established endemic area of Northwestern Italy. Zoonoses and Public Health 65, 675–682.

Frey, R.S., Ushio-Fukai, M., Malik, A.B., 2009. NADPH oxidase-dependent signaling in endothelial cells: role in physiology and pathophysiology. Antioxid Redox Signal 11, 791–810.

Frézard, F., Aguiar, M.M.G., Ferreira, L.A.M., Ramos, G.S., Santos, T.T., Borges, G.S.M., Vallejos, V.M.R., De Morais, H.L.O., 2022. Liposomal Amphotericin B for Treatment of Leishmaniasis: From the Identification of Critical Physicochemical Attributes to the Design of Effective Topical and Oral Formulations. Pharmaceutics 15, 99.

Garin, J., Diez, R., Kieffer, S., Dermine, J.F., Duclos, S., Gagnon, E., Sadoul, R., Rondeau, C., Desjardins, M., 2001. The phagosome proteome: insight into phagosome functions. J Cell Biol 152, 165–180.

Gioseffi, A., Hamerly, T., Van, K., Zhang, N., Dinglasan, R.R., Yates, P.A., Kima, P.E., 2020. *Leishmania* - infected macrophages release extracellular vesicles that can promote lesion development. Life Sci. Alliance 3, e202000742.

Glaser, T.A., Baatz, J.E., Kreishman, G.P., Mukkada, A.J., 1988. pH homeostasis in Leishmania donovani amastigotes and promastigotes. Proc Natl Acad Sci U S A 85, 7602–7606.

Gomez, M.A., Contreras, I., Hallé, M., Tremblay, M.L., McMaster, R.W., Olivier, M., 2009. Leishmania GP63 Alters Host Signaling Through Cleavage-Activated Protein Tyrosine Phosphatases. Sci. Signal. 2.

Gossage, S.M., Rogers, M.E., Bates, P.A., 2003. Two separate growth phases during the development of Leishmania in sand flies: implications for understanding the life cycle. International Journal for Parasitology 33, 1027–1034.

Goto, H., 2012. Review of the current treatments for leishmaniases. RRTM 69.

Goto, H., Lindoso, J.A.L., 2004. Immunity and immunosuppression in experimental visceral leishmaniasis. Braz J Med Biol Res 37, 615–623.

Goto, Y., 2025. Immunomodulation by Leishmania parasites: Potential for controlling other diseases. Parasitology International 104, 102987.

Gotthardt, D., Warnatz, H.J., Henschel, O., Brückert, F., Schleicher, M., Soldati, T., 2002. High-resolution dissection of phagosome maturation reveals distinct membrane trafficking phases. Mol Biol Cell 13, 3508–3520.

Gradoni, L., 2018. A Brief Introduction to Leishmaniasis Epidemiology. The Leishmaniases: Old Neglected Tropical Diseases 1–13.

Gupta, G., Oghumu, S., Satoskar, A.R., 2013. Mechanisms of Immune Evasion in Leishmaniasis, in: Advances in Applied Microbiology. Elsevier, pp. 155–184.

Gupta, N., Goyal, N., Rastogi, A.K., 2001. In vitro cultivation and characterization of axenic amastigotes of Leishmania. Trends Parasitol 17, 150–153.

Gupta, N., Goyal, N., Singha, U.K., Bhakuni, V., Roy, R., Rastogi, A.K., 1999. Characterization of intracellular metabolites of axenic amastigotes of Leishmania donovani by 1H NMR spectroscopy. Acta Trop 73, 121–133.

Gurjar, D., Bodhale, N., Shukla, D., Nayak, D., Lenka, N., Saha, B., 2025. Manipulation of macrophage signaling by Leishmania virulence factors. Virulence 16, 2549802.

Handman, E., Bullen, D.V.R., 2002. Interaction of Leishmania with the host macrophage. Trends in Parasitology 18, 332–334.

Henriques, C., Atella, G., Bonilha, V.L., de Souza, W., 2003. Biochemical analysis of proteins and lipids found in parasitophorous vacuoles containing Leishmania amazonensis. Parasitology Research 89, 123–133.

Herwaldt, B.L., Berman, J.D., 1992. Recommendations for Treating Leishmaniasis with Sodium Stibogluconate (Pentostam) and Review of Pertinent Clinical Studies. The American Journal of Tropical Medicine and Hygiene 46, 296–306.

Herweg, J.-A., Hansmeier, N., Otto, A., Geffken, A.C., Subbarayal, P., Prusty, B.K., Becher, D., Hensel, M., Schaible, U.E., Rudel, T., Hilbi, H., 2015. Purification and proteomics of pathogen-modified vacuoles and membranes. Front Cell Infect Microbiol 5, 48.

Hoffmann, E., Machelart, A., Song, O.-R., Brodin, P., 2018. Proteomics of Mycobacterium Infection: Moving towards a Better Understanding of Pathogen-Driven Immunomodulation. Front. Immunol. 9, 86.

Hostettler, L., Grundy, L., Käser-Pébernard, S., Wicky, C., Schafer, W.R., Glauser, D.A., 2017. The Bright Fluorescent Protein mNeonGreen Facilitates Protein Expression Analysis *In Vivo*. G3 Genes|Genomes|Genetics 7, 607–615.

Howell, J., Omwenga, S., Jimenez, M., Hammarton, T.C., 2024. Analysis of the Leishmania mexicana promastigote cell cycle using imaging flow cytometry provides new insights into cell cycle flexibility and events of short duration. PLoS One 19, e0311367.

Hurrell, B.P., Beaumann, M., Heyde, S., Regli, I.B., Müller, A.J., Tacchini-Cottier, F., 2017. Frontline Science: *Leishmania mexicana* amastigotes can replicate within neutrophils. Journal of Leukocyte Biology 102, 1187–1198.

Huynh, K.K., Eskelinen, E.-L., Scott, C.C., Malevanets, A., Saftig, P., Grinstein, S., 2007. LAMP proteins are required for fusion of lysosomes with phagosomes. EMBO J 26, 313–324.

Ilg, T., 2000. Lipophosphoglycan is not required for infection of macrophages or mice by Leishmania mexicana. EMBO J 19, 1953–1962.
Isnard, A., Shio, M.T., Olivier, M., 2012. Impact of Leishmania metalloprotease GP63 on macrophage signaling. Front. Cell. Inf. Microbio. 2.

Jara, M., Berg, M., Caljon, G., de Muylder, G., Cuypers, B., Castillo, D., Maes, I., Orozco, M.D.C., Vanaerschot, M., Dujardin, J.-C., Arevalo, J., 2017. Macromolecular biosynthetic parameters and metabolic profile in different life stages of Leishmania braziliensis: Amastigotes as a functionally less active stage. PLoS One 12, e0180532.

Kima, P.E., 2007. The amastigote forms of Leishmania are experts at exploiting host cell processes to establish infection and persist. International Journal for Parasitology 37, 1087–1096.

Kima, P.E., Dunn, W., 2005. Exploiting calnexin expression on phagosomes to isolate Leishmania parasitophorous vacuoles. Microbial Pathogenesis 38, 139–145.

Kloehn, J., Saunders, E.C., O'Callaghan, S., Dagley, M.J., McConville, M.J., 2015. Characterization of Metabolically Quiescent Leishmania Parasites in Murine Lesions Using Heavy Water Labeling. PLoS Pathog 11, e1004683.

Körner, U., Fuss, V., Steigerwald, J., Moll, H., 2006. Biogenesis of *Leishmania major* -Harboring Vacuoles in Murine Dendritic Cells. Infect Immun 74, 1305–1312.

Kumar, R., Nylén, S., 2012. Immunobiology of visceral leishmaniasis. Front. Immun. 3.

Kumar, V., Bimal, S., Singh, S.K., Chaudhary, R., Das, S., Lal, C., Pandey, K., Das, V.R., Das, P., 2014. Leishmania donovani: Dynamics of L. donovani evasion of innate immune cell attack due to malnutrition in visceral leishmaniasis. Nutrition 30, 449–458.

Landfear, S.M., 2011. Nutrient Transport and Pathogenesis in Selected Parasitic Protozoa. Eukaryot Cell 10, 483–493.

Lang, T., Hellio, R., Kaye, P.M., Antoine, J.-C., 1994. *Leishmania donovani-infected* macrophages: characterization of the parasitophorous vacuole and potential role of this organelle in antigen presentation. Journal of Cell Science 107, 2137–2150.

Liévin-Le Moal, V., Loiseau, P.M., 2016. *Leishmania* hijacking of the macrophage intracellular compartments. The FEBS Journal 283, 598–607.

Lodge, R., Descoteaux, A., 2006. Phagocytosis of *Leishmania donovani* amastigotes is Rac1 dependent and occurs in the absence of NADPH oxidase activation. Eur J Immunol 36, 2735–2744.

Lodge, R., Descoteaux, A., 2005. Modulation of phagolysosome biogenesis by the lipophosphoglycan of Leishmania. Clinical Immunology 114, 256–265.

Lönnbro, P., Nordenfelt, P., Tapper, H., 2008. Isolation of bacteria-containing phagosomes by magnetic selection. BMC Cell Biol 9, 35.

Lysenko, A.J., 1971. Distribution of leishmaniasis in the Old World. Bull World Health Organ 44, 515–520.

Magalhães, L.S., Bomfim, L.G., Mota, S.G., Cruz, G.S., Corrêa, C.B., Tanajura, D.M., Lipscomb, M.W., Borges, V.M., Jesus, A.R. de, Almeida, R.P. de, Moura, T.R. de, 2018. Increased thiol levels in antimony-resistant Leishmania infantum isolated from treatment-refractory visceral leishmaniasis in Brazil. Mem Inst Oswaldo Cruz 113, 119–125.

Mandell, M.A., Beatty, W.L., Beverley, S.M., 2022. Quantitative single-cell analysis of Leishmania major amastigote differentiation demonstrates variably extended expression of the lipophosphoglycan (LPG) virulence factor in different host cell types. PLoS Negl Trop Dis 16, e0010893.

Mandell, M.A., Beverley, S.M., 2017. Continual renewal and replication of persistent *Leishmania major* parasites in concomitantly immune hosts. Proc. Natl. Acad. Sci. U.S.A. 114.

Mann, S., Frasca, K., Scherrer, S., Henao-Martínez, A.F., Newman, S., Ramanan, P., Suarez, J.A., 2021. A Review of Leishmaniasis: Current Knowledge and Future Directions. Curr Trop Med Rep 8, 121–132.

Marecic, V., Shevchuk, O., Ozanic, M., Mihelcic, M., Steinert, M., Jurak Begonja, A., Abu Kwaik, Y., Santic, M., 2017. Isolation of F. novicida-Containing Phagosome from Infected Human Monocyte Derived Macrophages. Front. Cell. Infect. Microbiol. 7, 303.

Martínez-López, M., Soto, M., Iborra, S., Sancho, D., 2018. Leishmania Hijacks Myeloid Cells for Immune Escape. Front. Microbiol. 9, 883.

Mayle, K.M., Le, A.M., Kamei, D.T., 2012. The intracellular trafficking pathway of transferrin. Biochimica et Biophysica Acta (BBA) - General Subjects 1820, 264–281.

McConville, M.J., De Souza, D., Saunders, E., Likic, V.A., Naderer, T., 2007. Living in a phagolysosome; metabolism of Leishmania amastigotes. Trends in Parasitology 23, 368–375.

McConville, M.J., Naderer, T., 2011. Metabolic Pathways Required for the Intracellular Survival of *Leishmania*. Annu. Rev. Microbiol. 65, 543–561.

McConville, M.J., Saunders, E.C., Kloehn, J., Dagley, M.J., 2015. Leishmania carbon metabolism in the macrophage phagolysosome- feast or famine? F1000Res 4, 938.

McConville, M.J., Turco, S.J., Ferguson, M.A., Sacks, D.L., 1992. Developmental modification of lipophosphoglycan during the differentiation of Leishmania major promastigotes to an infectious stage. EMBO J 11, 3593–3600.

Moradimotlagh, A., Chen, S., Koohbor, S., Moon, K.-M., Foster, L.J., Reiner, N., Nandan, D., 2023. Leishmania infection upregulates and engages host macrophage Argonaute 1, and system-wide proteomics reveals Argonaute 1-dependent host response. Front. Immunol. 14, 1287539.

Moradin, N., Descoteaux, A., 2012. Leishmania promastigotes: building a safe niche within macrophages. Front Cell Infect Microbiol 2, 121.

Moreira, D., Rodrigues, V., Abengozar, M., Rivas, L., Rial, E., Laforge, M., Li, X., Foretz, M., Viollet, B., Estaquier, J., Cordeiro da Silva, A., Silvestre, R., 2015. Leishmania infantum modulates host macrophage mitochondrial metabolism by hijacking the SIRT1-AMPK axis. PLoS Pathog 11, e1004684.

Morris, L., Klanke, C., Lang, S., Lim, F.-Y., Crombleholme, T., 2010. TdTomato and EGFP identification in histological sections: insight and alternatives. Biotechnic & Histochemistry 85, 379–387.

Mougneau, E., Bihl, F., Glaichenhaus, N., 2011. Cell biology and immunology of *Leishmania*. Immunological Reviews 240, 286–296.

Mukherjee, A., Padmanabhan, P.K., Singh, S., Roy, G., Girard, I., Chatterjee, M., Ouellette, M., Madhubala, R., 2006. Role of ABC transporter MRPA, -glutamylcysteine synthetase and ornithine decarboxylase in natural antimony-resistant isolates of Leishmania donovani. Journal of Antimicrobial Chemotherapy 59, 204–211.

Mutiso, J.M., Macharia, J.C., Kiio, M.N., Ichagichu, J.M., Rikoi, H., Gicheru, M.M., 2013. Development of Leishmania vaccines: predicting the future from past and present experience. J Biomed Res 27, 85–102.

Naderer, T., McConville, M.J., 2007. The Leishmania-macrophage interaction: a metabolic perspective: Leishmania metabolism in macrophages. Cellular Microbiology 10, 301–308.

Ndjamen, B., Kang, B.-H., Hatsuzawa, K., Kima, P.E., 2010. Leishmania parasitophorous vacuoles interact continuously with the host cell's endoplasmic reticulum; parasitophorous vacuoles are hybrid compartments. Cell Microbiol 12, 1480–1494.

Okwor, I., Uzonna, J., 2016. Social and Economic Burden of Human Leishmaniasis. Am J Trop Med Hyg 94, 489–493.

Olivier, M., Atayde, V.D., Isnard, A., Hassani, K., Shio, M.T., 2012. Leishmania virulence factors: focus on the metalloprotease GP63. Microbes and Infection 14, 1377–1389.

Ornellas-Garcia, U., Cuervo, P., Ribeiro-Gomes, F.L., 2023. Malaria and leishmaniasis: Updates on co-infection. Front. Immunol. 14, 1122411.

Pace, D., 2014. Leishmaniasis. Journal of Infection 69, S10–S18.

Panahi, E., I. Stanisic, D., S. Peacock, C., J. Herrero, L., 2022. Protective and Pathogenic Immune Responses to Cutaneous Leishmaniasis, in: De Azevedo Calderonon, L. (Ed.), Leishmaniasis - General Aspects of a Stigmatized Disease. IntechOpen.

Paterou, A., Sáez Conde, J., Týč, J., Sunter, J.D., Vaughan, S., Gull, K., Dean, S., 2025. A comprehensive toolkit for protein localization and functional analysis in trypanosomatids. Open Biol. 15, 240361.

Perezvictoria, F., Sanchezcanete, M., Seifert, K., Croft, S., Sundar, S., Castanys, S., Gamarro, F., 2006. Mechanisms of experimental resistance of Leishmania to miltefosine: Implications for clinical use. Drug Resistance Updates 9, 26–39.

Piscopo, T.V., Mallia Azzopardi, C., 2007. Leishmaniasis. Postgrad Med J 83, 649–657.

Podinovskaia, M., Descoteaux, A., 2015. *Leishmania* and the Macrophage: A Multifaceted Interaction. Future Microbiol. 10, 111–129.

Ponte-Sucre, A., Gamarro, F., Dujardin, J.-C., Barrett, M.P., López-Vélez, R., García-Hernández, R., Pountain, A.W., Mwenechanya, R., Papadopoulou, B., 2017. Drug resistance and treatment failure in leishmaniasis: A 21st century challenge. PLoS Negl Trop Dis 11, e0006052.
Ready, P., 2014. Epidemiology of visceral leishmaniasis. CLEP 147.

Real, F., 2020. Isolation of intact Leishmania amazonensis large parasitophorous vacuoles from infected macrophages by density gradient fractionation. Exp Parasitol 218, 107989.

Real, F., Mortara, R.A., 2012. The Diverse and Dynamic Nature of Leishmania Parasitophorous Vacuoles Studied by Multidimensional Imaging. PLoS Negl Trop Dis 6, e1518.

Roatt, B.M., De Oliveira Cardoso, J.M., De Brito, R.C.F., Coura-Vital, W., De Oliveira Aguiar-Soares, R.D., Reis, A.B., 2020. Recent advances and new strategies on leishmaniasis treatment. Appl Microbiol Biotechnol 104, 8965–8977.

Rodríguez, N.E., Gaur Dixit, U., Allen, L.-A.H., Wilson, M.E., 2011. Stage-Specific Pathways of Leishmania infantum chagasi Entry and Phagosome Maturation in Macrophages. PLoS ONE 6, e19000.

Rossi, M., Fasel, N., 2018. How to master the host immune system? *Leishmania* parasites have the solutions! International Immunology 30, 103–111.

Russell, D.G., 2001. Mycobacterium tuberculosis: here today, and here tomorrow. Nat Rev Mol Cell Biol 2, 569–578.

Sacks, D.L., Modi, G., Rowton, E., Späth, G., Epstein, L., Turco, S.J., Beverley, S.M., 2000. The role of phosphoglycans in Leishmania-sand fly interactions. Proc Natl Acad Sci U S A 97, 406–411.

Sanchiz, Á., Morato, E., Rastrojo, A., Camacho, E., González-de la Fuente, S.G. la, Marina, A., Aguado, B., Requena, J.M., 2020. The Experimental Proteome of Leishmania infantum Promastigote and Its Usefulness for Improving Gene Annotations. Genes (Basel) 11, 1036.

Santos, D.O., Coutinho, C.E.R., Madeira, M.F., Bottino, C.G., Vieira, R.T., Nascimento, S.B., Bernardino, A., Bourguignon, S.C., Corte-Real, S., Pinho, R.T., Rodrigues, C.R., Castro, H.C., 2008. Leishmaniasis treatment—a challenge that remains: a review. Parasitol Res 103, 1–10.

Sarkar, A., Mandal, G., Singh, N., Sundar, S., Chatterjee, M., 2009. Flow cytometric determination of intracellular non-protein thiols in Leishmania promastigotes using 5-chloromethyl fluorescein diacetate. Experimental Parasitology 122, 299–305.

Sasidharan, S., Saudagar, P., 2021. Leishmaniasis: where are we and where are we heading? Parasitol Res 120, 1541–1554.

Saunders, C., 2016. Characterising the association of CCR5 with Leishmania donovani infection and the protein composition of the Leishmania-containing intracellular phagolysosome. PhD thesis, University of York.

Schneider, P., Rosat, J.P., Ransijn, A., Ferguson, M.A., McConville, M.J., 1993. Characterization of glycoinositol phospholipids in the amastigote stage of the protozoan parasite Leishmania major. Biochem J 295 (Pt 2), 555–564.

Schwing, A., Pisani, D.F., Pomares, C., Majoor, A., Lacas-Gervais, S., Jager, J., Lemichez, E., Marty, P., Boyer, L., Michel, G., 2021. Identification of adipocytes as target cells for Leishmania infantum parasites. Sci Rep 11, 21275.

Séguin, O., Descoteaux, A., 2016. Leishmania, the phagosome, and host responses: The journey of a parasite. Cellular Immunology 309, 1–6.

Semini, G., Aebischer, T., 2018. Phagosome proteomics to study Leishmania's intracellular niche in macrophages. International Journal of Medical Microbiology 308, 68–76.

Shadab, Md., Ali, N., 2011. Evasion of Host Defence by *Leishmania donovani* : Subversion of Signaling Pathways. Molecular Biology International 2011, 1–10.

Shaner, N.C., Steinbach, P.A., Tsien, R.Y., 2005. A guide to choosing fluorescent proteins. Nat Methods 2, 905–909.

Shevchuk, O., Batzilla, C., Hägele, S., Kusch, H., Engelmann, S., Hecker, M., Haas, A., Heuner, K., Glöckner, G., Steinert, M., 2009. Proteomic analysis of Legionella-containing phagosomes isolated from Dictyostelium. International Journal of Medical Microbiology 299, 489–508.

Shweash, M., Adrienne McGachy, H., Schroeder, J., Neamatallah, T., Bryant, C.E., Millington, O., Mottram, J.C., Alexander, J., Plevin, R., 2011. Leishmania mexicana promastigotes inhibit macrophage IL-12 production via TLR-4 dependent COX-2, iNOS and arginase-1 expression. Molecular Immunology 48, 1800–1808.

Silva, A.M., Cordeiro-da-Silva, A., Coombs, G.H., 2011. Metabolic variation during development in culture of Leishmania donovani promastigotes. PLoS Negl Trop Dis 5, e1451.

Singh, A.K., Pandey, R.K., Siqueira-Neto, J.L., Kwon, Y.-J., Freitas-Junior, L.H., Shaha, C., Madhubala, R., 2015. Proteomic-Based Approach To Gain Insight into Reprogramming of THP-1 Cells Exposed to Leishmania donovani over an Early Temporal Window. Infect Immun 83, 1853–1868.

Singh, N., Mishra, J., Singh, R., Singh, S., 2013. Animal Reservoirs of Visceral Leishmaniasis in India. Journal of Parasitology 99, 64–67.

Soysa, R., Tran, K.D., Ullman, B., Yates, P.A., 2015. Integrating ribosomal promoter vectors that offer a choice of constitutive expression profiles in Leishmania donovani. Mol Biochem Parasitol 204, 89–92.

Späth, G.F., Epstein, L., Leader, B., Singer, S.M., Avila, H.A., Turco, S.J., Beverley, S.M., 2000. Lipophosphoglycan is a virulence factor distinct from related glycoconjugates in the protozoan parasite *Leishmania major*. Proc. Natl. Acad. Sci. U.S.A. 97, 9258–9263.

Späth, G.F., Garraway, L.A., Turco, S.J., Beverley, S.M., 2003. The role(s) of lipophosphoglycan (LPG) in the establishment of Leishmania major infections in mammalian hosts. Proc Natl Acad Sci U S A 100, 9536–9541.

Srivastava, P., Dayama, A., Mehrotra, S., Sundar, S., 2011. Diagnosis of visceral leishmaniasis. Transactions of the Royal Society of Tropical Medicine and Hygiene 105, 1–6.

Steiert, F., Petrov, E.P., Schultz, P., Schwille, P., Weidemann, T., 2018. Photophysical Behavior of mNeonGreen, an Evolutionarily Distant Green Fluorescent Protein. Biophysical Journal 114, 2419–2431.

Steinhäuser, C., Heigl, U., Tchikov, V., Schwarz, J., Gutsmann, T., Seeger, K., Brandenburg, J., Fritsch, J., Schroeder, J., Wiesmüller, K., Rosenkrands, I., Walther, P., Pott, J., Krause, E., Ehlers, S., Schneider-Brachert, W., Schütze, S., Reiling, N., 2013. Lipid-Labeling Facilitates a Novel Magnetic Isolation Procedure to Characterize Pathogen-Containing Phagosomes. Traffic 14, 321–336.

Stockmar, I., Feddersen, H., Cramer, K., Gruber, S., Jung, K., Bramkamp, M., Shin, J.Y., 2018. Optimization of sample preparation and green color imaging using the mNeonGreen fluorescent protein in bacterial cells for photoactivated localization microscopy. Sci Rep 8,

Subramanian, A., Sarkar, R.R., 2015. Comparison of codon usage bias across Leishmania and Trypanosomatids to understand mRNA secondary structure, relative protein abundance and pathway functions. Genomics 106, 232–241.

Sunyoto, T., Boelaert, M., Meheus, F., 2019. Understanding the economic impact of leishmaniasis on households in endemic countries: a systematic review. Expert Review of Anti-infective Therapy 17, 57–69.

Thomas, S.A., Nandan, D., Kass, J., Reiner, N.E., 2018. Countervailing, time-dependent effects on host autophagy promote intracellular survival of Leishmania. Journal of Biological Chemistry 293, 2617–2630.

Tobin Magle, C., Pittman, K.J., Moser, L.A., Boldon, K.M., Knoll, L.J., 2014. A toxoplasma patatin-like protein changes localization and alters the cytokine response during toxoplasmic encephalitis. Infect Immun 82, 618–625.

Torres-Guerrero, E., Quintanilla-Cedillo, M.R., Ruiz-Esmenjaud, J., Arenas, R., 2017. Leishmaniasis: a review. F1000Res 6, 750.

Trost, M., English, L., Lemieux, S., Courcelles, M., Desjardins, M., Thibault, P., 2009. The phagosomal proteome in interferon-gamma-activated macrophages. Immunity 30, 143–154.

Tsigankov, P., Gherardini, P.F., Helmer-Citterich, M., Späth, G.F., Zilberstein, D., 2013. Phosphoproteomic Analysis of Differentiating *Leishmania* Parasites Reveals a Unique Stage-Specific Phosphorylation Motif. J. Proteome Res. 12, 3405–3412.

Valigurová, A., Kolářová, I., 2023. Unrevealing the Mystery of Latent Leishmaniasis: What Cells Can Host Leishmania? Pathogens 12, 246.

Van Griensven, J., Carrillo, E., López-Vélez, R., Lynen, L., Moreno, J., 2014. Leishmaniasis in immunosuppressed individuals. Clinical Microbiology and Infection 20, 286–299.

Van Griensven, J., Diro, E., 2012. Visceral Leishmaniasis. Infectious Disease Clinics of North America 26, 309–322.

Vinet, A.F., Descoteaux, A., 2010. Leishmania donovani delays phagolysosomal acidification. Med Sci (Paris) 26, 227–228.

Vinet, A.F., Fukuda, M., Turco, S.J., Descoteaux, A., 2009. The Leishmania donovani Lipophosphoglycan Excludes the Vesicular Proton-ATPase from Phagosomes by Impairing the Recruitment of Synaptotagmin V. PLoS Pathog 5, e1000628.

Vinet, A.F., Jananji, S., Turco, S.J., Fukuda, M., Descoteaux, A., 2011. Exclusion of synaptotagmin V at the phagocytic cup by Leishmania donovani lipophosphoglycan results in decreased promastigote internalization. Microbiology 157, 2619–2628.

Vitzthum, F., Behrens, F., Anderson, N.L., Shaw, J.H., 2005. Proteomics: From Basic Research to Diagnostic Application. A Review of Requirements & Needs. J. Proteome Res. 4, 1086–1097.

Wanderley, J.L.M., Thorpe, P.E., Barcinski, M.A., Soong, L., 2013. Phosphatidylserine exposure on the surface of *L eishmania amazonensis* amastigotes modulates *in vivo* infection and dendritic cell function. Parasite Immunology 35, 109–119.

Wang, L., Xie, X., Cao, T., Bosset, J., Bakker, E., 2018. Surface-Doped Polystyrene Microsensors Containing Lipophilic Solvatochromic Dye Transducers. Chemistry 24, 7921–7925.

Werner, A., Otte, K.L., Stahlhut, G., Pöggeler, S., 2020. Establishment of the monomeric yellow-green fluorescent protein mNeonGreen for life cell imaging in mycelial fungi. AMB Expr 10, 222.

Yeshaw, Y., Tsegaye, A.T., Nigatu, S.G., 2020. Incidence of Mortality and Its Predictors Among Adult Visceral Leishmaniasis Patients at the University of Gondar Hospital: A Retrospective Cohort Study. Infect Drug Resist 13, 881–891.

Zaidan, A.L., Grossi de Oliveira, A.L., Brito, R.M. de M., Bueno, L.L., Oliveira, F.M.S., Fujiwara, R.T., 2025. Evaluation of MHC class I-binding peptides from Leishmania spp. for vaccine development against visceral leishmaniasis. Vaccine 62, 127531.

Zhou, M., Philips, M.R., 2017. Nitrogen Cavitation and Differential Centrifugation Allows for Monitoring the Distribution of Peripheral Membrane Proteins in Cultured Cells. J Vis Exp 56037.

Zilberstein, D., 2021. Lysosome Sensing Is a Key Mechanism in Leishmania Intracellular Development. Front. Microbiol. 12, 667807.

Zubarev, R.A., 2013. The challenge of the proteome dynamic range and its implications for in-depth proteomics. Proteomics 13, 723–726.

Chapter 7: Appendix

7.1 mNeonGreen plasmid pGL3093 full DNA sequence

TGAGGCCGGGCTGGCCAGATCTCCATCGATAGGACGTCGAGGAGTACTAAGGTAGACTCGTGCCGCGCGCTGA
TGATGTAGGTGCACGCGTGCGTGTGCTGCAGCGGAGCCGCCGCCACCGCGACTGTGTGTGTGTGTGCGCGCGT
GACGACCGGCTCGAGGAAGGAGGAGCGCGCGTGTGCGTGCGATGCGCCTCCTCTTTTTTTTTTTCGCCCTCGTC
GGTTTTTTTTTTTCTGAGAGGACGGCGGCGGCGGATGGCGGGGCGGCGGCGCTGACGGAGCGGCCACGCTCT
GCACCTCCCCGCCCTCCGCCGTCTCTCCGTTCGCCGTCCTCTCCTTCCTCGTGCGTGCGTCTGCCGCGCATGCACA
CGCGCGCGCGTTGCCGTAGCGCTGTGTATCTGTGGAGGAGGGCCTTGTCTCTCCCTCCCCGTCGCTGAGAGATG
AAGGGGCAAAAAGAGAGAGCAGTGCGCATGTGTGCCTCCGCTCCCTGGAGCTCCCCACGAGCCCCCTGCGCCA
CGCACCTGCGAACCTGCACAGCGGCCCACCTGCCCGCACACGTGAGCAGAAATGGGTGTGTGGAGCGGGTGA
TGTCGGCGCGCACACGCGCGCGCGCTGACCACTCCGACGTGAAAACACGGAAGAGCGAGGCTGGCAAGGCA
GGGCAGGAACCTGATCACGTGCGCGCGCACAAACGGAATGAGCAGCTCCTGAAGAGGAGATGGGGCTCATGC
ACGCAGACACGCACGTGCACACTCCTCCGTCTTCACGGAGCGCGGCCCTGCTGCTGCTGCCATGTGCCGGACGT
CTGCCACGCGTCTCTTCCCCACACCTTGCTCTTCCCCCCCCCTTCCCTCCCGGCGAACACAAAACACGCGCACGC
CCACCGAAACAACAACGCGCAGCTCTTCGCTCTCGTTCTTCGAGCTTGGCGCGGCCTGCAGGGAGAGAATGGT
TGACCATGAGGACGCCGATGGGCGATGCGCCAGCGCGTGCTTGCGTACTTCAATCGTTTTTCATCTTGATTCAGA
GCTAAGTAGTAGCACACCACAGCAAGCGTAATCATGTAGCATGTATGCAGGTGCACGAGTAGGCACTCTCTGTCT
CTGTCCGGCATCTATGATGCTCTCCGGCCGCGTGCGCGCGACGCCTCTGTGTGAGTGCTCGTGTGAGTGTGTGA
GAGCTGTCCAGGCCTTTCCTCTGCCTACTCGTCCCACGCTCAGGCAGGCACAGAGGAATGAAAAGGAAGACGA
GGACGCAACGCCAGGCGCATCGACATCGCGCACGTGTTTGCGGTGTACTGTGCGTCGATGATCGAGCGGCCAA
GCGTCCAGCTTCACGCGAGGAGGACTGCATCGCTGCTCCTGTGCGCGTGCGTGCACGCGTCAAGGCACGCTCG
ATTCGTTCCCAGGGTGGATACCCTCCCCCCTCCCCCAGCTGCAGACAACCCCCACCCTCTCGAGGCTTGCACCCA
GGCTCGTCAGTCTCTCTACCACTTTCTGCCTTCTGTAGTGCACCCCACCCCTGCATTCTCCTCTCTCTCACACACAC
ACACACACACACACACACACACACACACACACACACGTACACACGTACACACACGTGCGCATGCTTGACGCATACGCG
ACGAATTCGAAAGCTCACCTCATTCCTCCCTCCTCACACCATCATCGGCATCCATAGAGACACGTGCGCGTAGAAC
GATACAGCTCACGCGCACAGAGAGGCGTGTTCTGGTCGTGCGCATCATCGGCACAGCACTGGCGGACGAAACT
CGCACACAGGCACGCCGCCTCCTTTCACCCGTCATAGATAGTTGAATTAGACGCCCTCCTCCTCCCTCATCATCGC
CGTCGTCATCCGGGTCCGAGCACTAGTCGCGTGTGGCCTCGAACACCGAGCGACCCTGCAGCCAATATGGGATC
GGCCATTGAACAAGATGGATTGCACGCAGGTTCTCCGGCCGCTTGGGTGGAGAGGCTATTCGGCTATGACTGG
GCACAACAGACAATCGGCTGCTCTGATGCCGCCGTGTTCCGGCTGTCAGCGCAGGGGCGCCCGGTTCTTTTTGT
CAAGACCGACCTGTCCGGTGCCCTGAATGAACTGCAGGACGAGGCAGCGCGGCTATCGTGGCTGGCCACGACG
GGCGTTCCTTGCGCAGCTGTGCTCGACGTTGTCACTGAAGCGGGAAGGGACTGGCTGCTATTGGGCGAAGTGC
CGGGGCAGGATCTCCTGTCATCTCACCTTGCTCCTGCCGAGAAAGTATCCATCATGGCTGATGCAATGCGGCGGC
TGCATACGCTTGATCCGGCTACCTGCCCATTCGACCACCAAGCGAAACATCGCATCGAGCGAGCACGTACTCGGA
TGGAAGCCGGTCTTGTCGATCAGGATGATCTGGACGAAGAGCATCAGGGGCTCGCGCCAGCCGAACTGTTCGC
CAGGCTCAAGGCGCGCATGCCCGACGGCGATGATCTCGTCGTGACCCATGGCGATGCCTGCTTGCCGAATATCAT
GGTGGAAAATGGCCGCTTTTCTGGATTCATCGACTGTGGCCGGCTGGGTGTGGCGGACCGCTATCAGGACATAG
CGTTGGCTACCCGTGATATTGCTGAAGAGCTTGGCGGCGAATGGGCTGACCGCTTCCTCGTGCTTTACGGTATCG
CCGCTCCCGATTCGCAGCGCATCGCCTTCTATCGCCTTCTTGACGAGTTCTTCTGAGGGGATCGGCAATAAAAAG
ACAGAATAAAACGCACGGGTGTTGGGTCGTTTGTTCGGATCACTAGTAGTGATCCCGCCCGCACCCGCGCGCGC
TCAGGCCGCGTGTCGTCGTGCTCTTTCCATTTTTTTTTTGTGTGTGGTGGTGATTTGAGCTGCTCTCCGTTGTGTG
CTGGGGACCCTCCTTCCCTCGATCTCCTCGTGCGGGGTCTCCGACGCCGCAGACGCGGTGCGTGCGAGCGTGC
ACGTGGCTGTCGCCGTGGCTGTAGTTGCGAGCGGAGAGAGAGAGAGAGGGAGGGAGGGAGGGCAGAGGGC
AGAGGACATGCGGGTGGGAACGTGCACCGGCCTCGTCTCACGCAGCTGGAGCCCACGAATGCCACCACCACAC
CCTTCTTCCCCCCCCCCTCCCTCTTCTTCCCACGGCGGCGACGACGACGGGGCTCAGCTCACGCTTCTGTAGGGT
ATTATATTAAAGCACATGTGCGTGCTGTGCTTCGGCTTCTTGTTGGTGGTCGTTCGCTTTCAAGTCCACGACTCCT
GCCGTTGCTCACCGCCGGGCTGTCTTCTTTCGCCCCTCCCTCGGTGCCTCTTCCGCCGCCGCACGCGTGCGCTGA

TCACGCGTCTTGCGTGATGTGCCTGTGTGTATACACACCGTGCACGGAGAGAGCGAGCGAGCGAGAGAGAGAG
AGGGCGAGAGGAAGAATGGCCGGTGCCTCGCGTGGGCAAGCGTGCGCGAGTTTGTCGTGTCGCTGCGCCGCG
TGGATGTCGCGCAGCGCAAGACCCCGTGCGCCTGAAACGTGAAGGGAGGTCGAGAAGCGTGCCGCATGAGGC
CTTAAGGCAGGAAAGTGAAAAGAGCTCGACGCGAGTGCAGCACGCGCGCATCGACAGGACGGAATAGACACT
CAGCCCCTTCCCCTTTCAAAAACTGAATGGACGGACATCGTAACGCGCTTCTCTCCCCTCCACTCCCCCTGTCCCT
GTCTCCTTGACGTGTGCTGCTCTCGTGAGCGACAGATGAAGCGAGGCGTAGAAGGAAAGGGGGGGGGAGCA
GGCCTGCACACACACACACACACACACACACACACACACACACACACACACACACACACACACGAAAAGCAAGTTTGAGGCAG
ACGTGGTTTCACACGATTCCTGTGCAAGATGCGTGCCTGCGTGACGGGTGTGGCTGTGTATGCATGCGTGAAGG
GTTACCGCAACGATGCGCAATGGACTCCCCCGCTTTCCATTTCGTCACCTTCCGCCTCTCTCTCTCTCTCTCACC
ATCTACGCGTGCACATCATCAACTGTCTCTTGTCGGTGCTCACCACCCTCAACCACCCCTCACTTTCAAGGCTTCC
CGAACGCACACAAAAGGCGTGAAAACCGCTCGCGGTGTGTTGAGCCGTCCACCGGCGCGCCGGCCGCGGATC
GAAACCTGTCGTGCCAGCTGCATTAATGAATCGGCCAACGCGCGGGGAGAGGCGGTTTGCGTATTGGGCGCTC
TTCCGCTTCCTCGCTCACTGACTCGCTGCGCTCGGTCGTTCGGCTGCGGCGAGCGGTATCAGCTCACTCAAAGG
CGGTAATACGGTTATCCACAGAATCAGGGGATAACGCAGGAAAGAACATGTGAGCAAAAGGCCAGCAAAAGGC
CAGGAACCGTAAAAAGGCCGCGTTGCTGGCGTTTTTCCATAGGCTCCGCCCCCCTGACGAGCATCACAAAAATC
GACGCTCAAGTCAGAGGTGGCGAAACCCGACAGGACTATAAAGATACCAGGCGTTTCCCCCTGGAAGCTCCCT
CGTGCGCTCTCCTGTTCCGACCCTGCCGCTTACCGGATACCTGTCCGCCTTTCTCCCTTCGGGAAGCGTGGCGCT
TTCTCATAGCTCACGCTGTAGGTATCTCAGTTCGGTGTAGGTCGTTCGCTCCAAGCTGGGCTGTGTGCACGAACC
CCCCGTTCAGCCCGACCGCTGCGCCTTATCCGGTAACTATCGTCTTGAGTCCAACCCGGTAAGACACGACTTATC
GCCACTGGCAGCAGCCACTGGTAACAGGATTAGCAGAGCGAGGTATGTAGGCGGTGCTACAGAGTTCTTGAAG
TGGTGGCCTAACTACGGCTACACTAGAAGAACAGTATTTGGTATCTGCGCTCTGCTGAAGCCAGTTACCTTCGGA
AAAAGAGTTGGTAGCTCTTGATCCGGCAAACAAACCACCGCTGGTAGCGGTGGTTTTTTTGTTTGCAAGCAGCA
GATTACGCGCAGAAAAAAAGGATCTCAAGAAGATCCTTTGATCTTTTCTACGGGGTCTGACGCTCAGTGGAACG
AAAACTCACGTTAAGGGATTTTGGTCATGAGATTATCAAAAAGGATCTTCACCTAGATCCTTTTAAATTAAAAATG
AAGTTTTAAATCAATCTAAAGTATATATGAGTAAACTTGGTCTGACAGTTACCAATGCTTAATCAGTGAGGCACCTA
TCTCAGCGATCTGTCTATTTCGTTCATCCATAGTTGCCTGACTCCCCGTCGTGTAGATAACTACGATACGGGAGGG
CTTACCATCTGGCCCCAGTGCTGCAATGATACCGCGAGACCCACGCTCACCGGCTCCAGATTTATCAGCAATAAA
CCAGCCAGCCGGAAGGGCCGAGCGCAGAAGTGGTCCTGCAACTTTATCCGCCTCCATCCAGTCTATTAATTGTTG
CCGGGAAGCTAGAGTAAGTAGTTCGCCAGTTAATAGTTTGCGCAACGTTGTTGCCATTGCTACAGGCATCGTGGT
GTCACGCTCGTCGTTTGGTATGGCTTCATTCAGCTCCGGTTCCCAACGATCAAGGCGAGTTACATGATCCCCCATG
TTGTGCAAAAAAGCGGTTAGCTCCTTCGGTCCTCCGATCGTTGTCAGAAGTAAGTTGGCCGCAGTGTTATCACTC
ATGGTTATGGCAGCACTGCATAATTCTCTTACTGTCATGCCATCCGTAAGATGCTTTTCTGTGACTGGTGAGTACTC
AACCAAGTCATTCTGAGAATAGTGTATGCGGCGACCGAGTTGCTCTTGCCCGGCGTCAATACGGGATAATACCGC
GCCACATAGCAGAACTTTAAAAGTGCTCATCATTGGAAAACGTTCTTCGGGGCGAAAACTCTCAAGGATCTTACC
GCTGTTGAGATCCAGTTCGATGTAACCCACTCGTGCACCCAACTGATCTTCAGCATCTTTTACTTTCACCAGCGTT
TCTGGGTGAGCAAAAACAGGAAGGCAAAATGCCGCAAAAAAGGGAATAAGGGCGACACGGAAATGTTGAATA
CTCATACTCTTCCTTTTTCAATATTATTGAAGCATTTATCAGGGTTATTGTCTCATGAGCGGATACATATTTGAATGTA
TTTAGAAAAATAAACAAATAGGGGTTCCGCGCACATTTCCCCGAAAAGTGCCACCTAAATTGTAAGCGTTAATAT
TTTGTTAAAATTCGCGTTAAATTTTTGTTAAATCAGCTCATTTTTTAACCAATAGGCCGAAATCGGCAAAATCCCTT
ATAAATCAAAAGAATAGACCGAGATAGGGTTGAGTGTTGTTCCACACAAAATTTCATGCTCAGGGACACAAATAT
AGGAGGGGGGGGGGGTGAATACGTTATATATGTATAATGTGTGTCGCTTAGCTTCACAAACCCAGAAGGAACGG
TGCAAAGGACCCGACAACCAGCTGTGTGCGCGTATATATTTACGTCTGCATACACGGCTCGTTGTCGGGTCCTTG
CCCTTTTCCGTCCCCTTTTCCGTCCTGCGCGTGTGTGTATGGGCGCGGGTGGGGTGTGTGCATGCGGGGGGGG
GGGAGGATCGAGCACCCCCCAACACTACCTCCATCCAAAACAAACACACAGCAGAGAGTGCTCGCCAACCTTG
GGCGCTTCTCGGTTGCCGTGTGTGTCATTGCCCTGCAGAGAGAGCGGAACAGGGGGGTGGAGGTGGGAATGG
GGGGGCACGATTTCCACCACCAAAGTCTCTCCCTACGGGAACACGCCAATAGGCATGCCCTTTGACTGTAAGTT
ACAGTCAAGCAATACGGCGGCTTACCTCCGCCACCCGACCCGGCAACCAGCTGCGCCCAACCGCGCGGCTCGT
TGTCGGGTCCTTGCCCTTTTTTCACTGCGACCCTCAAAGACAGTGTACGCCAGTCCAACGATCCCACTCCCAGCG
ATGGACCGCGCCCAACGTTCACCCGCAACCCACATTCGGAATTCGACATCATGCCCTAGGATTTAAATGCGGCCG
CGAGGTCTGCGATTGACGTAGGAGTTGCAAGGGGGAGGGGGTATGAACGGGGTGGGTAGAGCTTTTTTAGGT
GGAAGTAGTGAGATGGTGGGCTTGAGAGAATTTGAGGTGTGTTCGTGATGTGTGGATCTTATCGGGGGCTCGG

TTGAGTTTTTGGTTTGGTGATTTTGTAGGGGTGAAGGGCGGTGGAAGGGTTGCTGTGTGCGTGCCATTCCGTG
AAGCGTCATTCCTATGTCCGACACTGAAATGCGTCCGCGATCGTGTGGATTGTGTGGAAGTGTTTGGGCGACGA
CTGAATTGAGAAGGGGAGTCGAAACGGTGCGTGGATGCCGTGTTTGTGCTACACACAAGCAAAGGCAACAAC
GCAAGCGCATCGAGCCAGACGAACCAACCCAAAATTCACACAACTGTACGTGGCAGCGCGCTGTATCGTTGGA
AAGACGATGCGTGTGCGCGTGCCACCACCATGTACTAGTTTCCAGCCTAACTGCTTGTATACCTTGTCTTTTGCGT
TGTGCCTGCGCGTGCTGTGTACCTCTGCTCGTGTGTCCCTTCGGTCTCACGTAGCTAGCACCGACAAGACCAGAA
TAGCGCTTATGTGTGTGTGTTTGTGTGTGGGTGTGTGTGCCCATGTGTGACAAAGAGGCCAGTGCTTTCTCTAAA
GCAAGAGCGCGAGGTTGCTGGCTAAGGACTCTAAGTCCCTCACAGTGATGGCGTGTTGCATTTTCTAAACCGTC
AATCCAACACGTCGGTAGCATATCGGTTTTGTAGGCTCTTCTGGATACCTTCCCCAGTAAGACCGCCACTGCTTCG
TGACTGAAGCACTGTAAATATCACTGAAACCGTCGCGTTGCTTTGTCTAATTATCACCGCCTTTGCCAGCTATCGC
CTCAGGCTGCGCTCTTTGACTAATCCACTCACCACTTCTCTGCCTTCTTCCTCCGGTTGTTGTTGTGTCCTGCGTGT
ACATGGCGCGTGTCCTTTTCGAGCAAACAGCTGTCTTTTCTTTCACGATAACACACTCATATTAAACGCGAGTATT
ACTCATCAGTCAACGTCACATTCCGCTCTGTCCACTTCGACCTTACACCTCTACTTGTCCAACTATCTTCCACTTGT
CAAGCTCCGGAGGCCACCTGGGCCATGGTCTCGAAAGGTGAGGAAGACAATATGGCCAGCTTGCCAGCAACGC
ACGAGCTTCATATATTTGGGTCGATCAACGGTGTGGATTTCGACATGGTGGGTCAAGGCACAGGTAATCCTAATG
ACGGGTATGAAGAACTCAATTTGAAGAGCACTAAGGGAGATCTCCAGTTTTCCCCGTGGATTCTTGTGCCGCATA
TTGGTTATGGTTTTCATCAGTACTTACCATACCCCGATGGAATGTCGCCCTTCCAAGCAGCTATGGTGGACGGCTC
GGGGTATCAAGTACATCGCACCATGCAATTTGAGGACGGAGCATCCCTCACCGTAAACTACCGCTATACGTATGA
GGGGAGCCACATAAAAGGTGAGGCTCAAGTTAAAGGCACAGGCTTCCCAGCTGACGGCCCGGTCATGACCAAT
TCATTAACCGCTGCTGATTGGTGCCGTTCTAAGAAGACCTACCCTAACGACAAGACGATCATTAGTACTTTTAAGT
GGAGTTATACCACAGGAAACGGAAAGCGGTATCGAAGCACTGCTCGAACAACCTACACATTTGCGAAGCCAATG
GCCGCGAACTACTTGAAGAACCAGCCAATGTATGTGTTTCGAAAAACGGAACTGAAGCATTCGAAAACCGAGCT
TAATTTTAAAGAGTGGCAGAAGGCGTTTACAGACGTGATGGGGATGGACGAATTGTATAAG